Design and Synthesis of CdS Quantum Dots and CdS-Fe_3O_4 Hybrid Nanoparticles in Aqueous Solution

by

SERDAR ÇELEBİ

A Thesis Submitted to the
Graduate School of Engineering
in Partial Fulfillment of the Requirements for
the Degree of

Master of Science
in
Materials Science and Engineering

Koc University

October 2007

Koc University

Graduate School of Sciences and Engineering

This is to certify that I have examined this copy of a master's thesis by

Serdar Çelebi

and have found that it is complete and satisfactory in all respects,
and that any and all revisions required by the final
examining committee have been made.

Committee Members:

_____

Havva F. Yağcı Acar, Ph. D. (Supervisor)

_____

Alphan Sennaroğlu, Ph. D.

_____

Mehmet Somer, Ph. D.

Date: _____

ABSTRACT

Realization of control over structures at the nanoscale revolutionized today's science and technology. Nanomaterials with unique properties created new opportunities in a variety of scientific and technological fields. Among many, quantum dots (QDs) can be considered as one of the most impressive nanomaterials with size dependent optical and electrical properties that are valuable in a variety of areas, especially biotechnology, microelectronics, and optoelectronics. Superparamagnetic iron oxide nanoparticles are also of great interest and subject of continuous research in areas where magnetic recognition or separation is desired. Ever increasing demand to push the borders of existing technologies requires better control of the particle properties and development of multifunctional materials. A highly desirable, multifunctional entity would be magnetic quantum dots (MQD) where particles can be recognized both optically and magnetically.

In realization of such hybrid nanoparticles, a two-step approach was followed: first, preparation of stable and highly luminescent cadmium sulfide (CdS) QDs in water; then, synthesis of MQDs in QD solution. Initially, poly(acrylic acid) (PAA) capped CdS nanoparticles were prepared and characterized. Influence of coating amount, Cd/S ratio, polymer molecular weight and reaction pH on the particle size and quantum yield (QY) were investigated. Results indicate that PAA coating provides excellent stability in water, yet size tunability is limited and QYs are low (5-17 % with respect to rhodamine B). More importantly, a critical ratio of carboxylic acid to cadmium of 1.5-2.0 emerged as the optimum value that provides the highest QY.

Secondly, CdS QDs coated with PAA and MAA (mercaptoacetic acid) were developed. Utilization of MAA, which bonds to the surface of CdS through thiol group, provided ability to alter crystal size and improved QY. Good QY for MAA coated QDs is known but stability of these particles is not good. Therefore, by the use of a binary mixture of PAA

and MAA, a synergy in all properties was expected. Effect of composition and reaction temperature on optical properties was also investigated. 50 % QY was achieved with 40/60 PAA/MAA (COOH/Cd = 11) coating. Attempt to combine the optimum coating amount (COOH/Cd = 2) and the best PAA/MAA ratio (40/60) improved QY up to 98%.

Lastly, first example of one pot synthesis of CdS-Fe_3O_4 particles was demonstrated. PAA and PAA/MAA coated CdS solutions were used as the synthesis medium for the iron oxide nanoparticles. A red shift of 50 nm in the emission maximum (PL_{max}) of the QDs indicates quite intriguing events that are under current investigation.

Development of new highly luminescent CdS QDs and hybrid MQDs create an exciting opportunity for multifunctional materials that would impact the fields of biological labeling, medical imaging, sensing and separation with an advantage of multiplexing and combined action of dual sensing and separation.

ÖZET

Malzemelerin yapılarının nano boyutta kontrolünün sağlanması, bilim ve teknolojide bir devrim yaratmıştır. Eşsiz özelliklerdeki nano-malzemeler, çeşitli teknoloji ve bilim alanlarında yeni fırsatlar sunmaktadır. Kuantum noktaları, biyomedikal ve elektronik alanlarındaki çeşitli uygulamaları sebebiyle en dikkat çeken nano-malzemeler arasında yer almaktadır. Bunun yanında, süperparamanyetik demir oksit nanoparçacıkları da çok ilgi çeken ve özellikle manyetik tanımlama ve manyetik ayırma işlemlerini gerektiren sahalarda çokça araştırılan nano-parçacıklardandır. Gelişen teknolojinin sınırlarını ileriye taşıma isteği, partiküller üzerinde hassas bir kontrolün sağlanmasını ve birden çok işlevi yerine getirebilen akıllı malzemelerin geliştirilmesini gerektirmektedir. Manyetik demir oksit ve kuantum noktalarının tek bir yapıda birleştirilmesi, optik ve manyetik tanımlamanın aynı anda elde edilmesini olanaklı kılacaktır.

Bu çalışmamızda, manyetik ve optik tanımlama imkanı bulunan bu parçacıkları (süperparamanyetik kuantum noktaları) geliştirebilmek için iki adımdan oluşan bir yaklaşım izlenmiştir. İlk olarak, yüksek ışımaya ve kuantum verimine sahip olan kadmiyum sülfit (CdS) nanoparçacıkları suda sentezlenmiştir. Bu sentezleri takiben süperparamanyetik demir oksit nanoparçacıkları (CdS) QD çözeltisi içinde sentezlenmiştir. Bunun için öncelikli olarak Poli(akrilik asit) (PAA) kaplı CdS nanoparçacıkların sentezi ve karakterizasyonu yapılmıştır. Kaplama miktarının, kadmiyum sulfite oranının (Cd/S), polimer molekül ağırlığının ve reaksiyon pH'ının, partikül büyüklüğü ve kuantum verimi üzerindeki etkileri detaylarıyla araştırılmıştır. Sonuçlar, PAA kaplamasının sulu ortamda üstün bir kararlılık sağladığını göstermektedir. PAA ile kaplanan CdS malzemelerinin, PAA miktarına göre kristal büyüklüklerinin değiştirilemediği ve düşük kuantum verimine sahip olduğu (5-17 %; Rhodamine B referans alındığında) görülmüştür. En yüksek

kuantum veriminin, COOH/Cd oranının 1.5-2.0 aralığında tutulmasıyla elde edilebileceği önemli bir bulgu olarak ortaya çıkmıştır.

Çalışmanın ikinci aşamasında, PAA ve merkaptoasetik asit (MAA) karışımıyla kaplanmış CdS kuantum noktaları geliştirilmiştir. Kaplama malzemesine (PAA), yüzeye sülfür bağı ile bağlanan MAA'in eklenmesi kristal büyüklüğünü değiştirmeye ve kuantum verimini arttırmaya olanak sağlamıştır. MAA'in iyi kuantum verimine sahip olduğu bilinmektedir ancak MAA kaplı parçacıkların sudaki kararlılığı iyi değildir. Bu nedenle, iki kaplama malzemesinin karıştırılarak nanoparçacıkların özelliklerinde sinerjik bir etkinin elde edilmesi planlanmıştır. Sabit COOH/Cd oranında, PAA/MAA oranının ve reaksiyon sıcaklığının bahsedilen optik özellikler üzerindeki etkileri incelenmiştir. CdS noktaları, COOH/Cd oranı 11 tutulup, 40/60 PAA/MAA oranı ile kaplandığında, 50 % kuantum verimi elde edilmiştir. Ancak, çalışmanın ilk safhasında bulunan optimum kaplama miktarı, (COOH/Cd = 2), uygulandığında kuantum verimi 98 %' e ulaşmıştır.

Son olarak, ilk kez CdS-Fe_3O_4 partiküllerinin aynı sistem içinde sentezlenebilirliği gösterilmiştir. PAA ve PAA/MAA kaplamalı CdS çözeltileri, demir oksit sentezi için başlangıç çözeltisi olarak kullanılmıştır. Işıma ölçümlerinde kuantum noktalarının ışıma maksimumlarının sürekli olarak (50 nm) kırmızı dalga boyuna kaydığı görülmüştür. Işıma kaymasının sebepleri araştırılmaya devam edilmektedir.

Yüksek ışıma verimine sahip CdS kuantum noktalarının suda hazırlanabilmesi ve böylelikle birden fazla işlevi olan manyetik kuantum noktalarının geliştirilmesi; biyolojik etiketleme, tıbbi görüntüleme, algılama ve ayırma fonksiyonlarının bir arada bulunmasını sağlayıp, önemli bir yenilik yaratacaktır.

ACKNOWLEDGEMENTS

I am deeply indebted to my supervisor Asst. Prof. Dr. Havva Funda Yağcı Acar from Koç University for her help, stimulating suggestions, encouragement and motivation at all stages of my research and during the preparation of this thesis. I would like to express my gratitude to Prof. Alphan Sennaroğlu and Adnan Kurt for their support, interest and valuable hints on my studies. I also want to thank A. Koray Erdamar for his collaboration and assistance on the PL and UV visible measurements and for his friendship.

I would like to acknowledge Assoc. Prof. A.Levent Demirel and Prof. Mehmet Somer for their helpful and friendly approach to my problems. I also have to thank my lab mates S. Sinan Öztürk and Recep Kaş for their friendship and help during the experimental part. Mr Öztürk provided a different perspective that helped me to understand and solve the technical problems easily. I deeply appreciate N. İpek Serttunalı assistance on the experimental part of my research and her help on the characterization part. I also would like to thank Özlem Tekmek for her valuable insight, Feyza Selcuk for endless understanding and friendship, Miray Demirer for her support during the initial stages of my research and her friendly attitude. I also would like to thank Ilkin Kokal and Selcuk Acar for their guidance on collection and evaluation of XRD and FT-IR data. I am also grateful to Muharrem Güler for his help for all the difficult events taking place in the lab and for all lab equipment problems. Without him, we could not carry out any reaction!

I would like to thank Prof. Somer and Prof. Sennaroğlu for taking part in my thesis committee. Especially, I would like to give my special thanks to my mother, father and brother (sarı) who's love and encourage enabled me to complete this work.

TABLE OF CONTENTS

Appendix B

LIST OF TABLES

LIST OF FIGURES

NOMENCLATURE

m^*	Effective Mass of Electrons
E_g	Energy Gap
BE	Binding Energy
CdS	Cadmium Sulfide
COOH	Carboxylic Acid
Dh	Average hydrodynamic size
DLS	Dynamic Light Scattering
EBR	Electron Bohr Radius
EMA	Effective Mass Approximation
Fe_3O_4	Iron Oxide (magnetite)
FTIR	Fourier Transform Infrared Spectra
FWHM	Full Width at Half Maximum
LED	Light Emitting Diodes
MAA	Mercaptoacetic acid
MM	Multiple Measurement
MNP	Magnetic NanoParticle
MQD	Magnetic Quantum Dot
MRI	Magnetic Resonance Imaging

NC	Nano Container
OA	Oleic Acid
Aº	Angstrom
PAA	Poly(acrylic acid)
PL	PhotoLuminescence
QD	Quantum Dot
QY	Quantum Yield
–SH	Thiol
SM	Single Measurement
SPIO	Super Paramagnetic Iron Oxide
T_c	Curie Temperature
TOPO	Tri-Octyl Phosphine Oxide
UV	Ultra Violet
XPS	X-ray Photoelectron Spectroscopy
XRD	Xray Diffraction
α-Fe_2O_3	Iron Oxide (maghemite)

Chapter 1

INTRODUCTION

Smart materials with novel or improved properties are necessary for the future fabrication of our universe. In order to produce these smart and novel materials, spatial organization in nanoscale should be realized through engineering at the molecular level. In the fast-growing *nano world* a considerable attention has been devoted to nanoparticles which usually exhibit different properties than their bulk or macroscopic forms. Among these, probably the most exciting ones are the semiconductor nanoparticles called *quantum dots (QDs)* and *superparamagnetic iron oxides (SPIOs)*. These nanoparticles created advancement and lead into many innovations in diverse areas across many industries as non-traditional materials with unique properties crossing over the limitations of existing materials and going beyond. Size dependent fluorescent properties of QDs are being exploited for many applications from fluorescent tags to lasers. QDs impacted the development of electronic and optical devices dramatically. On the other hand, superparamagnetism in addition to biocompatibility of SPIOs made them very attractive for the biomedical applications, yet they found use in the other areas ranging from audio speakers to sensors. Major impact of SPIOs originates from its dragging and detection ability in a magnetic field. Today, although there are commercially available products from both of these families, there is a continuing extensive research on QDs and SPIOs both in the academia and industry, for the advancement of the scientific and technological frontiers

as well as to make these nanoparticles more accessible, cheaper, faster, and with tailored properties.

Majority of the research summarized in this MS thesis is focused on the QD synthesis and characterization with the ultimate goal of achieving magnetic quantum dot (MQD) hybrid nanoparticles that combines the unique properties of both in a single body. Following sections would introduce the major terminology and concepts in addition to a brief review of the related literature on QDs, SPIOs and MQD.

1.1 Quantum dots (QDs)

QDs are unique class of semiconductors with small crystal size of usually below 10 nm and composed of group II-VI, III-V, or IV-VI atoms. Nearly 7.5 million QDs could be lined up end to end and fit within the width of a 50 Turkish Kuruş (Figure 1.1).

Material properties change dramatically at this small size regime in which the motion of conduction band electrons and valence band holes are confined. This confinement can be due to the presence of electrostatic potential; an interface between different semiconductor materials and the semiconductor surface or a combination of these.

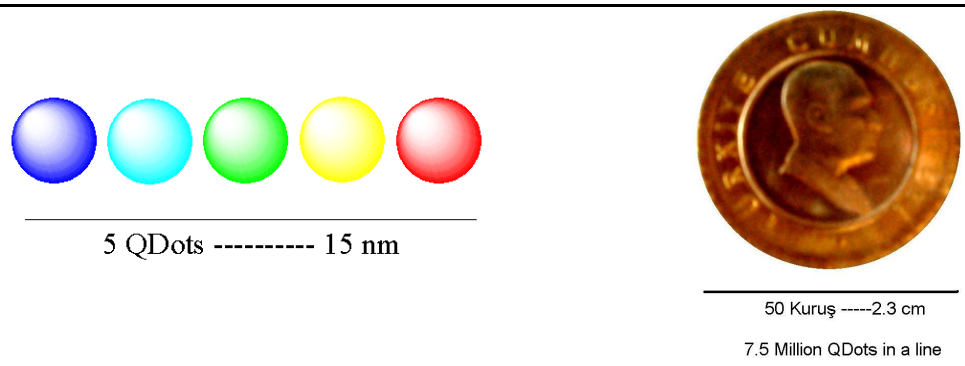

Figure 1.1 QDs comparable sizes (www.evidenttech.com)

1.2 Energy bands and bandgap

In a bulk nanocrystal, energy levels are so close to each other that they are considered as continuous. Moreover, some energy levels are calculated quantum mechanically as forbidden energy levels and called as *bandgap*, which is different for each bulk material. Energy levels below the bandgap are defined as the valence band and energy levels above the bandgap are defined as the conduction band (Figure 1.2). If an electron in the valence band acquires enough energy to cross the bandgap, it jumps to the conduction band leaving a positive *hole* behind. An external stimulus such as photon flux, voltage or heat can provide the necessary energy for the jump. The conduction band electron and the valance band hole are called an *exciton* as a pair (Figure 1.2). The distance between the electron and the hole is called as *Exciton Bohr Radius (EBR)* (Figure 1.3) and is the minimum radius of a semiconductor nanocrystal having continuous energy bands. EBR differentiates a QD from a bulk semiconductor. Fluorescence of QDs originates from the release of energy in the form of photon during the electron-hole recombination.

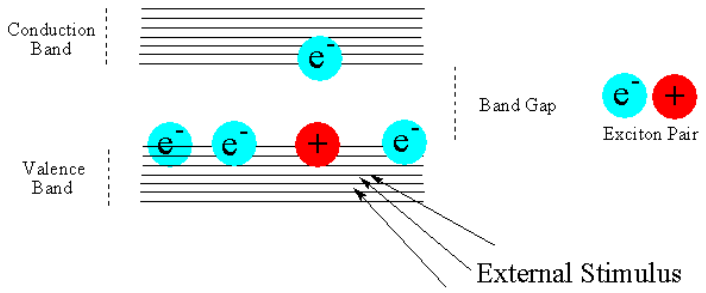

Figure 1.2 Semiconductor crystal levels and creation of exciton (www.evidenttech.com)

In bulk semiconductors, energy levels are continuous and band gaps are fixed. However, when the size of the crystal is as small as the EBR, electron energy levels are no

longer continuous but rather discrete. This is called as *quantum confinement*. Size dependent fluorescence of QDs originates from this phenomenon. As a result of such confinement, band gap of the QD varies with the size of the nanocrystal and is always larger than the band gap of its bulk form (Figure 1.3a). This also causes a blue shift in the emission with decreasing crystal size, providing QDs of various *colors* (Figure 1.3b).

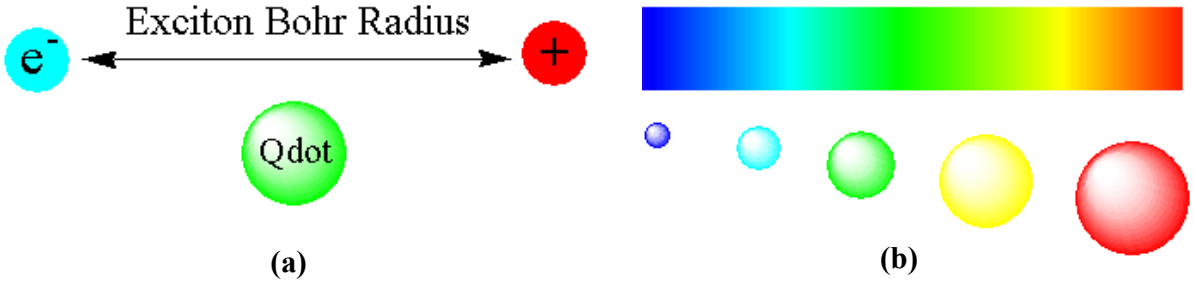

Figure 1.3 a) Size difference between QD and exciton Bohr radius b) Emission color change of QDs with respect to their sizes. (www.evidenttech.com)

1.3 Tunable absorption and emission behavior

Absorption spectrum of QDs can be considered as overlapping peaks corresponding to a transition between different exciton energy levels, getting larger at shorter wavelengths. The wavelength corresponding to the first exciton absorption in UV visible spectrum of a QD is called *absorption onset* and depends on the size of the nanocrystal. Absorption onset of smaller dots is blue shifted with respect to larger ones because of the quantum confinement.

Excited electron returns to ground state through radiative recombination with the hole. Energy loss corresponding to this transition is generally lower than the energy necessary for the excitation hence; the emission wavelength is longer than the absorption onset. This energy separation is referred as the *Stoke's Shift* and originates from the loss of some energy during the excited lifetime (Figure 1.4). Emission wavelength of a QD is

independent of the excitation wavelength for wavelengths shorter than the absorption onset. This along with the broad absorption spectrum of the QDs allows excitation of various sizes at a single wavelength and emission in different colors. For the minimum overlap of emitted colors, narrow emission profile is required which is one of the many advantages of QDs over organic fluorophores. The bandwidth of the emission spectra expressed as the *Full Width at Half Maximum (FWHM)* gets larger with the increasing size distribution of the QDs. Besides it depends on the temperature and natural spectral line width of the dots.

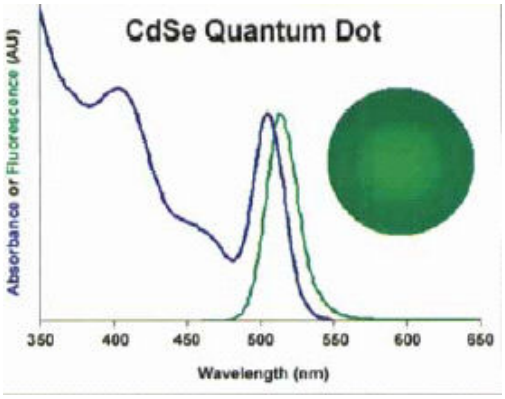

Figure 1.4 Representation of Stoke's shift in green emitting CdSe QD.[1]

QDs can be compared with other semiconductor nanostructures: quantum wires (1D), which confine the motion of electrons and holes in two directions and, quantum wells, which have confinement in one direction and allow free propagation in two directions (Figure 1.5). In QDs, the confinement results in discrete energy levels whereas in quantum wells and wires, energy levels are continuous.

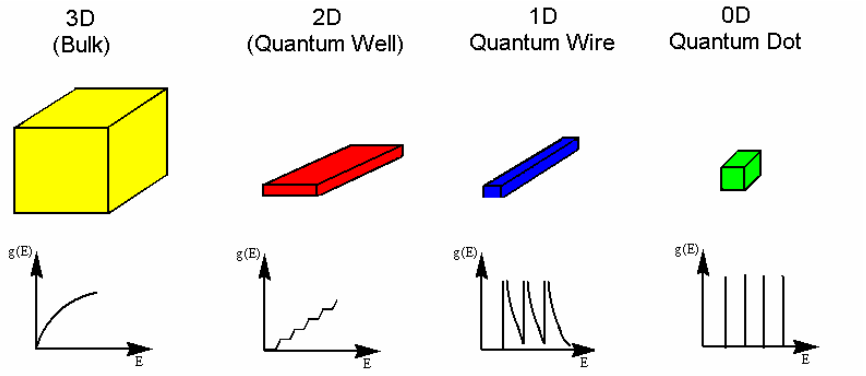

Figure 1.5 Bulk and confined structures of nanocrystals. [2]

1.4 Brus equation and crystal size determination

First in-depth investigation of electron confinement in QDs was done by Brus et al in 1984.[3] They tried to solve the quantum well problem for zero dimensional systems. They found out that the minimum energy (energy gap), E_g, required for creating an exciton mainly depended on three important contributors: The first contributor was the bulk band gap energy of the nanocrystal, $E_g(bulk)$. The second one was stated as the confinement energy for the carriers, described as $E_{well} = E_{well}(e^-) + E_{well}(h^+)$.[4] In a spherical QD, well energy can be easily calculated from the potential box problem (eqn 1.1),

$$E_{well} = \frac{h^2}{2m^* d^2} \tag{1.1}$$

where h is Planck constant, d is the average diameter of the particles and m^* is the effective mass of the electrons and holes given by $\frac{1}{m^*} = \frac{1}{m_e} + \frac{1}{m_h}$. The third contributor is the coulomb screening interaction potential and determined experimentally. The strength of the

screening depends on the screening coefficient that is the dielectric constant of the semiconductor (ε) (eqn 1.2).

$$E_{Coul} = -1.8\frac{e^2}{2\pi\varepsilon\varepsilon_0 d} \tag{1.2}$$

By combining these three terms, $E_g(dot)$ can be written as;

$$E_g(dot) = E_g(bulk) + E_{well} + E_{Coul} \tag{1.3}$$

$$E_g(dot) = E_g(bulk) + \frac{h^2}{2m^* d^2} - 1.8\frac{e^2}{2\pi\varepsilon\varepsilon_0 d} \tag{1.4}$$

The crystal anisotropy and the spin-orbit coupling are not taken into account in the basic equation (eqn 1.4). In this equation, the confinement energy term varies with $1/d^2$ whereas the coulomb term varies with 1/d. Confinement term is a positive term that raises the energy of the first possible state. On the other hand, coulomb interaction term is always attractive and lowers the energy. Since the dependence of $E_g(dot)$ on confinement term is $1/d^2$, confinement effect is dominant in the size calculation. Coulomb term affects the crystal size calculated by the Brus Equation by 10 %. Detailed calculations and size-color relationship based on the Brus Equation are given in Appendix A.

1.5 Synthesis of QDs

QD production has been considered as a very hot topic for the last two decades. In general, QDs can be produced by colloidal methods, lithography, epitaxial growth or other solid state methods. However, these techniques are beyond the scope of this thesis and only a review of colloidal preparation methods will be discussed here.

Controlled growth of the nanocrystals should be done in suitable surfactant liquid mixture. Molecules that can adsorb on the crystal surface and prevent growth are considered as *surfactants* or *ligands*. The choice of the surfactant is very important since it

should not prevent the growth completely. On the other hand, weak coordinating agents results in a particle aggregation and does not allow effective control of the particle size and size distribution. Surfactant selection depends on the type of the QD, solvent and the synthesis temperature. Therefore, organic and aqueous routes for the QD synthesis should be reviewed separately.

In nonaqueous synthesis approach, Bawendi et al achieved nearly monodisperse QDs ranging in size from 12 – 115 Aº where a fast nucleation at high temperature is followed by a slow growth at lower temperatures.[5] Their synthesis of CdE (E=S, Se, Te) was based on the pyrolysis of organometallic reagents upon injection into a hot coordinating solvent. There are many other groups investigating the same method.[6, 7] The most widely used method utilizes tri-octyl phosphine (TOP) to dissolve the S, Se or Te, tri-octyl phosphine oxide (TOPO) as the coordinating solvent and dimethyl cadmium. In a typical preparation of TOPO capped CdSe nanocrystals, dimethyl cadmium and TOPSe were mixed at 300 ºC. This method was generally used in mass production of the QDs. Recent advances in colloidal preparation of II-IV QDs were discussed by Esteves et al.[8] It was found that the dominant binding between the organic ligands, such as phosphonic acid, phosphine oxide or carboxylic acid, and CdSe surface was through the oxygen atoms of the ligand and the cadmium atoms on the nanoparticle surfaces.[9] Later on, epitaxial growth of a wider band-gap materials such as CdS on CdSe core was demonstrated as a preferred method to improve the QY (to 50%) of the QDs.[10] This surface coverage was effective in reduction of non-radiative electron-hole recombination by elimination of the surface defects and confinement of the exciton. Surfactants used as the coating material around the semiconductor core were also influential in surface passivization to enhance luminescence.

An alternative system, Octadecene/Oleic acid, was also successfully adopted for the preparation of CdSe QDs.[11] Effect of the reaction temperature and concentration on the nucleation and crystal growth were studied in detail. It was shown that capping agents not

only affected the rate of growth but also made a great contribution in determining the number and the size of the nuclei. In another study using the same system, it was claimed that the ligand concentration changed the growth mechanism and different sized QDs could be obtained. Moreover, Octadecene/Oleic acid system was reported as a simpler, safer and economical alternative to TOPO method.[12]

Despite the fact that the organic methods give rise to highly luminescent particles of different colors, transfer of QDs to water is necessary for many biological applications. Ligand exchange of TOPO with water soluble molecules and bilayer formation are proven methods to provide aqueous suspension of QDs.[13-15] On the other hand, they suffer from drawbacks such as dramatic reduction in the QY, colloidal stability or increase in overall hydrodynamic size. It was shown that the CdS-QDs produced in organic media had very weak luminescence after being extracted into water with carboxylic acid containing ligands.[16]

The aqueous route for QD production is more challenging than the organic route. Yet, it is desired to prepare QDs in controlled size, in narrow size-distribution with high QY and colloidal stability utilizing aqueous synthetic routes. Molecules with thiol (–SH) groups were proven to be effective coatings for CdS and CdSe. In aqueous systems, bifunctional molecules were desired where the thiols adsorb on the crystal surface and the other functional groups provide a favorable interaction with the solvent to suspend the particles. Few examples are thioacetamide [17], cysteine [18], mercaptoethanol [19], mercaptopropionic acid [19, 20] and mercaptopropyl-trimethoxysilane.[21] Investigations were mainly concentrated on the types of surfactant and precursors, addition sequence of the reagents, duration of the reaction and reaction parameters such as concentration and pH. Korgel et al reported a detailed study on mercaptoacetic acid (MAA) coated CdS nanoparticles prepared in water and discussed the influence of pH and coating amount on

the size and QY of CdS.[22] Preparation of the QDs was also carried out in microemulsion suspensions.[23-25]

Colloidal QDs are free floating and can be attached to a variety of molecules via metal coordinating functional groups, such as those mentioned above. These groups include but are not limited to thiol, amine, nitrile, phosphine, phosphine oxide, phosphonic acid, carboxylic acid or others. By bonding appropriate molecules to the surface, QDs can be dispersed in nearly any solvent or incorporated into a variety of inorganic and organic films.

1.6 Superparamagnetism

Superparamagnetism is a type of paramagnetism where the material is paramagnetic even below the *Curie temperature (T_c)*. In order to explain the superparamagnetic behavior, other type of magnetism such as ferromagnetism, paramagnetism and diamagnetism should be discussed. In **ferromagnetism**, magnetic moments of the atoms in the material are aligned within the domains, but the material has no net magnetic dipole as the net direction of each domain is random. Placement of this type of materials in a weak external magnetic field causes alignment of the spins of different domains, creating net magnetization which remains for a long time even after the removal of the magnetic field. Above the T_c, the thermal motion of the atoms is so strong that the electrons in bonds are no longer able to keep the dipole moments aligned and the long range order of the spins is lost. The other type of magnetism called "**diamagnetism**" occurs in a material whose atoms have no permanent dipole moment. When diamagnetic materials are placed in a strong magnetic field, an atomic dipole moment appears directed opposite to the direction of the magnetic field caused by the change of the force acting onto the orbiting electrons. Magnetic susceptibility (amount of magnetization in an applied magnetic field) of diamagnetic materials is negative, but it is quite small in magnitude, the order of 10^{-5} and10^{-4}.

Magnetic levitation is an outcome of diamagnetism. Unpaired electron of an orbital in a material is the main source of **paramagnetism**. Magnetic dipoles created by the presence of unpaired electrons are normally randomly oriented in a paramagnetic material. If a magnetic field is applied to such a material, dipole moments line up in the direction of the external field, creating a net magnetization. So, the magnetic susceptibility of such materials are positive, and are usually in the range 10^{-5} and10^{-3}. A paramagnetic material shows magnetic behavior in the strong magnetic field like ferromagnetic materials, and it attracts and repels other magnets. However, unlike ferromagnetism, magnetization disappears when the external field is removed.

Superparamagnetism emerges when a paramagnetic material is confined into small scale (1-10 nm). Nanocrystals below 10 nm size are usually single crystals in which no separate magnetic domains exist. So, the entire crystallite responds to the external field. Elimination of magnetic domains enhances the net magnetization since these domains usually do not perfectly align with the external magnetic field. Therefore, superparamagnetic nanoparticles show higher magnetization than paramagnetic materials. At this small scale, energy required to change the direction of the magnetic moment of a particle is comparable to the ambient thermal energy. In superparamagnetism, even at the temperatures below the T_C, the thermal energy is sufficient to cause fluctuation of the dipoles and no net magnetization occurs. This behavior is size dependent. The energy required to disturb the alignment of magnetic dipoles depends on the size, and the corresponding temperature decreases with the decreasing crystal size.

1.7 Superparamagnetic iron oxides

SPIOs are usually in the forms of magnetite (Fe_3O_4) or maghemite (γ-Fe_2O_3). Oxidation of synthesized SPIO converts Fe_3O_4 to γ-Fe_2O_3. This results in a change of the material appearance from a black-brown to a red-brown as Fe^{2+} in the magnetite lattice oxidizes. It

is important to note that these two iron oxide structures possess similar magnetic properties, but maghemite has a slightly lower saturation magnetization. The mean core diameter of SPIO is usually between 4-10 nm.

Ferrofluids are the most well-known examples of SPIOs which are dispersed in a carrier solvent (polar or non polar). Ferrofluids are utilized in a variety of interesting applications including damping in audiospeakers, magnetic separation, cell sorting and sensing as well as a tremendous presence in the biotechnology and medicine. (Figure 1.6) Current use in MRI as a contrast agent and potential for drug delivery, hyperthermia, and magnetic transfection increased the importance of small and stable aqueous colloidal SPIOs. Aqueous SPIOs are usually provided by coating the magnetic cores with a suitable hydrophilic surfactant such as dextran, poly(vinyl alcohol), poly(ethylene glycol), polyacrylic acid, etc.[26-29] Although, the size of the magnetic crystalline core is important for the magnetic properties, overall hydrodynamic size and the size of the aggregates that might be formed are important for the applications. For the magnetic separation or magnetic dragging, relatively large hydrodynamic sizes (in the order of few hundred nm to microns) are beneficial since a reasonable magnetic field can be applied to drag and fix the magnetic nanoparticles at target (Figure 1.6b). Yet, for biomedical applications, especially in-vivo applications, smaller sizes (200 nm and below) are required. Recent advancements in the medical imaging and therapy indicates that ultrasmall size of less than 50 nm is desired to achieve special tasks such as molecular targeting (Figure 1.6d).

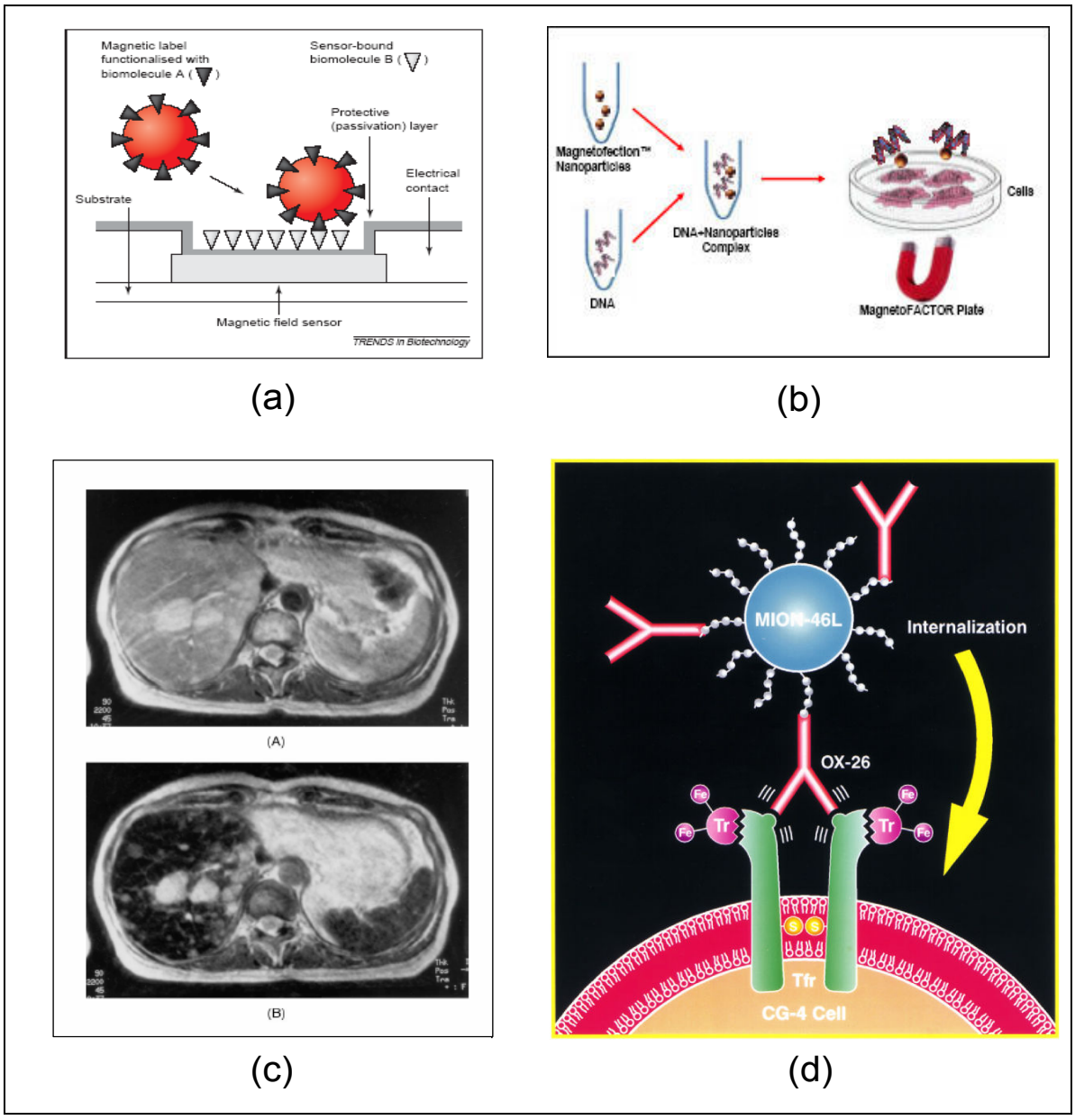

Figure 1.6 (a) Schematic fort magnetically labeled biomolecule detection in biosensor.[30] (b) Method of magnetofection: the transfection of cells with with DNA (magnethttp://www.chemicell.com) (c) Cancer imaging with MRI. A, before and B, after contrast introduction. T2-weighted SE image shows two metastases and many small ones in the right liver lobe.[31] (d) Internalization of an antitransferrin receptor with MAB-SPIO construct.[32]

1.8 Quantum dot / superparamagnetic iron oxide hybrid nanocomposites

Recently, hybrid nanoparticles are emerging as novel multifunctional entities. Development of composite nanoparticles of luminescent QDs and magnetic nanoparticles (MNPs) offers a tremendous opportunity to create multifunctional single entities addressable by a magnetic field and detectable optically and magnetically at the same time. QDs with narrow emission bands at specific wavelengths (particle size) act as luminescent markers while magnetic nanoparticles allow manipulation by an external magnetic field and/or a second sensing mechanism based on magnetization. MQDs have an enormous potential in the medical imaging, immunoassays, transfection, sensor, multiplexed arrays, nanobarcode technologies and many more where optical and magnetic detection as well as magnetic dragging have been individually utilized. A few reports on magnetic microbeads labeled with fluorescent compounds for diagnostic and magnetic detection/separation appeared in the literature. An example of a magnetic separation of breast cancer cells with fluorescent/magnetic nanoparticles is presented in Figure 1.7. The antibodies labeled with luminescent/magnetic nanoparticles were separated easily from the solution by using a magnet.

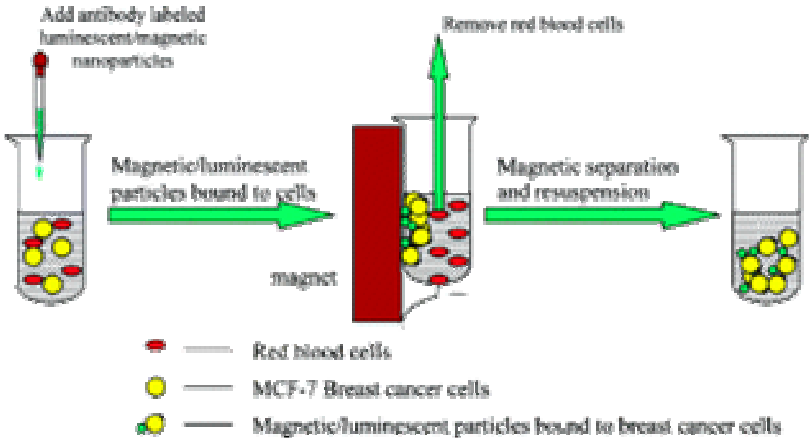

Figure 1.7 Magnetic separation of cancer cells bound to magnetic/luminescent particles [33]

The synthesis of QD-MNP nanocomposite carried out by Rosenzweig et al was consisted of polymer coated γ-Fe_2O_3 superparamagnetic cores and CdSe/ZnS QDs shell.[34] A single layer of QDs was bound to the surface of thiol-modified magnetic beads through the formation of thiol-metal bonds to form luminescent/magnetic nanocomposite particles. Their average diameter was 30 nm with a size variation of ±15% determined by TEM. A 3-fold decrease in the QY of the nanocomposites and a slight blue shift in their emission peaks compared to the individual luminescent QDs were observed. Incompatibility between the surface polarities of the two particles makes the fabrication of composite particle difficult, causing aggregation. The luminescent/magnetic nanoparticles were easily separated from the solution by magnetic decantation using a permanent magnet. To demonstrate their utility they immobilized anticycline E antibodies on their surface and used the antibody coated particles to separate MCF-7 breast cancer cells from serum solutions. The separated breast cells were easily identified by fluorescence microscopy due to the strong luminescence of the nanocomposites. Li et al expanded this strategy to deposition of QDs on MNPs in a layer-by-layer assembly.[35] Dubertret et al developed a QD-MNP using commercially available γ-Fe_2O_3 nanoparticles (around 10 nm in diameter) and 3 nm CdSe/ZnS/TOPO QDs in an oil/water emulsion using octane and oleic acid (OA).[36] It is important to note that particles are just mixed not conjugated with each other. They have pointed out an important problem: As the concentration of the MNP increased, fluorescence decreased due to the strong absorption of MNP at the fluorescence wavelength of the QDs.

Use of silica as an encapsulant is another demonstrated strategy. Hyeon et al showed that the hybridized particles can be stacked in mesoporous SiO_2 and fluorescent magnetic beads can be obtained with an average particle size of 150 nm.[37] These hybrid nanoparticles were demonstrated as effective drug carriers when ibuprofen (nonsteroidal anti-inflammatory agent) was loaded into the mesoporuos silica spheres. A relatively fast

preparation method for silica coated Magnetic Florescent beads was claimed in inverse sol-gel technique.[38] Spherical, transparent beads that are able to encapsulate bio and fluorescent substances could be achieved. In another study, incorporation of QDs and fluorescent dyes into magnetic beads were performed by Whitman et al.[39] They described a method to modify polystyrene based magnetic microbeads to give uniform fluorescence without affecting the magnetic or surface chemical properties.

All these methods use the preformed MNPs and QDs and focused on the methods of combining the two in the most effective way.

1.9 Purpose of the research and objectives

The main objective of this research is to develop an efficient method for the preparation of superparamagnetic QDs, or in another word fluorescent SPIOs, which we will refer as MQDs in water (Figure 1.8). MQDs with different sizes and colors would offer tremendous advantages especially if differently sized particles can be engineered to emit different colors. These MQDs would impact the research in areas where dual sensitivity, multiplexing, sensing and magnetic separation are required. If successful, having the ability to excite different colors with a single source could allow multiplexing in sensors, imaging, immunoassays, bioseparation where each color detect a different analyte in a single sample allowing multi-analyte detection simultaneously. Control of the size, color, QY and stability are crucial. Small sized MQDs would impact the in vivo imaging tremendously where dual imaging (MRI and optical), magnetic delivery with external magnetic field as well as molecular targeting can be achieved.

Our approach in preparing such MQDs involves a novel one pot route where NPs are coated with functional surfactants capable of stabilizing both types of NPs. Yet, in order to achieve such goal, first highly efficient QDs need to be prepared as aqueous colloidal systems in order to eliminate the problems encountered in the previous literature (as

detailed in previous sections) originating from the incompatibility of NP mediums or due to the transfer of NPs from organic to aqueous medium.

In the majority of this thesis work, development of highly luminescent QDs in aqueous media is discussed. As CdS emit in the visible region, it was chosen as the target QD for this work. In order to synthesize the MNP-QD hybrid system poly(acrylic acid) (PAA) and mercaptoacetic acid (MAA) were used as surfactants. PAA is a biocompatible polymer with multiple functional groups (carboxylic acid) to adsorb on the crystal surface and also provide steric and electrostatic stabilization. In our group, Miray Demirer, studied PAA coated SPIOs and demonstrated that small and ultrasmall sized SPIOs with long term stability can be achieved.[40] MAA is very effective in CdS surface passivization. Based on this approach, we first investigated the synthesis and properties of MAA and PAA coated CdS, PAA and MAA binary coated CdS for achieving highly stable and luminescent NPs. In the last phase of this research, PAA/MAA coated CdS colloidal solution is used to prepare SPIOs which would lead the way to a practical one pot synthesis.

Figure 1.8 Schematic of magnetic nanoparticles labeled in different QD colors.

Chapter 2

SYNTHESIS AND CHARACTERIZATION OF POLY(ACRYLIC ACID) STABILIZED CDS QDs

2.1 Introduction

Semiconductor QDs have been the subject of extensive research due to their unique size-dependent optical properties and widespread applications in science and technology. Quantum confinement of excitons at crystal sizes comparable to or below the exciton Bohr radius creates size-tunable narrow bandwidth photoluminescence.[2] As the size of the semiconductor crystal decreases, the band gap between the conduction and the valence bands increases.[3] This results in a size-dependent absorption onset and emission wavelength, both becoming blue-shifted with decreasing particle size.[4] Therefore, the color output can be tuned by varying the size and the nature of the QD. Group II-VI semiconductor nanocrystals, such as CdS, CdSe, and CdTe have been studied widely as they emit in the visible region.[41, 42] There is a tremendous effort to improve and control QDs which enable innovations in a broad spectrum of areas including solar cells, light emitting diodes (LEDs), sensors, lasers, medical imaging, and biological labeling.[43-47] Long term photostability, high quantum yield (QY) and narrow spectral band width make QDs excellent fluorescent tags with better sensitivity compared to organic fluorescent molecules. Possibility to excite various size QDs simultaneously with a single excitation

wavelength, provided opportunity for color multiplexing which is revolutionary in barcoding and labeling.[43, 48]

Since the unique properties of QDs are based on size, controlling size and size distribution as well as crystallinity and surface defects is crucial. NPs are usually prepared as core-shell structures, in which an organic shell is adsorbed on the crystal surface to control the particle growth through surface passivization (arrested).[49] Organic shell is also responsible for the dispersion of particles in a carrier solvent, prevention of aggregation and colloidal stability. Effective surface passivization is also crucial for the optical properties such as photobleaching and QY. Surface defects usually cause radiationless recombination of the excitons which limits QY.[50]

Best quality QDs are generally provided by the high temperature synthesis using the stringent Schlenk techniques from toxic organometallic precursors with hydrophobic coatings such as TOPO.[5] However, for many biological applications, transfer of QDs to water is necessary. Ligand exchange of TOPO with water soluble molecules and bilayer formation are proven methods to provide aqueous suspensions of QDs.[13-15] However, they usually suffer from drawbacks such as dramatic reduction in the QY, colloidal stability or increase in the overall hydrodynamic size. Therefore, preparation of particles directly in aqueous solutions is a very practical approach and, usually, a milder, greener synthetic route. Yet, it is a challenge to prepare QDs in desired sizes and narrow size-distribution with high QY and colloidal stability with the aqueous synthetic routes. Molecules with thiol (–SH) groups are proven to be effective coatings for CdS and CdSe. In aqueous systems, bifunctional molecules are desired where the thiols adsorb on the crystal surface and the other functional groups provide a favorable interaction with the solvent to suspend particles. Few examples are thioacetamide [17], cysteine [18], mercaptoethanol [19], mercaptopropionic acid [19, 20] and mercaptopropyl trimethoxysilane.[21] Korgel et al. reported a detailed study on mercaptoacetic acid (MAA)-coated CdS QDs prepared in water, and discussed the influence of pH and coating amount on the size and luminescence.[22] In MAA-CdS, thiolates bind competitively to the

surface cations. Although QYs were not reported, maximum PL intensity was reported to be achieved at pH range of 6-8 at MAA/Cd ratio of 11-20. The ligand concentration does not have a significant effect on the absorption wavelength or the PL peak position of the MAA-CdS particles. However, both of these have a red shift with increasing pH of the solution before Na_2S addition. Such behavior was attributed to HS^- mediated crystal growth and the thiol complexes formed between the ligand and Cd^{2+} ions. They also suggest that many times, the changes in the size and luminescence is not due to the ligand concentration but the related change in pH.

We are interested in the preparation of PAA-CdS in a low temperature aqueous process. Polymeric coatings are effective on providing steric stabilization for colloidal nanoparticles. PAA, a polyelectrolyte, would also provide electrostatic stabilization. In addition, each polymer chain provides multiple adsorption sites and the coated particles would have free carboxylate groups available for further functionalization.

There are few reports on the templated synthesis of CdS in PS-b-PAA block-copolymer micelles with a focus on the ionic core size and the aggregation number. These particles had a hydrophobic PS shell, and all QDs were prepared in the PAA core.[51, 52] Eisenberg expanded this system to PEO-b-PS-b-PAA triblock polymers to create different morphologies such as multicore and warm like micelles.[53] Zhang, reported an example of PAA(1000 g/mole)-coated CdS nanoparticles to prepare polyaniline wires through complex formation but did not focus on PAA-CdS system itself or its optical properties.[54]

To the best of our knowledge, this is the first report in the literature investigating the influence of PAA molecular weight and amount on particle properties such as crystal size, photoluminescence (PL) emission intensity, QY and colloidal stability of aqueous CdS-PAA-QDs. PAA with 2100 and 5100 g/mol molecular weights were used as coatings. We also investigated the influence of reaction pH on the size and optical properties. CdS QDs were prepared at a pH of 7.5 with varying amounts of PAA at both molecular weights. In a different set of reactions, QDs were prepared at pH 5.5 using PAA 2100 g/mol. Effect of

the Cd/S ratio on particle properties was also studied. Influence of the variables on size and optical properties was determined through absorption (UV-Vis range) and photoluminescence analysis.

2.2 Experimental section

2.2.1 Materials

All chemicals were analytical grade or of the highest purity available. Sodium sulfide trihydrate ($Na_2S{\cdot}3H_2O$), mercaptoacetic acid ($HSCH_2COOH$), cadmium nitrate tetrahydrate ($Cd(NO_3)_2{\cdot}4H_2O$), Rhodamine B and HNO_3 (65 %) were purchased from Merck. Sodium hydroxide and PAA sodium salts (PAA2K: 2100 g/mol and PAA5K: 5100 g/mol) were purchased from Aldrich. Only double distilled Milli-Q water (Millipore) was used as the solvent.

2.2.2 Synthesis of CdS stabilized with PAA

In a typical synthesis, 64.3 mg of $Cd(NO_3)_2{\cdot}4H_2O$ was dissolved in 100 ml water and transferred into a 500 ml, three-necked round-bottomed flask fitted with a mechanical stirrer. Appropriate amount of PAA (Mw = 2100 g/mol) was dissolved in 150 ml water, added to Cd solution and deoxygenated with nitrogen for ten minutes. For reactions run at pH 7.5, pH was adjusted with 10 M NaOH and/or 10 M HNO_3. Sulfide solution was prepared by dissolving 25 mg $Na_2S{\cdot}3H_2O$ in 50 ml of water and injected into the reaction mixture. Reaction was kept stirring at room temperature under nitrogen for an hour. pH usually increases by 0.5-1.0 units after Na_2S addition and the reaction ends around pH 8.0-8.5. No further pH adjustment was done before UV-Vis or PL measurements. Appropriate amount of PAA was calculated based on the desired COOH/Cd ratio. All ratios are listed in Table 2.1.

2.2.3 Instrumentation

FTIR spectra were recorded on Jasco FT-IR-600 spectrometer. Absorption spectra were recorded with a Schimadzu UV-Vis-NIR spectrophotometer model 3101 PC in the 300-600 nm range. Absorption of samples at the excitation wavelength was kept in the 15 % range

by diluting the samples with water. Size of the CdS nanoparticles was calculated by using Brus Equation [3] given in Appendix A (equation A-2.1). For the evaluation of photoluminescence and calculation of quantum efficiencies, samples were excited at the wavelength of 355 nm. The luminescence measurements were carried out in Koc University Laser Research Lab.[55] The XPS measurements were performed on a VG Ionex system equipped with a Clam II analyzer and a mono-chromatic Al K_α X-ray source ($h\gamma$ =1486.6 eV) at the Eindhoven University of Technology. The photoelectron take-off angle was 90° with respect to the sample surface. Sampling depth is in the range of 10nm, depending on the kinetic energy of the ejected electrons. Excess coating was removed by dialysis before the analysis. X-ray diffraction analysis was performed by using HUBER G670 diffractometer with a germanium monochromator and CuKα radiation (λ = 1.5406 Å). Data collection was done in the range of $5^o<2\theta<100^o$ with 0.005º increments. Data were analyzed by using STOE WinXPOW software. Excess coating was removed by the precipitation of QDs in isopropanol before the XRD measurements.

Table 2.1. Average size and band gap of CdS nanoparticles calculated from UV–vis spectrum

Sample ID	COOH / Cd	Cd / S	Absorption cutoff (λ)	Size (nm)	Band gap (eV)	FWHM (nm)
PAA 2K-1a	1.0	1.1	460	3.6	2.70	181.5
PAA 2K-2a	**1.6**	**1.1**	**464**	**3.7**	**2.68**	**161.0**
PAA 2K-3a	2.1	1.1	486	4.5	2.55	176.5
PAA 2K-4a	2.5	1.1	488	4.6	2.54	179.5
PAA 2K-5a	3.3	1.1	492	4.9	2.52	177.0
PAA 2K-6a	11.2	1.1	459	3.6	2.71	153.0
PAA 2K-1b	0.8	1.1	490	4.8	2.53	189.5
PAA 2K-2b	**1.5**	**1.1**	**487**	**4.6**	**2.55**	**163.5**
PAA 2K-3b	2.0	1.1	477	4.1	2.60	165.5
PAA 2K-4b	3.0	1.1	477	4.1	2.60	182.5
PAA 2K-5b	5.0	1.1	484	4.4	2.57	193.5
PAA 2K-6b	8.1	1.1	488	4.6	2.54	173.0
PAA 2K-7b	11.2	1.1	490	4.8	2.53	196.5
PAA 2K-8b	13.1	1.1	489	4.7	2.54	201.5
PAA 5K-1	**1.6**	**1.1**	**463**	**3.7**	**2.68**	**161.0**
PAA 5K-2	2.5	1.1	476	4.1	2.61	160.5
PAA 5K-3	5.0	1.1	508	6.5	2.44	143.0
PAA 5K-4	12.5	1.1	506	6.2	2.45	133.5
PAA 5K-5	1.6	2.5	470	3.9	2.64	164.5
PAA 5K-6	1.6	0.6	490	4.8	2.53	152.5

2.3 Results and discussions

2.3.1 Synthesis and characterization of CdS-PAA.

CdS nanocrystals coated with PAA have been successfully prepared at room temperature in water from non-toxic precursors. PAA/Cd^{2+} ratio was varied at each formulation based on the mole ratio of carboxylic acid to Cd^{2+} (reported as COOH/Cd for simplicity) since two different molecular weights (2100 and 5100 g/mole) of PAA were studied. Carboxylates can chemically adsorb on the crystal and passivate the surface, controlling crystal growth and minimizing the surface defects.[51, 52] Unbound carboxylate groups provide electrostatic stabilization to the aqueous CdS colloidal system. CdS with COOH/Cd ratio of 0.8 precipitated right after the reaction and ratio of 1.0 started to flocculate after 10 days. All other samples showed excellent colloidal stability over a period of more than eight months so far.

FTIR spectrum of the PAA-coated CdS NPs (Figure 2.1) shows a characteristic C=O stretching peak for carboxylic acid at 1710 cm^{-1}. Peaks at 1565 and 1410 cm^{-1} correspond to antisymmetric and symmetric stretching modes of carboxylate (COO^-) which are generally used to determine the binding mode of carboxylates to a surface or to a cation. A monodentate binding (from one oxygen) is usually associated with the existence of both symmetric and antisymmetric stretching modes.[56] However, since only a part of the functional groups adsorbs on the CdS, it would not be possible to provide a full interpretation here. Peaks at 1455 and 1280 cm^{-1} are CH_2 bending and wagging modes of PAA backbone. The very weak peak observed around 406 cm^{-1} was attributed to the Cd-S bond.[54]

XRD analysis of CdS (PAA 2100 g/mol) shows broad peaks that are normal for nanocrystals. Two theta peaks at 26.5º, 30.7º, 44.0º, 52.1º, 70.5º, 72.6º, 80.8º are consistent with the cubic crystal structure (a = 5.82 nm) of CdS (Figure 2.2). Calculated size according to the Debye-Scherrer formula [57] is 3.8 nm which is little lower than the size

calculated from UV-Vis spectrum (4.6 nm) (Table 2.1). Broad peaks at such small sizes make size calculations difficult.

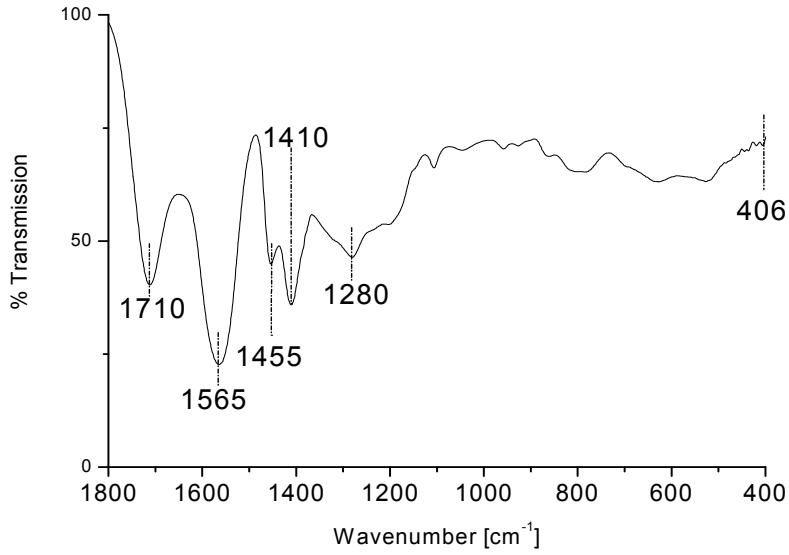

Figure 2.1. IR spectra of PAA2K-6a coated CdS.

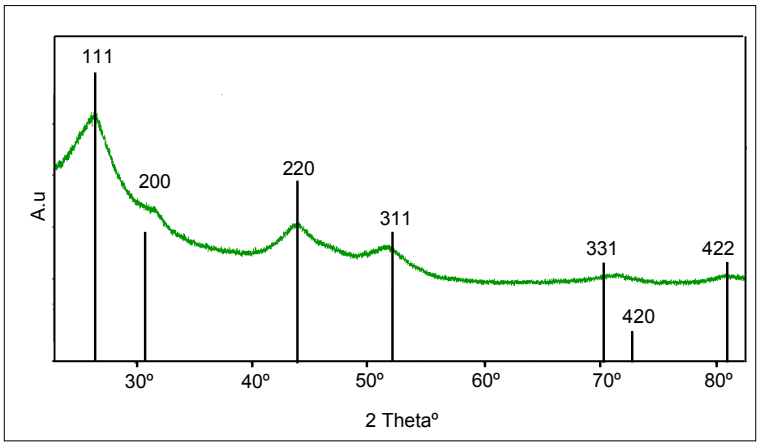

Figure 2.2 X-Ray powder diagram of PAA 2K-2b.

XPS analysis provided information about the existence of Cd, S, C and O elements constituting the CdS core and the coating adsorbed on its surface (Figure 2.3a). Peaks at 405.6 eV and 162.2 eV correspond to the binding energies (BEs) of Cd $3d_{5/2}$ and S $2p_{3/2}$ consistent with the reported values for CdS (Figure 2.3b and c).[58] Integration of the peak areas after background subtraction and correction for atomic sensitivity factors provides information about the relative amounts of the elements. Calculated Cd/S ratio of 0.997 is consistent with the theoretical ratio of 1. There are two overlapping O 1s peaks at 532.4 and 535.4 eV, usually assigned to the carbonyl and the hydroxyl oxygen of the carboxylic acids, respectively (Figure 2.3d).[59] Ratio of the two is 0.994 close to theoretical ratio of 1:1. The two overlapping peaks for C 1s at 285.4-288.3 eV are in agreement with the reported binding energies for the aliphatic (backbone CH_2) and the COOH carbon, respectively (Figure 2.3e).[60] Ratio of the low and the high BE peaks of C 1s is 2.33, little over the theoretical 2:1 ratio for PAA. Little higher amount of C might be due to the atmospheric contaminants. This also results in C/O ratio of 2.1 which is also slightly higher than the theoretical value of 1.5.

In the UV-Vis absorption spectra of the NPs (Figure 2.4), a blue shift (shorter wavelength) of the absorption onset was observed in comparison with bulk (2.41 eV) as a result of quantum confinement.[61] The sizes of the CdS nanocrystals were determined from the absorption onset wavelengths by using the Brus equation (see Eq. 1) based on the effective-mass approximation (Table 2.1). The absence of strong excitonic peaks on the absorbance spectra was attributed to the strong Coulomb screening and/or broad size distributions of the NPs.[62, 63] All samples emit around yellow-orange when excited with UV lamp at 365 nm but they differ in the color intensity. In order to compare the luminescence efficiencies of the samples, the emission spectra were calibrated with respect to absorption at 355 nm, and with respect to the emission strength of Rhodamine B where samples were excited. Calibrated emission spectra are shown in Figure 2.5. Note that the sharp peak is due to the stray 532-nm light that could not be completely filtered. The second peak near 404 nm is the Raman emission of water due to 355-nm excitation. The

emission spectra of all samples are broad band emissions, indicating broad particle size distribution (Figure 2.5 and Table 2.1).[64] Peak widths are larger than MAA-CdS system.[22]

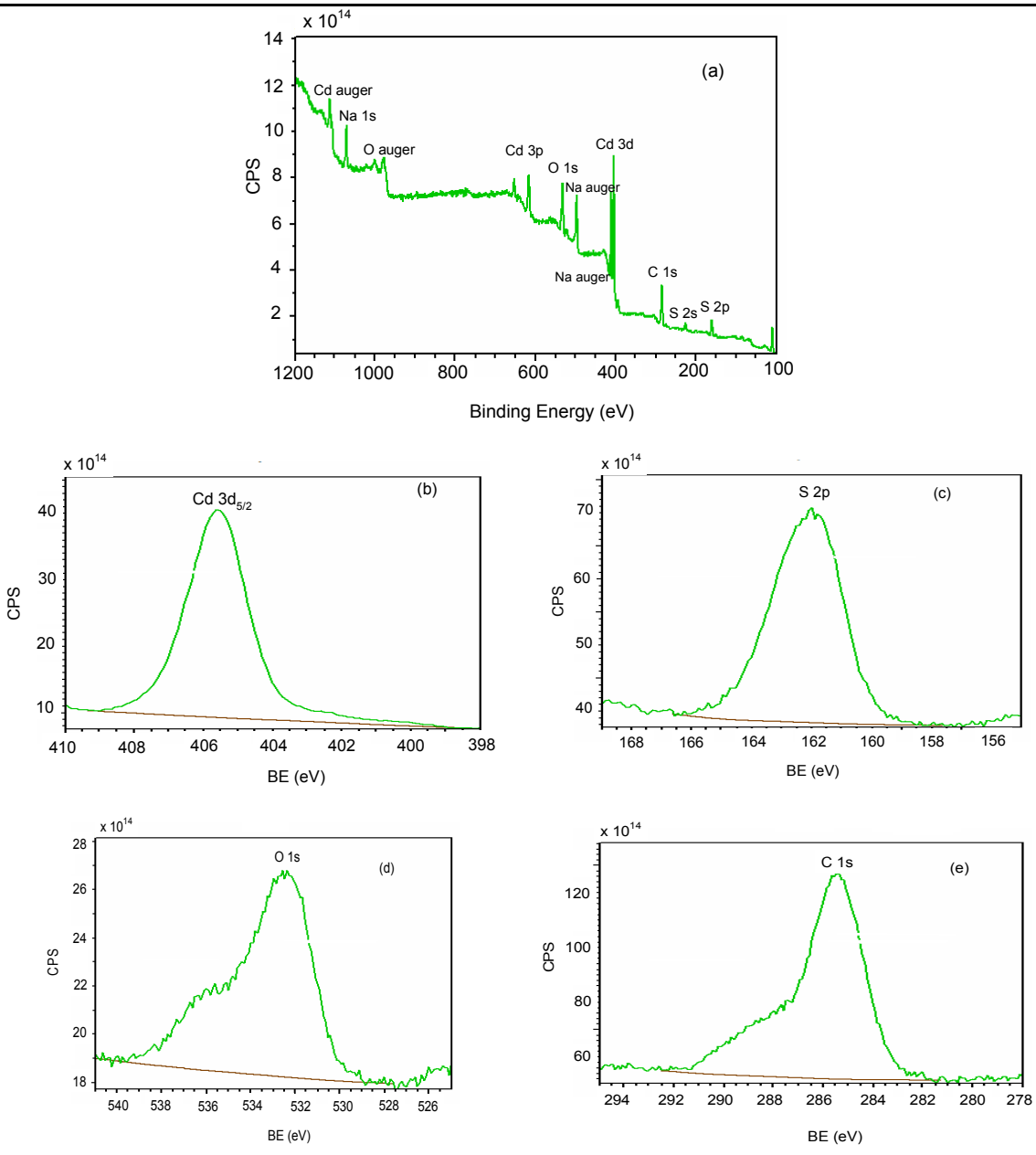

Figure 2.3 XPS spectra of the (a) PAA 2K-2b; (b) Cd 3d (c) S 2p (d) O 1s (e) C 1s.

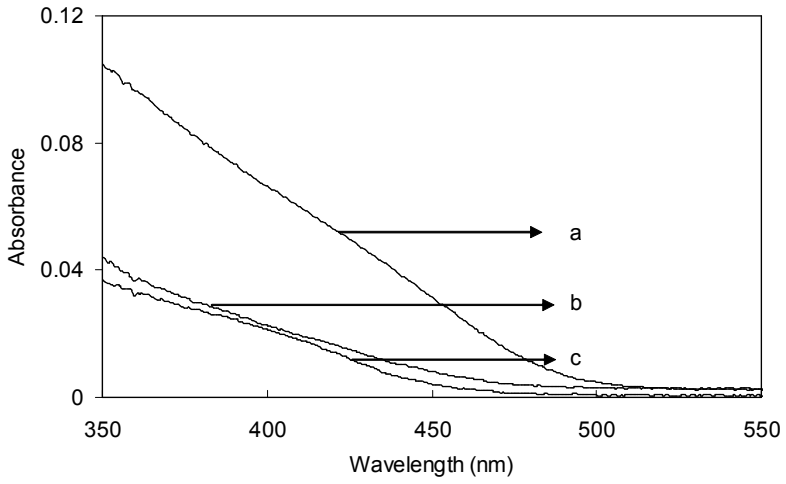

Figure 2.4 Absorption spectra of CdS nanoparticles coated with a COOH / Cd = 1.6 (a) PAA2K at pH=5.5 and (b) PAA5K at pH 7.5 (c) PAA2K at pH=7.5.

2.3.2 Cd/S ratio

Cd/S ratio has been reported to be important for the size and properties of QDs coated with thiolated species.[22] Crystal sizes of 4.8, 3.7, and 3.9 nm were obtained at the Cd/S ratio of 0.6, 1.1 and 2.5, respectively, with PAA5K coating (Table 2.1). Major difference occurs when S^{2-} amount exceeds Cd^{2+}. Surface passivization depends on the interaction of the carboxylates with the surface atoms. A strong adsorption of the coating on the crystal surface retards growth at that site. Carboxylates would not bind to anionic sulfur atoms on the crystal surface, eliminating an efficient surface capping and the desired arrested growth.

PL maximum is red shifted by 110 nm, in agreement with larger crystal size, when Cd/S ratio was reduced to 0.6 (Figure 2.5a). PL intensity was affected by the Cd/S ratio as well. At the compositions where Cd^{2+} is in excess (Cd/S=1.1 and 2.5), PL intensities were comparable, but showed a 3-fold decrease at the Cd/S ratio of 0.6.

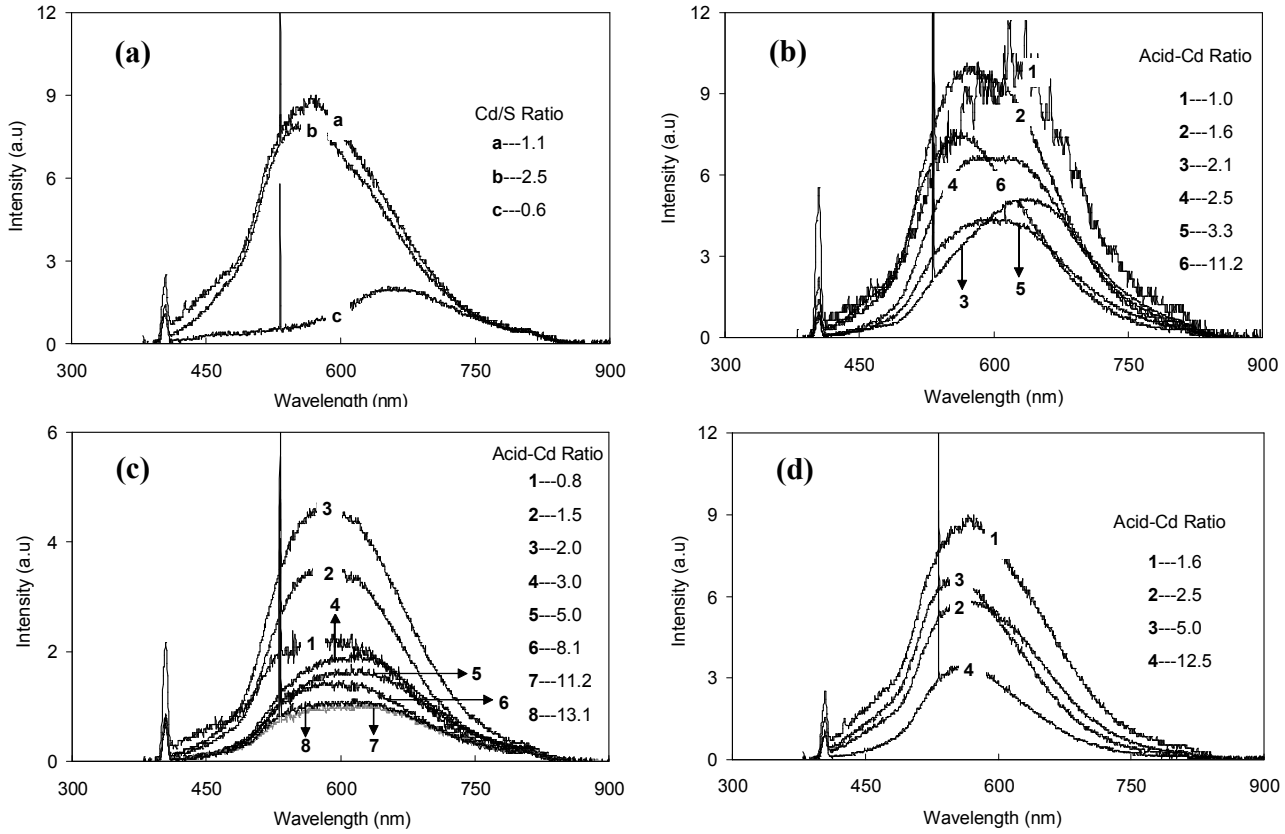

Figure 2.5 (a) Calibrated PL spectra of PAA5K coated CdS with varying Cd/S ratio. Reaction pH=7.5 and COOH/Cd=1.6. (b) Calibrated PL spectra of PAA2K coated CdS prepared at pH=7.5. (c) Calibrated PL spectra of PAA2K coated CdS prepared at pH=5.5. (d) Calibrated PL spectra of PAA5K coated CdS prepared at pH=7.5

Similar results were also obtained for MAA stabilized CdS nanocrystals.[22] However, in that system there was a about a 4-fold increase in PL intensity going from Cd/S ratio of 1 to 2. Improved luminescence with the use of excess Cd^{2+} supports the discussion of ineffective coating of sulfur-rich crystal surface with the negatively charged carboxylate groups, creating dangling bonds on the surface acting as surface traps. It has also been reported that S^{2-} vacancies can act as deep traps for photogenerated electrons in the

conduction band, resulting in the red luminescence of CdS through transfer to surface molecules or to a preexisting trapped hole.[65]

Therefore, Cd/S ratio was fixed at 1.1 for the reactions designed to study the influence of polymer amount, polymer molecular weight, and reaction pH.

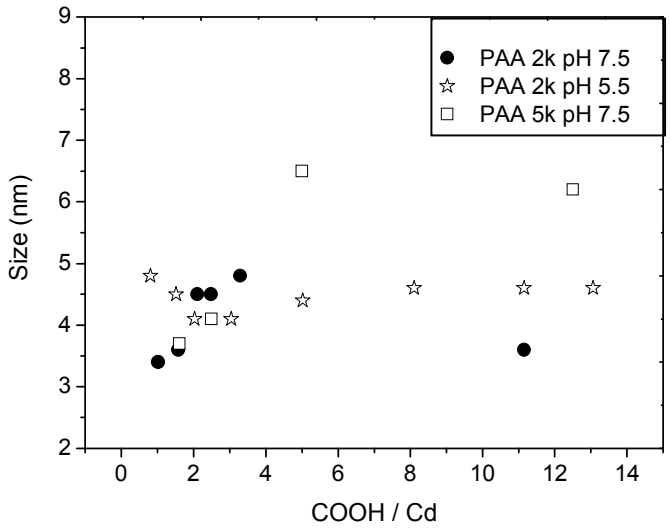

Figure 2.6 Size dependence of CdS dependence wrt COOH / Cd ratio, molecular weight and starting solution pH at fixed Cd/S.

2.3.3 PAA amount and molecular weight

The crystal size increases slightly with increasing amount of polymer (increasing COOH/Cd ratio from 1-12.5) at pH 7.5 (Figure 2.6) from 3.6 to 4.9 nm for PAA2K and from 3.7 to 6.5 nm for PAA5K (Table 2.1). It is important to note that crystal sizes are close to each other around a critical COOH/Cd ratio of 1.5-2 for both PAA molecular weights. Above this ratio, increasing the amount of polymer increases the crystal size at pH 7.5. Along with this, emission spectra showed maximum PL intensity around COOH/Cd = 1.5-2 as well (Figure 2.5). This should correspond to a ratio where critical amount of

surface cations are bound to the carboxylates, creating a relatively defect-free surface. Further increase in the coating amount causes a decrease in PL intensity. This is quite interesting since increasing the amount of surface capping agent is generally expected to decrease the crystal size and ensure full surface coverage, decreasing non-radiative coupling. However, PAA may behave differently than a monomeric carboxylate. The observed trend here points out ineffective or incomplete surface capping with increasing coating amount. A combination of factors such as particle bridging, extended polymer conformation, high charge density, and repulsion of the neighboring carboxylates that would adsorb on the particle surface could play a role in such a trend. These factors would be imposing more dramatic effects especially at higher COOH/Cd ratios and high molecular weights. Above the mentioned critical COOH/Cd ratio, PAA5K-coated NPs have larger crystal size (Figure 2.6) and lower PL intensity than PAA2K-coated ones (Figure 2.5-b, d). Decreasing PL intensity with increasing coating amount have been reported with mercaptoacetic acid [22] and cysteine [18] coated CdS QDs recently, but these systems contain thiols as surface binding moiety and the behavior, although not known exactly, was attributed to the competitive binding of Cd^{2+} to S^{2-} versus RS^- or the resulting change in pH. In our study, all reactions were performed at a fixed pH. Besides, affinity of Cd^{2+} to thiol is much higher than to carboxylate. PAA forms complexes with the free Cd^{2+} in the solution and the particle surface during growth. Dynamic adsorption allows the crystal to grow through deposition of ions on the surface in a mechanism similar to ligand exchange and is known as cluster-cluster aggregation.[66] Since smallest crystal sizes are obtained at around COOH/Cd ratio of 1.5-2, best balance of surface and cation complexation should be achieved at this ratio. In his studies, Moffit focused on the synthesis of CdS in micelles of PAA/PS core/shell structures and emphasized the importance of kinetic control on particle size.[67] He suggests that the size of the CdS formed within micelles depends on the size of the ionic core and is limited by the viscosity that slows diffusion. In our case, there is no micelle but PAA-Cd^{2+} complexes might be considered as polymeric networks or clusters where many Cd^{2+} ions can form a complex with a single chain or where Cd^{2+} can form complex with two different chains. Charge

neutralization collapses the polymer to some extent, which would prefer rather extended conformation otherwise due to charge repulsion. Growth will be influenced by the diffusion rate of the ions and clusters in such network limiting the ability to tune particle size. This may also explain why blue or red luminescent particles could not be achieved with PAA in our work. At a fixed COOH/Cd ratio, less amount of PAA5K is used in comparison to PAA2K, so the number of coating molecules decreases. As the size of the polymer chain increases, not only does the possibility of binding multiple Cd^{2+} increase, but also bridging between primary particles is enhanced. This would increase the cluster-cluster collisions as well, enhancing growth. In addition, longer chains and the repulsion between the repeat units prevent effective passivization of the surface which allows growth through deposition of ions on the surface. Such a decrease in the surface passivization also leads to the observed drop in the luminescence of QDs with increasing COOH/Cd ratio and PAA molecular weight. Increasing amount of coating does not help beyond the critical ratio since these charged macromolecules repel each other and prefer extended confirmation which is difficult for wrapping around the crystal surface. Negative influence of the chain-length and increased charge density on the capping of the crystal surface and arresting crystal growth could explain the increasing size and decreasing luminescence. Incomplete surface capping/passivization would leave uncoordinated sites as surface traps resulting in non-radiative recombination of the electron and the hole, and hence reduced luminescence.

2.3.4 pH

CdS QDs were synthesized at pH 5.5 and 7.5. The initial complex formed between PAA and Cd^{2+} is insoluble below pH 4.0. In order to increase the binding capacity of PAA, higher pH value of 7.5 was also adopted. Reaction pH has a significant influence on the crystal size and luminescence. Although overall variation in the crystal size as a function of COOH/Cd ratio is less dramatic at pH 5.5, as the ratio increased from 0.5 to 2, size decreased from 4.8 to 4.1 nm and stayed around 4.7 nm above this ratio. This indicates the existence of a two-way interaction between the pH and the polymer amount in affecting the crystal size. At fixed COOH/Cd ratio, particles prepared at pH 5.5 absorb at longer

wavelengths (Figure 2.4), suggesting less effective surface capping as a means to arrest the particle growth. At pH 5.5, luminescence intensities also dropped significantly (Figure 2.5 b, c) and the PL maximum shifted to longer wavelengths in agreement with the absorbance spectra (Figure 2.4). Yang and Gao [20] reported pH-dependent luminescence for 3-mercaptopropionic acid (MPA) and thioglycolic acid (TGA) coated CdTe, showing a maximum at pH 6 and 4.5, respectively. They have adjusted the pH during the measurements. They suggest that surface passivization is enhanced though secondary interaction of the carbonyl of the protonated carboxylic acid group with the CdTe surface and the pH where protonation takes place depends on the pKa of the acid. According to this hypothesis, PAA (pKa = 4.75) should provide better luminescence at higher pH than MPA (pKa = 4.32). More importantly, partial protonation of carboxylates at low pH results in a decrease in the electrostatic repulsion, collapses the polymer, and decreases the cation and surface binding ability. According to Rivas et al, PAA binds 50% more Cd^{2+} at pH 7.5 than at pH 5.5.[68] Parallel to this, surface binding ability of PAA would also decrease with the protonated acids since carboxylate is the effective surface binding group, resulting in larger crystal sizes and uncoordinated sites on the surface. One should consider that carboxylates are linked together on a polymer chain and electrostatic repulsion of the unprotonated carboxylates as well as H-bonding in the protonated acids would be influential in determining the adsorption of carboxylates in close proximity. After MPA addition to PAA-coated QDs, we have seen an increase in the fluorescence intensity of the particles qualitatively. This observation also points out that the bonding strength, coating chemistry, surface coverage and the pKa values of the surfactants are significant contributors to the fluorescence intensity. Based on the above discussion, for effective capture of surface cations with carboxylates, higher amount of polymer might be needed at pH 5.5. This could explain the decreasing crystal size with increasing polymer amount at pH 5.5 as we approach the critical COOH/Cd ratio (Figure 2.6).

PL spectra showed a similar trend. pH also influences the optimum polymer amount required for the maximum luminescence intensity. At pH 5.5, PL intensity increases with

increasing coating amount until COOH/Cd ratio of 2 is reached and afterwards it shows a downward trend as seen for both molecular weights at pH 7.5 and 5.5 (Figure 2.5-b,c,d).

2.3.5 Quantum yield (QY)

Comparison of the luminescence of QDs and the trend observed as a function of our variables can be clearly seen in the QYs calculated against a Rhodamine B reference. Figure 2.7 shows calculated relative QYs (η) for all samples. QY of CdS QDs is slightly better with PAA2K (8-17 %) than with PAA5K at pH 7.5 (5-13 %). Maximum QY obtained from CdS QDs prepared in a PS(300)-block-PAA(20) micelle was reported as 4%.[52] At similar sizes, we have obtained better QYs. In the reported example, COOH/Cd ratio of 0.66 (Cd/COOH=1.5) was used. At this ratio, insufficient surface coverage could diminish QY. We believe that PAA-CdS QDs is resulted into better surface passivization reducing the extent of nonradiative relaxations and improved the QY over the reported values.

Overall, a significant decrease in the QY is observed at reaction pH 5.5. QY decreases with increasing coating amount at pH 7.5 but at pH 5.5, it has a bell-shaped trend with a maximum around COOH/Cd=2, in agreement with PL intensity. CdS crystal size decreased as the COOH/Cd ratio increased to 2 as discussed in previous sections (Figure 2.6). It is important to note that this COOH/Cd ratio is the same critical ratio observed in UV analysis and corresponds to the smallest crystal sizes for the stable colloids in each series. Smaller crystal sizes may contribute to enhanced QY as well. This further supports the importance and dependence of size and luminescence on polymer amount-pH interaction.

No significant decrease in the QY of the particles was observed for over 8 months. Optimum COOH/Cd ratio for best QY appears to be around the critical ratio of 1.5-2 for both molecular weights and pH without loosing colloidal stability.

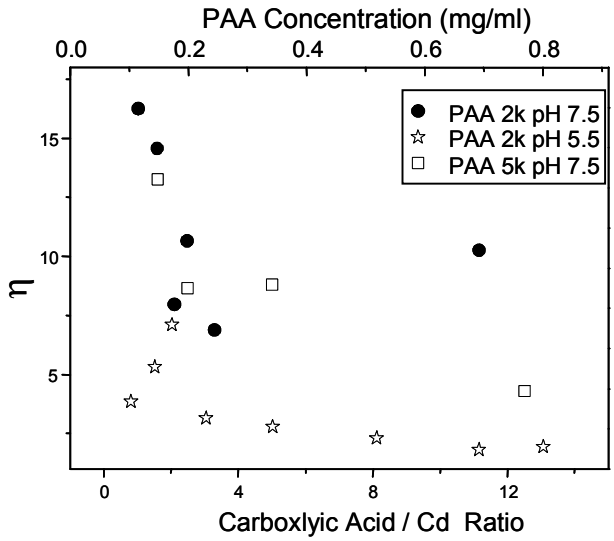

Figure 2.7 QY (η) of the samples wrt Carboxylic Acid / Cd ratio or PAA concentration.

2.4 Conclusions

CdS QDs were prepared successfully in a simple aqueous and relatively green route with PAA coating of 2100 and 5100 g/mol molecular weight. An excellent long-term colloidal stability of the CdS QDs with functional surfaces was achieved, far beyond what we have observed with MAA systems. PAA-CdS NPs are luminescent mostly in the light yellow-orange with absorption in the range of 460-508 nm. Small size alterations between 3.6 to 6.5 nm can be achieved by increasing the amount (COOH/Cd in the range of 0.8-12.5) and molecular weight of PAA. However, significant size tuning accompanied with luminescence in a broader visible range cannot be achieved with this polyelectrolyte. PAA provides surface adsorbing groups that are dependent on each other. Repulsion of neighboring chains and COO^- groups would impact chain conformation, cause expansion and impose restrictions in adsorption on the crystal surface and limitation in further size tuning. Complex formed between PAA and Cd^{2+} is influential on the size as well. Such complexes are formed by binding of multiple cations to a single PAA chain. Therefore, at a

fixed COOH/Cd ratio, lower molecular weight polymers, providing more polymer chains, are more desirable. Carboxylates of PAA adsorb on Cd^{2+} rich surface much more effectively, and therefore, Cd/S ratio above 1 is desirable for better surface capping, enabling better size control and better luminescence.

QYs of the PAA coated CdS QDs are in the range of 5-17%. Data indicate that use of large excess of PAA increases the crystal size and decreases the PL intensity. A very important outcome of this study is the identification of an optimum COOH/Cd ratio around 1.5-2 for the highest PL intensity and QY for both molecular weights and pH (5.5 and 7.5) within the limits of colloidal stability. NPs prepared with COOH/Cd ratio above one showed both colloidal and luminescence stability over eight months so far. Reaction pH is also identified as a critical parameter for the QY and the particle size. NPs prepared at higher pH values where the polymer is mostly ionized provided better surface passivization and better QYs. For maximum QY and smaller crystal sizes, larger amount of polymer is needed at lower pH where some protonation of the acid takes place. It is crucial to understand this critical ratio and the pH sensitivity for tuning particle size while keeping colloidal stability.

Here, we provided the first detailed study of PAA-coated CdS NPs. Although extremely stable and more luminescent than those reported by Moffit, PAA-coated CdS NPs do not have very high QY.[52] It is possible to improve the luminescence intensity and QY of these particles further by coating CdS crystals with ZnS or CdSe/ZnS as described in the literature.[10, 69, 70] The results gained from this study can be applied to other polymers and QDs. CdS was used as a model QD here, especially because it emits in the visible range.

Chapter 3

SYNTHESIS AND CHARACTERIZATION OF CADMIUM SULFIDE QUANTUM DOTS IN A NOVEL PAA/MAA BINARY SURFACTANT SYSTEM

3.1 Introduction

Development of semiconductor nanoparticles created a tremendous excitement both in the industry and academia due to unique size dependent electrical and optical properties. As the dimensions of the crystal approach the exciton Bohr radius, energy levels are quantized causing a blue shift in the absorbance spectrum. As the crystal size decreases, allowed energy levels spread and the gap between the conduction and the valance band increases, providing size dependent chemical and optical properties that are dramatically different than the bulk materials. Most significant outcome of such quantum confinement is the size tunable luminescence of semiconductor QDs. Tunable band gap, photostability, narrow emission profile, broad absorption range and ability to excite different sized QDs at a single excitation wavelength accelerates the development of new materials crossing the limitations of existing bulk materials. Luminescent QDs are being extensively investigated for a variety of applications such as fluorescent labeling, optical imaging, sensors, lasers, optoelectronics, inks, barcodes and photovoltaics.[45-47, 71] Such properties and better sensitivity make QDs superior to organic fluorophores. Therefore, aqueous suspensions of QDs are gaining more and more importance in biotechnology and medicine.

Synthesis of QDs in solutions utilizes surface adsorbing molecules as capping agents which serves to four major purposes: control of particle growth during the synthesis, suspension of particles in a solvent, passivization of surface to improve surface quality and prevention of particle aggregation. Luminescence and QY are largely affected by the surface properties. Core-shell structures generated by growing a larger band gap semiconductor and activation with high power UV source do improve the luminescence of the particles. [72-74]

Among different synthetic techniques, so far the best quality colloidal QDs are produced through the high temperature processes based on pyrolysis of organometallic precursors and using TOPO as a capping agent.[5] Transfer of TOPO capped QD to water is often accompanied with a drop in the luminescence or increase in the particle size.[15, 73, 75]. Synthesis of QDs in aqueous solutions offers a direct, simpler and much greener alternative, yet luminescence and size control are often inferior to high temperature pyrolysis method. A considerable amount of research has been devoted to elucidate the effect of different capping agents, ion concentration, pH, length of the hydrocarbon chains of thiolated molecules and the reaction time on the particle size and optical properties.[19, 22, 76] However, much less attention has been paid to the temperature dependence in the aqueous path.

In order to suspend QDs in water, various molecules, especially thiols with hydrophilic functional groups such as amine, carboxylic acid or hydroxyls have been applied.[62, 77] MAA is one of the most effective coating materials enabling aqueous dispersions of QDs. MAA provides efficient surface passivization through thiol-Cd interaction on the surface of the CdS.[19] However, we have observed that MAA coated CdS nanoparticles lack long term colloidal stability. On the other hand nanoparticle-polymer composites are also being investigated due to attractive properties of polymers.[78-80] We are interested in exploring PAA as a coating by itself for QDs as means to control particle size and impact QY in a simple aqueous preparation. PAA provides multiple attachment sites, hydrophilic and

functional surface, steric and electrostatic stabilization. Recently, stabilization of CdS nanoparticles and nanoplates with PAA was demonstrated by Lu and Pan.[54, 81] These reports do not provide information about the stability, size tuning or QY of the QDs. Moffitt et al has been working on CdS synthesis in self-aggregated PS-block-PAA micelles as templates since mid 90s.[52, 53, 67] His reports have less focus on the CdS properties than the larger micellar morphologies obtained.

We have performed a detailed study on the synthesis and properties of PAA coated QDs prepared in water and demonstrated that PAA provides excellent colloidal stability.[82] Although, luminescence was not as good as MAA stabilized CdS, QY up to 17% was achieved. PAA-CdS QDs emitted mostly in the yellow-orange range and different colors, so different sizes, were not easily achieved simply by changing the coating amount. Non-covalent attachment of carboxylates and poorer surface passivization in comparison to thiolated small surfactants was suggested as the main reason for such difference in the luminescence.

In an effort to achieve highly luminescent and stable aqueous CdS QDs in different sizes and colors, we used a binary mixture of MAA and PAA as the coating material. PAA (Mn 2100) sodium salt has 22 carboxylic acids and each molecule provides multiple sites for binding. MAA contributes with a single carboxylic acid and a thiol unit which has high affinity for cadmium. In this chapter, we will report the first examples of aqueous synthesis of CdS nanoparticles with binary surfactant mixture of PAA/MAA. As a part of this study, influence of temperature on the size and the properties of the PAA-CdS QDs were also determined. We investigated the size of the nanoparticles and QY as a function of coating composition (PAA/MAA ratio) and the reaction temperature which were both influential in the particle growth and surface passivization.

3.2 Experimental section

3.2.1 Materials

All chemicals were analytical grade or of the highest purity available and used as received. Sodium sulfide trihydrate ($Na_2S{\cdot}3H_2O$) and cadmium acetate two hydrate ($Cd(Ac)_2{\cdot}2H_2O$), Rhodamine B, acetic acid (99.8 %), nitric acid and mercaptoacetic acid (MAA) were purchased from Merck. NaOH pellets and poly(acrylic acid) sodium salt (PAA, Mn 2100) were purchased from Aldrich. Milli-Q water (Millipore) was used as a solvent.

3.2.2 Synthesis of CdS nanoparticles stabilized with PAA/MAA

In all reactions, total $COOH/Cd^{2+}$ and Cd^{2+}/S^{2-} mole ratios were kept constant at 11 and 2.5, respectively.

Preparation of Cd^{2+} solution. In a typical synthesis, 333.2 mg $Cd(Ac)_2{\cdot}2H_2O$ was dissolved in 250 ml deionized water (DI water) and added to 1L three-necked round-bottomed flask fitted with a mechanical stirrer. In order to have a COOH/Cd molar ratio of 11, total of 13.8 mmol COOH was required. Depending on the desired PAA/MAA ratio, necessary PAA and MAA amounts were calculated and added into the reaction flask. Solution pH was adjusted to 7.5 by using 10M, 5M and 1M concentrated NaOH and/or HNO_3 solutions drop by drop. This solution was deoxygenated for 15 minutes, and brought to the desired reaction temperature in an oil bath. Synthesis of CdS was performed at 30, 60 and 90 °C for all coating compositions.

Preparation of S^{2-} solution. 66.0 mg $Na_2S{\cdot}3H_2O$ was dissolved in 250 ml DI water in an ultrasonic bath and transferred into an addition funnel and deoxygenated for 15 min.

Preparation of CdS nanoparticles. Sodium sulfide solution was added to the cadmium acetate solution in portions of 25 ml in 5 minute intervals. After the addition was completed, reaction was stirred under nitrogen at set temperature for additional one hour.

Then, the reaction mixture was left to cool down to room temperature and stored in the refrigerator. At this stage, the solution pH was usually around 8-8.5.

3.2.3 Characterization

Absorption spectra were recorded on a UV-Vis-NIR spectrophotometer (Schimadzu, model 3101 PC) in the 300-500 nm range. Photoluminescence measurements were performed on a Horiba Jobin Yvon–Fluoromax 3 spectrofluorometer at 355 nm excitation wavelength. A 370 nm band pass filter was used to eliminate the second harmonic emission of the 355 nm excitation at 710 nm. PL spectra were recorded between 365-900 nm with slid widths set at 2 nm for both excitation and emission monochromators. All measurements were done on three different dilutions of the aqueous samples with absorbance ≤ 0.1 at excitation wavelength. All PL spectra were calibrated with respect to their absorptions at the excitation wavelength. QYs were calculated by comparing the integrated emission of the samples with that of Rhodamine B reference (Rhodamine B in water QY= 31 % at 514 nm) [83] according to the procedure published by Horiba.[84] Details of the QY measurements and calculations are available in the supplementary information. Hydrodynamic sizes of the nanoparticles were measured as intensity and number average on a Malvern Zetasizer Dynamic Light Scattering Unit. Infrared spectra of the samples were obtained from Jascow FT-IR spectrophotometer using KBr pallets of the dried samples. X-ray diffraction analysis were performed on a HUBER G670 diffractometer with a germanium monochromator and $CuK\alpha_1$ radiation (λ = 1.5406 Å). Data was collected in the range of $5^{o}<2\theta<100^{o}$ with 0.005º increments and analyzed using STOE WinXPOW software. Excess coating was removed by precipitation before the XRD measurements. TEM measurements were done at Max-Plank Institute at Mainz with a FEI Tecnai F20 operated at an acceleration voltage of 200 kV. TEM samples were prepared by applying a drop of aqueous sample on a carbon coated copper TEM grid, followed by blotting off the excess solution with a filter paper. EDX examination was performed in

TEM bright-field mode, illuminating the area of interest (approx. 10 μm in diameter) by focusing the electron beam to the desired area using the condenser system of the TEM.

3.3 Results and discussions

3.3.1 Synthesis of PAA/MAA-CdS

CdS QDs were successfully prepared in homogenous aqueous reactions with PAA/MAA coating where the ratios of PAA/MAA and reaction temperature were altered systematically. CdS nanoparticles with coating compositions of 100/0, 80/20, 60/40, 40/60, 0/100 % PAA/MAA were prepared at 30, 60, and 90 ºC to investigate the influence of the composition and temperature on crystal size and optical properties. Variations in the coating composition were done at a fixed COOH/Cd ratio of 11.

All particles were luminescent in the visible range upon excitation with 365 nm. Figure 3.1 shows the UV-Vis absorption spectra of the CdS nanoparticles prepared at (a) 30 ºC, (b) 60 ºC, (c) 90 ºC. All samples showed a clear blue shift of the absorption onset with respect to the bulk absorption of CdS (514 nm, 2.41 eV) and larger bandgap as a result of quantum confinement.[62] Crystal sizes of CdS nanoparticles were calculated by applying the Brus equation (eqn 1) [3] and were in the range of 2.6-3.9 nm (Table 1). We have noticed that in some of the reports, the coulomb interaction term was left out when applying Brus equation for size calculations, which could cause at least 10 % error (eqn 1).[62, 85] Details on the Brus equation as well as particle size calculated with and without coulomb term were presented in the supplementary document.

$$\Delta E = \left(\frac{\hbar^2\pi^2}{2R^2}\right)\left(\frac{1}{m_e}+\frac{1}{m_h}\right) - 1.8\frac{e^2}{\varepsilon_{CdS}R} \qquad \text{eqn (1)}$$

Confinement Effect — Coulomb Effect

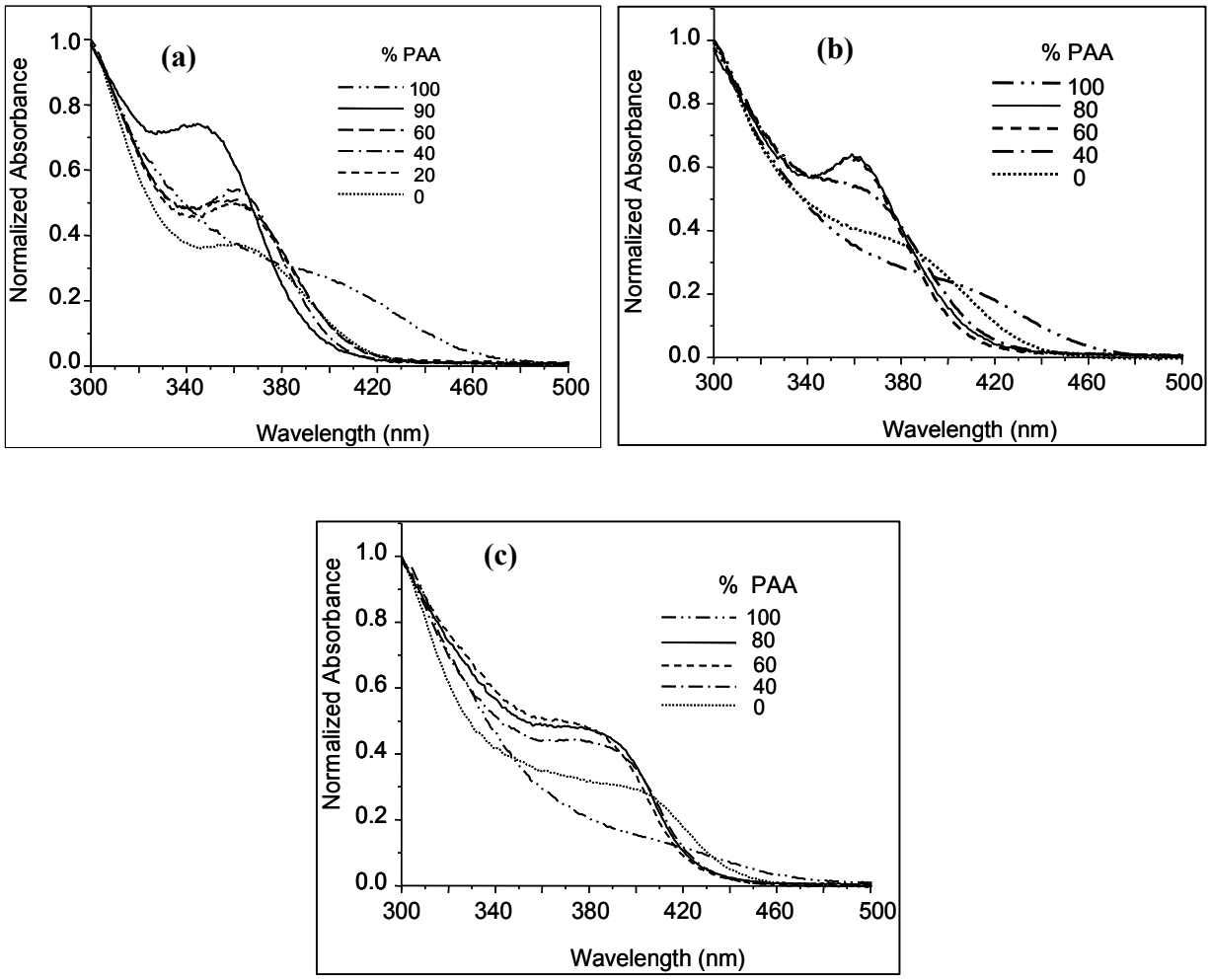

Figure 3.1 UV-Visible absorption spectra of CdS nanocrystals coated with various PAA/MAA ratio and prepared at (a) 30 ºC, (b) 60 ºC, (c) 90 ºC

Table 3.1 PL and UV-VIS data of CdS nanoparticles

PAA (mole %)	MAA (mole %)	Temperature (ºC)	Absorption cutoff (λ)	Size[a] (nm)	Band gap[b] (eV)	PL[c] Maximum (nm)	FWHM[d] (nm)
100	0	30	459	3.6	2.71	544.0	187
80	20	30	416	2.8	2.98	519.0	153
60	40	30	408	2.7	3.04	510.0	148
40	60	30	401	2.6	3.10	503.5	143
0	100	30	416	2.8	2.98	517.5	151
100	0	60	459	3.6	2.71	553.5	191
80	20	60	407	2.7	3.05	517.0	153
60	40	60	405	2.6	3.05	514.0	148
40	60	60	415	2.8	2.99	523.5	153
0	100	60	434	3.1	2.86	536.5	161
100	0	90	469	3.9	2.65	554.5	174
80	20	90	425	2.9	2.92	543.5	162
60	40	90	425	2.9	2.92	532.5	163
40	60	90	427	2.9	2.91	545.5	167
0	100	90	443	3.1	2.80	643.5	171

* All Samples are synthesized at pH 7.5 with Cd/S ratio of 2.5 and COOH/Cd ratio of 11

[a] Calculated by Brus Effective Mass Approximation[3]

[b] Corresponding band gap energy calculated by Planck's Equation ($E = hv$)

[c] Corresponding wavelength at highest photoluminescence intensity

[d] Full width at half maximums calculated from PL spectra

FTIR spectrum of PAA, MAA and PAA/MAA coated CdS nanoparticles were shown in Figure 3.2. Weak peaks around 407 cm^{-1} seen in all spectra were attributed to the Cd-S bond.[54] Absence of a –SH band at ca 2600 cm^{-1} confirms binding of thiols to particle surface in all the samples. CdS-MAA showed two significant peaks at 1560 and 1384 cm^{-1} corresponding to the antisymmetric and symmetric stretching modes of carboxylate.[56] CdS-PAA showed antisymmetric and symmetric stretching modes of carboxylate at 1560 and 1408 cm^{-1} and a C=O stretching band for the carboxylic acid at 1710 cm^{-1} indicating a COO^- binding on crystal surface and existence of some unbonded carboxylic acid groups. Peaks at 1455 and 1285 cm^{-1} are CH_2 bending and wagging modes. $–CH_2$ asymmetric stretching band for MAA and PAA coated particles are at 2921 and 2941 cm^{-1}, respectively. A 20cm^{-1} shift to lower frequency indicates denser packing of MAA on the particle surface. Peaks observed for CdS-PAA/MAA (80/20) at 2944, 1560, 1455, 1408, 1352 cm^{-1} are indicative for $-CH_2$ stretching (asym), $-COO^-$ stretching (asym), $-CH_2$ bending, $-COO^-$ stretching (asym), $-CH_2$ wagging modes. Absence of clear carbonyl peak at 1710 cm^{-1} may indicate an interaction between the coating molecules as well. Shoulders at 1634 and 1734 cm^{-1} might indicate H-bonded systems.

Peaks appeared around 25.5º (111), 30.8º (200), 44.1º (220), and 52.18º (311) in the X-ray powder diagrams of samples are in agreement with the cubic CdS structure (Figure 3.3). However, except the (111) one, all the peaks are weak, broad and slightly shifted towards higher 2θ values that is usual for the small size crystals.[54, 62, 86]

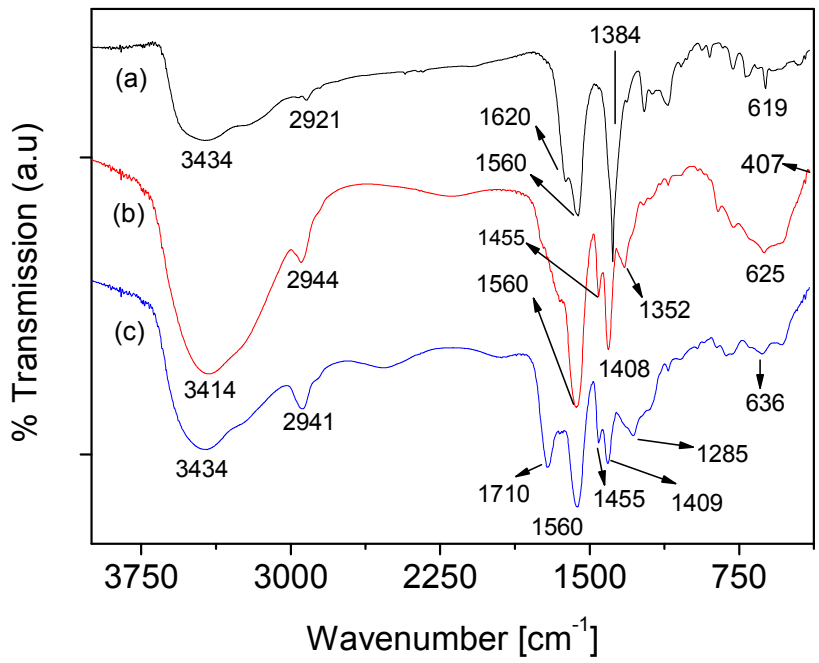

Figure 3.2 IR spectra of (a) MAA, (b) PAA/MAA (80/20), (c) PAA coated CdS QDs.

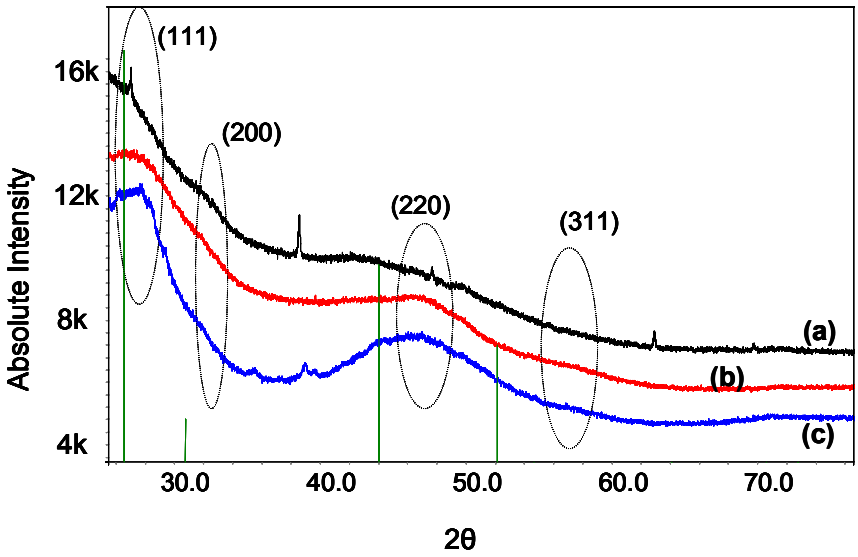

Figure 3.3 X-Ray powder diagrams for (a) PAA, (b) PAA/MAA 80/20-CdS and (c) MAA coated CdS QDs.

TEM of the samples indicate formation of small crystalline structures with the clearly seen lattice fringes (Figure 3.4). Although it was difficult to clearly visualize the individual particles and get a good size average due to the excess organic material, size of the crystals decrease in the order of coating composition of PAA, PAA/MAA (80/20), MAA. EDX indicates the presence of O, S and Cd. Difference in the relative intensities of these atoms roughly reflects the ratios of these elements coming from the coating and CdS itself but, presence of excess amount of coating material that contributes to the intensity of the peaks makes the quantification of PAA and MAA bound on the particle difficult.

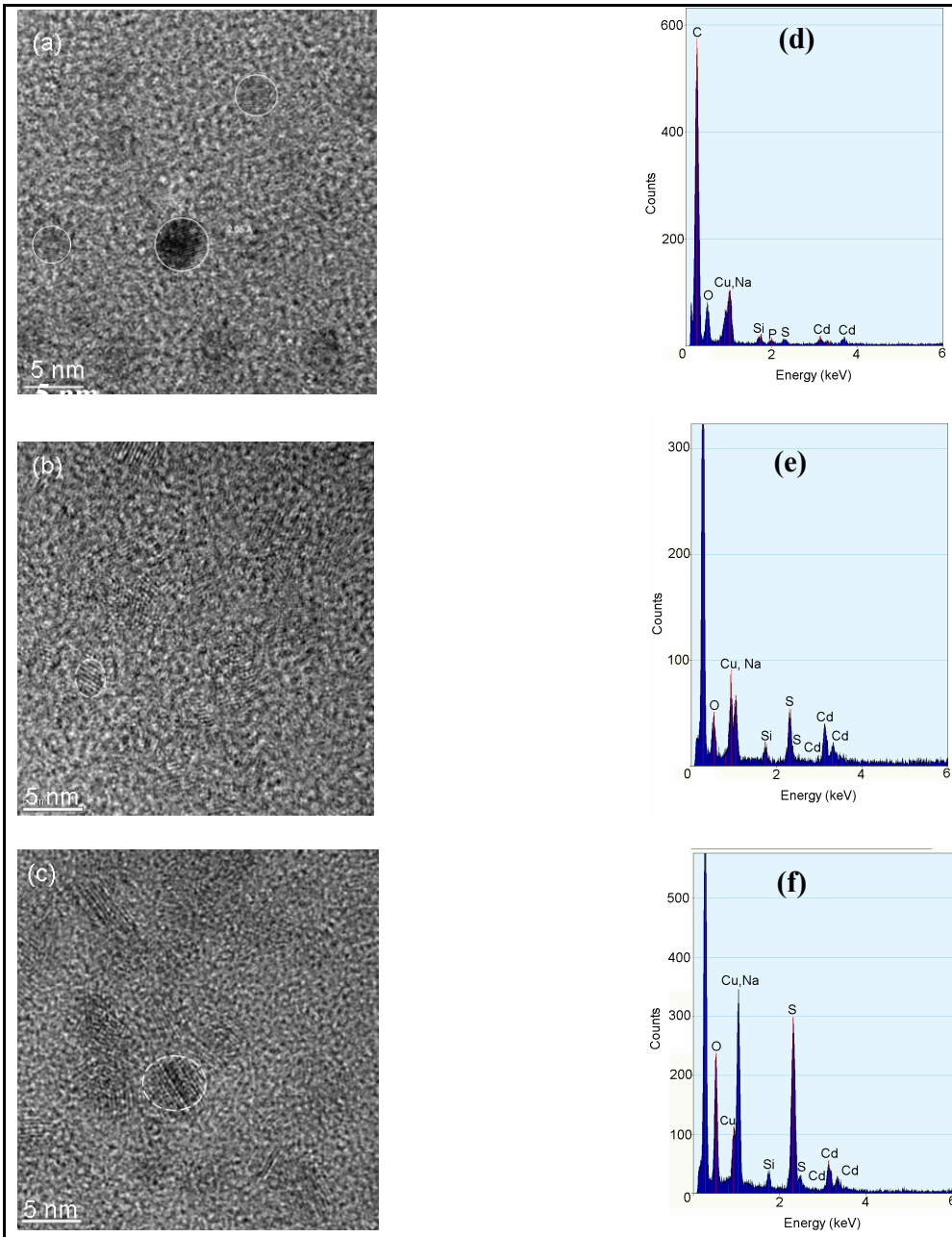

Figure 3.4 TEM and EDX images for a&d) 100, b&e) 80, c&f) 0 % PAA coated CdS nanoparticles synthesized at 60ºC (bars=5nm).

3.3.2 CdS QDs coated with MAA versus PAA

100% PAA coated CdS nanoparticles (CdS-PAA) have an absorption onset and PL maximum at a longer wavelength than 100% MAA coated ones (CdS-MAA), indicating larger crystal sizes at all temperatures (Table 3.1). This is also accompanied with a narrower full-width at half maximum of the PL peak for CdS-MAA which does indicate narrower particle size distribution at lower reaction temperatures. MAA is quite effective in arresting the crystal growth during the synthesis since not only S^{2-} but also the sulfur of the MAA reacts with the surface Cd^{2+} passivating the surface and limiting the growth. On the other hand, PAA adsorb on the crystal through carboxylates and does not compete with the S^{2-} for the Cd^{2+} sites on the crystal surface, therefore exposing a milder constraint on the crystal growth. Desorption of the capping agent for brief moments leaves the surface accessible for growth.[49] PAA seems to favor such process more than MAA based one according to the above discussion.

These capping agents not only bind to the crystal surface but also complex Cd^{2+} ions in the solution. MAA forms Cd-thiol, PAA forms Cd-carboxylate complexes with Cd^{2+} ions prior to nucleation. These complexes are not important only in setting reaction conditions but also are influential in the crystal growth. Ste-Marie et al defines different Cd-thiol complexes in a broad pH range and Nosaka reports $[Cd(SR)_4]^{2-}$ complex as the major one for CdS-mercaptoethanol system when RSH/Cd $\geq$4 at pH 7.[87, 88] Korgel draws attention to the formation of this complex as an important factor in the formation of MAA capped CdS QDs.[22] At the RSH/Cd = 11 and at pH 7.5, we assume all the Cd^{2+} formed such polynuclear complexes with the MAA which allowed crystal growth through cluster-cluster aggregation and ligand exchange as discussed by Meisel on the study of CdS-3-mercapto-1,2-propanediol system (using radiolytic release of sulfur).[66] Such growth kinetics seems to narrow down the particle size distribution as well.

PAA also forms complex with Cd^{2+} prior to nucleation. Torrents reported complexation of more than 90% Cd^{2+} with PAA above pH 7 within a broad range of Cd/PAA concentration including ours.[89] However, larger particle size and broader FWHM may indicate a different growth mechanism for the CdS-PAA QDs. Such thought is supported by the insensitivity of CdS-PAA to temperature (Figure 3.5a) or to PAA amount that we have reported earlier.[90] Presence of the excitonic peak (1s-1s` absorption) with MAA but not with PAA also enhances our belief for narrow size distribution for CdS-MAA QDs (Figure 3.1 Figure 3.5).[62] One could think since clusters are highly charged and polymers induce strong steric repulsion between different clusters, cluster-cluster aggregation will be more limited for PAA, which would limit focusing in size. Yet, non-covalent attachment of the PAA and high affinity of S^{2-} to Cd^{2+} can increase the rate of reaction/ligand exchange at the crystal surface with respect to MAA. Also, same line of thinking suggests more soluble primary particles with PAA that is more prone to size defocusing through Ostwald ripening. This might be even elevated with the proximity of each complex and primary particles which are all entrapped within the polymeric matrix since many polymers may adsorb on a single crystal and/or many clusters can be formed with a single polymer. It is also important to consider partial charge neutralization and collapse of the polymer upon complex formation with Cd^{2+}. Such proximity of clusters or primary particles can enhance diffusion and aggregation within the polymer matrix.

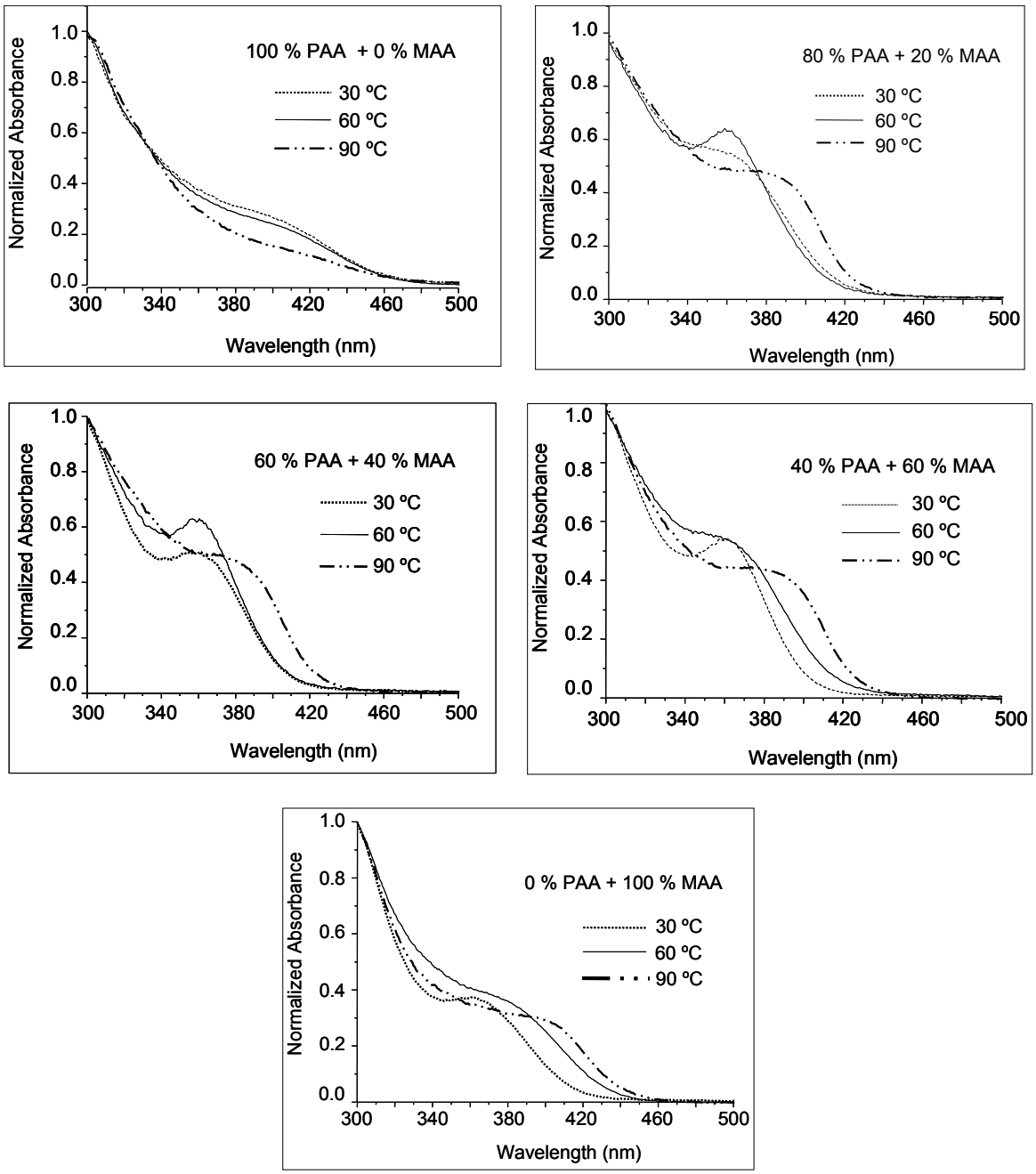

Figure 3.5 UV-Vis absorption spectra of each composition a) 100, b) 80, c) 60 d) 40 e) 0 PAA % at different reaction temperatures (30, 60, 90 ºC).

It is desired to have a narrow and symmetrical emission profile and high PL intensity with the QDs. Absorption corrected PL spectra of all samples can be seen in Figure 3.6. PL maximum intensity of PAA coated CdS nanoparticles are about 90 % less than MAA coated ones at every temperature. This difference is also visible to the naked eye. QY of CdS-MAA and CdS-PAA at 90°C are 1.6 and 7.7 % with respect to Rhodamine B in water and although the latter does not change with the increasing temperature, the former decreases with the temperature especially at 90°C. MAA coated CdS nanoparticles are known with their good surface passivization through Cd-SR bond formation as also discussed above.[19] However, PAA chemically adsorbs on the surface through carboxylates.[54] Yet, each carboxylate of PAA is influenced by the neighboring group. Ionized PAA prefers more extended conformation which may limit dense adsorption of carboxylates on the crystal surface, creating surface defects. Such inferior surface coverage would lead to a weaker luminescence than MAA coated particles, since surface defects result in non-radiative recombination.

Effect of Temperature. Figure 3.5 provided a good visualization of the temperature's impact on the particle size for each composition. Size of the nanocrystals or exciton energy of PAA coated CdS nanoparticles were not affected by the temperature (Figure 3.5a) except a small increase at 90 °C, yet there was a clear red shift for MAA coated particles as the temperature increases (Figure 3.5e). Increasing temperature can impact the nucleation and growth in three ways: increases the diffusion rate; increases the desorption rate of capping agents from the surface; and decreases the stability of the complexes favoring nucleation and growth.[49] Significantly higher sensitivity of Cd-MAA to temperature than Cd-PAA suggests that the thiol binding and thiol complex stability is more sensitive to temperature. Since adsorption of PAA is through weaker Cd-OOCR interaction rather than a Cd-SR bond, an increased desorption rate causing larger sizes compared to Cd-MAA can be expected. In case of PAA, 22 carboxylates are attached to each other so it certainly shows different behavior than monomeric species. PAA adsorbs on the surface through

multiple sites which would limit complete removal. It is reported that, T_g and thermal stability of polymer increases with cadmium complexation [91], which would decrease the surfactant mobility and desorption rate of the polymer compared to MAA. If the growth is taking place in a polymeric matrix formed initially with complexed cadmium ions, size can be limited with the size of this sort of nano-reactor. Moffit reported that during the synthesis of CdS within PAA cores of PS-block-PAA micelles, size of the CdS reaches a plateau above 10 nm as the viscosity and diffusion within the cores become the limiting factor and the kinetic control dominates the growth. [67] As discussed earlier, larger size of the complexes, therefore slower diffusion of CdS-PAA and Cd-PAA clusters and electrostatic repulsion between particles would limit further cluster and particle aggregation with increasing temperature.

Impact of temperature on the photoluminescence and QY can be visualized in Figure 3.7 Figure 3.8. CdS-PAA showed only a minor increase in the PL maximum and FWHM with increasing temperature. QY of the CdS-PAA is around 7-8 % and does not change much with the temperature, in agreement with the discussions provided above. Yet, CdS-MAA showed a dramatic red-shift in the PL maximum and a dramatic drop in the luminescence at 90°C, indicating higher sensitivity to temperature. QY dropped from 43.6 % to 1.6 % (with respect to Rhodamine B in water) as temperature increased from 30° to 90°C. This dramatic drop in the luminescence also suggests inferior surface binding of more mobile and small MAA with respect to bulkier, multi functional PAA at elevated temperatures.

3.3.3 CdS QDs coated with PAA/MAA binary mixture

All nanoparticles with the binary surfactant coating showed a blue shift in the absorbance onset and PL maximum with respect to PAA coated CdS nanoparticles (Figure 3.1). This is quite reasonable since smaller crystals were obtained with 100% MAA compared to 100% PAA. However, more interestingly, all QDs with the binary coating absorbed at lower wavelengths than MAA coated CdS nanoparticles, as well. The existence

of more obvious first excitonic peak for CdS-PAA/MAA QDs in the absorption spectra (Figure 3.5) indicates smaller size distribution than even CdS-MAA which is also reflected in the narrower FWHM values. All FWHM were decreased in binary synthesis about 4-30 nm (Table 3.1).

A very important outcome of utilizing a PAA/MAA binary coating is the enhanced luminescence of CdS QDs (Figure 3.8a): Addition of only 10% MAA caused more than 100% improvement in QY with respect to 100 % PAA coating. Most rapid increase in QY occurred with up to 40% MAA incorporation. We believe that the surface defects left on the crystal surface with PAA due to the steric limitations are trapped effectively with the small MAA molecules, decreasing non-radiative coupling events. Surprisingly, the binary coating system improves QY over not only PAA coated QDs but also MAA coated ones up to 60% PAA in the mixture at lower temperatures and for all compositions at 90°C. Nanoparticles with PAA ≤ 40 % in the coating composition have higher luminescence intensity and QY than all the other compositions including the pure MAA at 30° and 60 °C (Figure 3.7 andFigure 3.8a). At these two synthesis temperatures, PL intensity of the samples decreased in the order of 40-20>0>60>80>100 % PAA (Figure 3.6a,b). This indicates that, in the presence of sufficient amount of PAA (possibly maximum 50 %), nucleation and growth follows a similar route to 100% PAA and not dramatically affected by the temperature. Increasing the temperature further to 90 °C caused a significant decrease in the PL intensity and the QY for all QDs. QDs with 60% PAA displayed the highest PL intensity at 90 °C. For the two lower temperatures, QY of the QDs with up to 60% PAA are around 45 %, similar or better than CdS-MAA, and then starts to decrease towards Cd-PAA values. On the other hand, at 90 °C, QY increases over the value of MAA up to 20 % as the PAA content increases, then declines. Increasing PAA amount in the coating composition reduces the sensitivity of QY to temperature, similar to CdS-PAA case. Also, existence of PAA, through possible interactions with MAA and steric as well as electrostatic stabilization, increased the colloidal and oxidative stability of the MAA

patches on the surface. These QDs are stable over nine months so far. All these suggest that a balance between PAA and MAA is needed to control the complexes, growth kinetics, surface passivization and stability all at the same time: As MAA content increases, better surface passivization and higher QY are obtained in the expense of temperature sensitivity. As PAA content increases, QY becomes less sensitive to temperature, size is varied in a narrower range and above 60% PAA, QY falls below the value of CdS-MAA. A synergy between the two exists at PAA content of ≤ 60%.

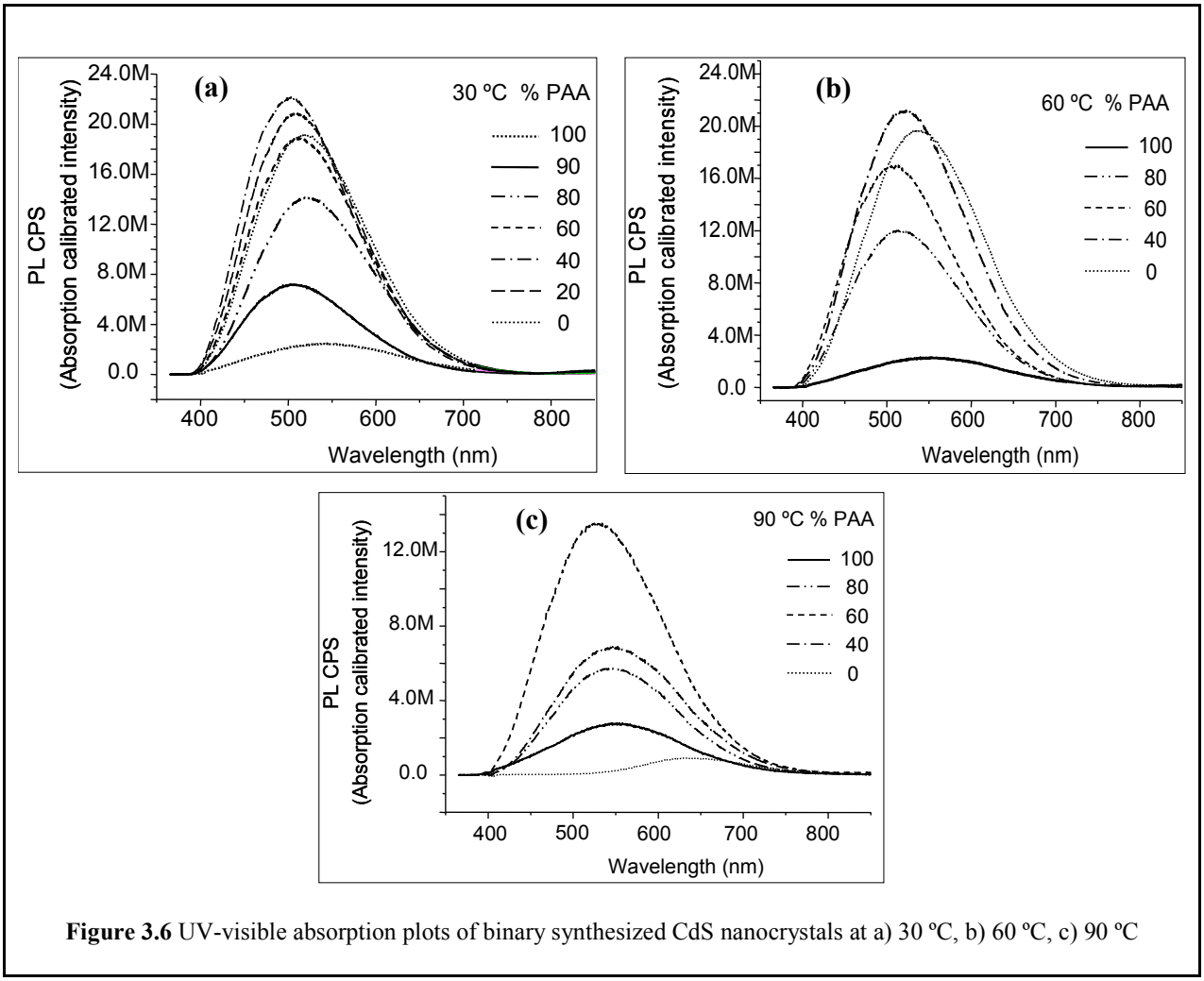

Figure 3.6 UV-visible absorption plots of binary synthesized CdS nanocrystals at a) 30 ºC, b) 60 ºC, c) 90 ºC

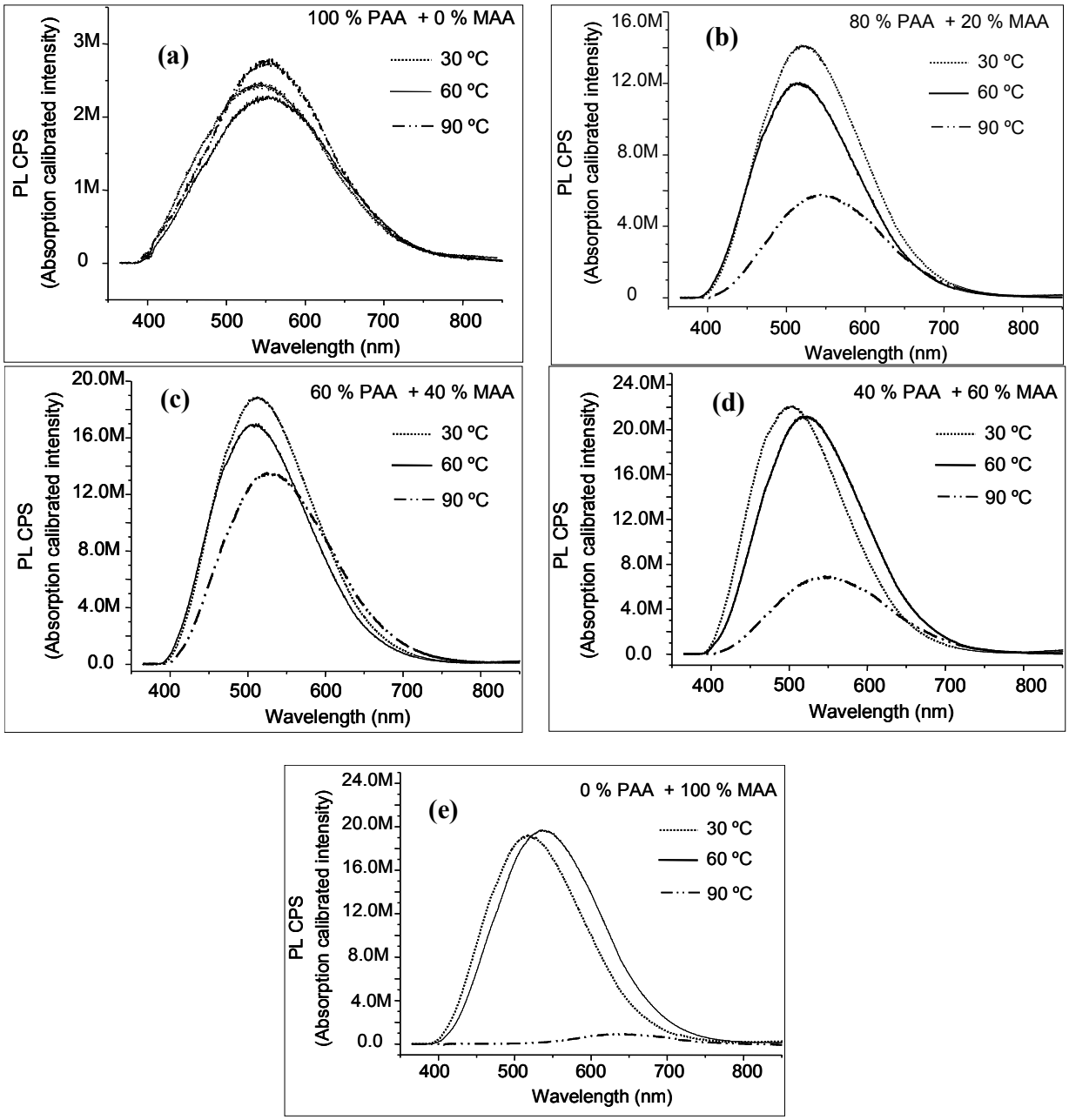

Figure 3.7 Representation of the PL plots of fixed composition with respect to temperature variation: a) 100, b) 80, c) 60 d) 40 e) 0 PAA % compositions.

A ratio of the two determines the sensitivity to temperature, size, size distribution and the QY. So overall, with PAA above 40 %, not only the sensitivity to temperature is decreased but also the QY. Color can be tuned from blue to greenish yellow with the mixed surfactants. In order to achieve red high MAA amount and high T is required.

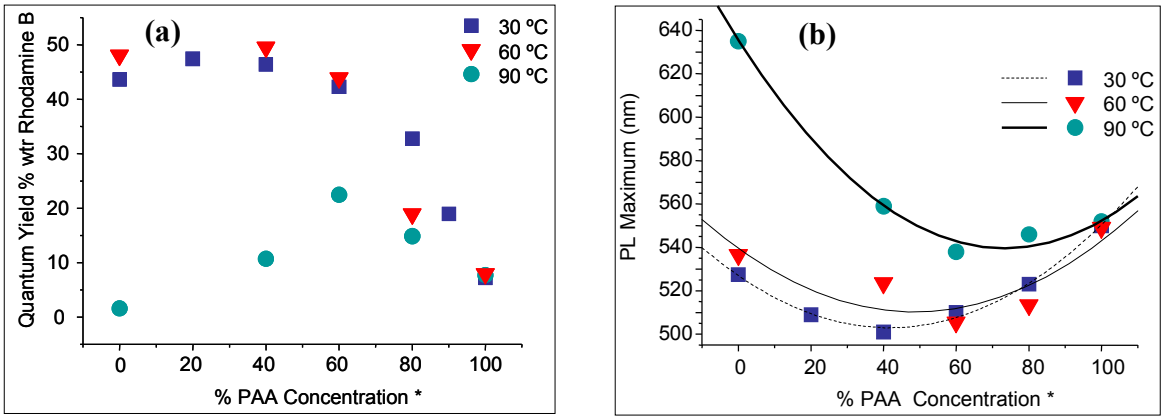

Figure 3.8 Dependence of a) QY b) PL maximum to temperature and coating composition.

Regarding the ability of size and color tuning of CdS QDs utilizing the novel PAA/MAA coating system, we should indicate that for coating having more than 40 % PAA, size and color can be tuned by the composition. Decreasing PAA amount would require the aid of temperature for color tuning, specifically high temperatures such as 90 °C. Figure 3.9 shows pictures of three CdS QDs prepared at 60°C. QDs with 100% PAA (cuvette A-Orange) coating have larger crystal size and lower PL intensity than the 100% MAA coated ones (cuvette C-Yellow). It is important to note that 100 % PAA coated particles are orange luminescent at all temperatures and 100 % MAA coated particles are yellow at low temperatures. Red luminescent particles are only obtained at 90 °C with 100 % MAA. QDs capped with 80/20 PAA/MAA (cuvette b-blue) resulted in smaller crystals

that luminesce blue-green. Due to limitation in size, we could not achieve red luminescing particles with the mixed coating.

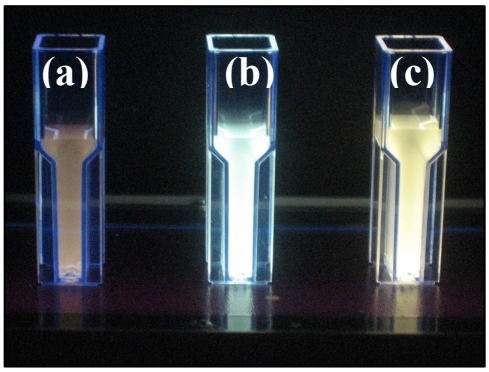

Figure 3.9 Picture of the luminescing QDs with a) 100 % PAA, b) 80 % PAA, c) 0 % PAA in the coating composition and synthesized at 60°C. Samples were excited with a UV lamp at 360 nm.

Yang and Gao reported that addition of PAA to 3-mercaptopropionic acid stabilized CdTe nanoparticles enhances the photoluminescence based on a strong secondary interaction between the CdTe surface and the oxygen of the carboxylic acid.[20] It was also stated that no particle growth was observed after the addition of PAA. However, in our study, PAA addition during the synthesis changes the particles size from yellow to blue indicating that the growth of the particles were hindered by the PAA. Blue luminescing particles could not be obtained using 100% PAA. So, existence of two types of capping agents controls particle size as well. We believe that the surface defects left on the crystal surface with PAA due to the sterics of the polymer chain are trapped effectively with the small MAA molecules, improving the QY dramatically over CdS-PAA. Also, existence of PAA chain and the sterics exerted by it increased the colloidal and oxidative stability of the MAA CdS patches on the surface. Together, they both impact the nucleation and growth and surface quality of the CdS QDs.

Smaller crystal sizes indicate that surface passivization and growth is not solely depend on MAA and strong Cd-S bond but also to the strong stabilization from PAA and limited the diffusion and growth observed with PAA. In other words, we believe that PAA, MAA and Cd^{2+} form a ternary complex in the solution, and nucleation and growth kinetics are influenced by both.

In order to follow the size in the solution we performed DLS measurements. Average hydrodynamic size (Dh) of the CdS coated with PAA/MAA 80/20, MAA and PAA are 3, 4 and 10 nm, respectively (Figure 3.10). This trend is in agreement with observed blue shift in the emission wavelength of CdS-PAA/MAA. Crystal size calculated from absorbance onset for these samples are 2.7, 3.1 and 3.6, respectively (Table 3.1). Larger Dh values than crystal sizes are expected since DLS gives the size for the whole nanoparticle including the hydrated coating and clusters if any exists. Intensity based size distribution of the samples shows peaks at the same small sizes as well as a second peak around 250 nm (data not shown). These solutions were filtered from 20 nm syringe filters and all peaks remained unchanged. Therefore, we believe that they are not hard aggregates. Therefore, for simplicity and better relation to crystal size we preferred to use number averaged values for the comparison.

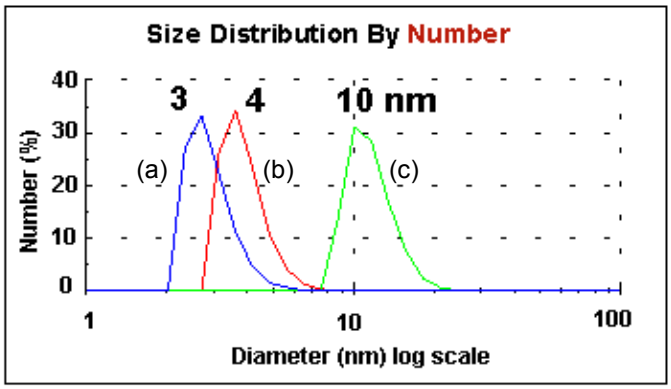

Figure 3.10 Size distribution by number of the CdS nanocrystals synthesized at 60 ºC: (a) blue: CdS-PAA/MAA (80/20), (b) red: CdS-MAA and (c) green: CdS-PAA.

DLS study of the reaction mixture right before Na_2S addition revealed an interesting phenomenon (Figure 3.11). Hydrodynamic size of the complex formed with PAA/MAA mixture is much smaller than pure PAA or MAA system. Same trend was observed in intensity and volume based averages (data not shown) which supports formation of a ternary compact complex of cadmium with PAA and MAA, may be regarded as a nano-container.

Formation constant of Cd-SR complex is much larger than Cd-OOCR (log K_{CdSR} = 11.5, log K_{CdOOCR} = 3.2).[92] So, more Cd-SR complex can be formed. However, when both surfactants are available in the solution complexation with both is expected. Complexation of Cd^{2+} with carboxylates of different chains as well as complexation of many Cd^{2+} with carboxylates of the same chain creates a rather compact structure. DLS indicates much more collapsed structure for the ternary system. H-bonding between PAA and MAA might be one of the possible reasons for the smaller structure formed. Details of the ternary complex are not clear to us at the moment. Nucleation and growth with existing Cd-SR complexes would follow a cluster-cluster aggregation, yet existence of a surrounding large multidentate molecule (PAA), imposes a kinetic control as discussed for CdS-PAA.

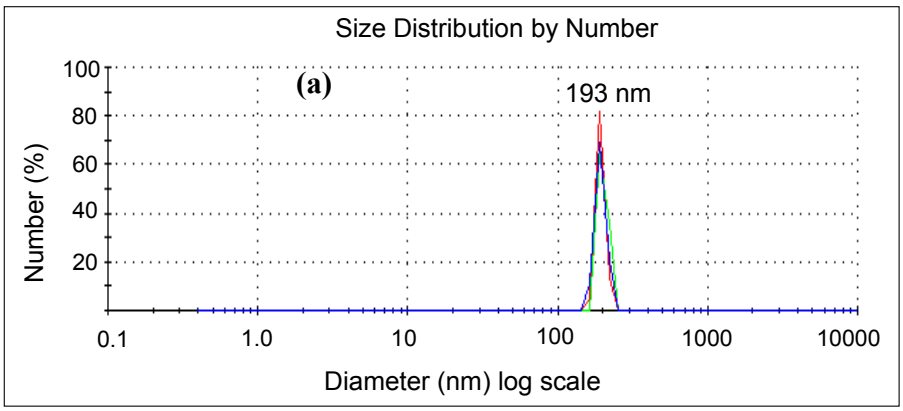

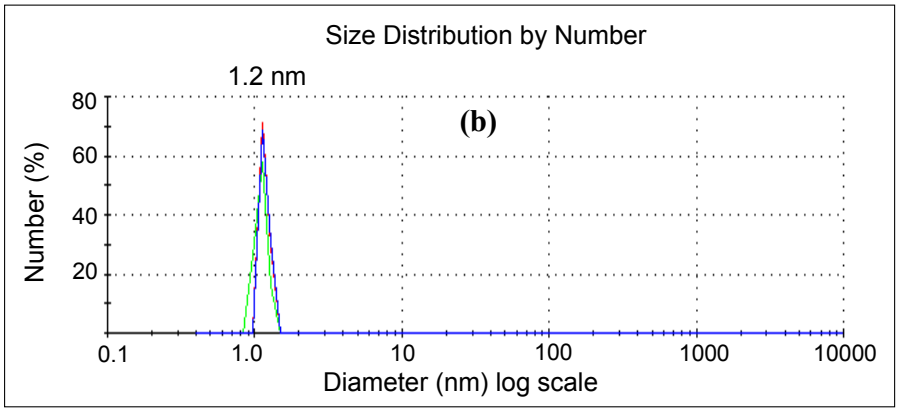

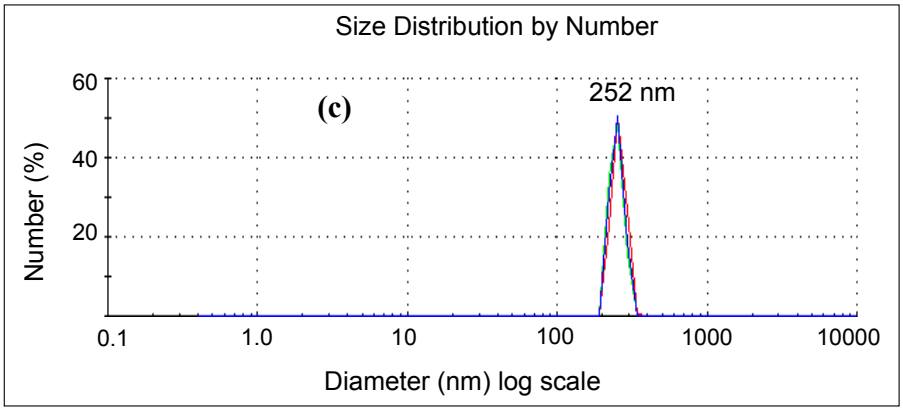

Figure 3.11 Size distribution by number measured by DLS: (a) CdS-PAA (b) CdS-PAA/MAA 80/20 and (c) CdS -MAA- nanoparticles at 60 ºC. Three runs for each sample were performed.

Therefore, particles prepared with the binary surfactant system are always smaller than CdS-MAA and particles prepared with high PAA content shows more limited growth at high temperature. PL maximum size shows a minimum at around 40-60% PAA. This should provide the best balance between the Cd-SR, Cd-OOC complexes as well as the thermodynamic and kinetic control of the growth (Figure 3.8b).

3.4 Optimization of the photoluminescence for PAA/MAA-CdS

In chapter 2 and 3, we analyzed two different variables on the size and QY of CdS QDs. In chapter 3, influence of PAA/MAA ratio was studied at a fixed COOH/Cd ratio of 11. Highest QY was achieved at 40/60 (PAA/MAA). In chapter 2, investigation of the relationship between the COOH/Cd ratio and the QY, indicated an optimum ratio of 2. When the results of these two studies are evaluated, QY of the PAA/MAA coated system is expected to improve when COOH/Cd ratio is reduced to 2. In order to test this assumption and to improve the luminescent properties of the QDs, PAA/MAA-CdS was prepared at 40/60 PAA/MAA ratio and COOH/Cd=2. The experimental and characterization procedures are same as detailed in section 3.2.

There is a clear blue shift in the UV-Vis absorbance spectrum of the CdS QDs prepared at COOH/Cd ratio of 2 compared to those prepared at the ratio of 11 (Figure 3.12). The size of the CdS decreased from 2.6 to 2.2 nm with the reduction of the coating amount to the optimized value. Nanocontainers formed between PAA, MAA and Cd^{2+} ions before the reaction is possibly smaller at lower coating loadings since more cation will form a complex with the –COOH. At lower doses of PAA, more Cd^{2+} can be bound to a single PAA molecule and collapse system due to charge neutralization more dramatically than a PAA loaded with less number of Cd^{2+}. In a smaller cluster, it is possible to have smaller crystals with better surface coverage.

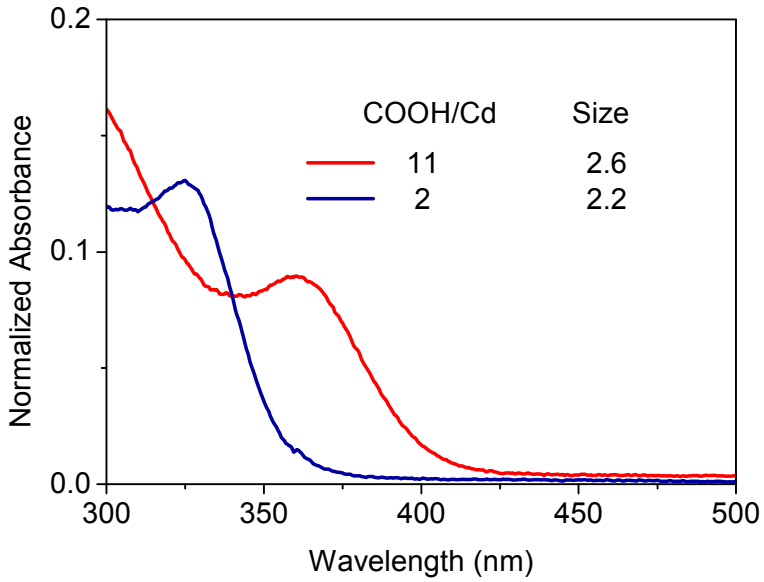

Figure 3.12 Uv-Visible absorbance spectra of PAA/MAA 40/60 – CdS at a COOH/Cd of 11 and 2.

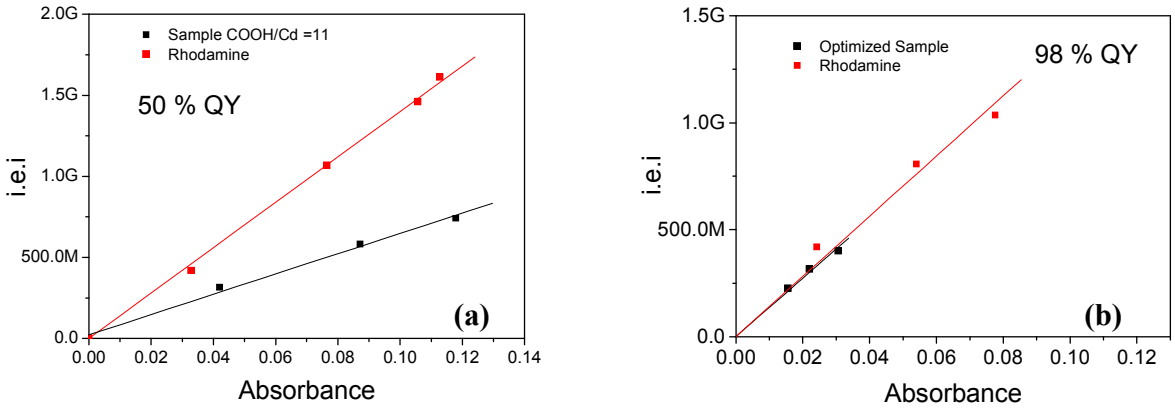

Figure 3.13 Calculation of QY for 40/60 PAA/MAA coated CdS at a COOH/Cd ratio of **(a)** 11.0 **(b)** 2.0

Optimization of the coating amount had a tremendous improvement in the QY. As seen in Figure 3.13, the QY of the optimized sample (b) was doubled with respect to the QD synthesized at the COOH/Cd of 11 (a). Figure 3.13 indicates the total integrated emission intensity of the QDs and the reference (Rhodamine B) at three different concentrations. The dramatic enhancement in the luminescence is clearly seen in the absorbance calibrated luminescence data (Figure 3.14). *QY of 98% is so far the highest that we have seen in the literature for an aqueous CdS QD.*

This increase in QY may partly represent smaller crystal size but a better surface passivization as well. If crystals do have significant amount of surface defects this would be more detrimental in a smaller particle where surface/volume ratio increases significantly. In chapter 2, COOH/Cd ratio of 2 was suggested to provide the best balance for the complexation of cadmium ions and growing surface, reaction on the surface of the crystal and diffusion limited growth. Density of –COOH groups and coating composition of the crystal surface should be studied in detail in order to understand the effects better.

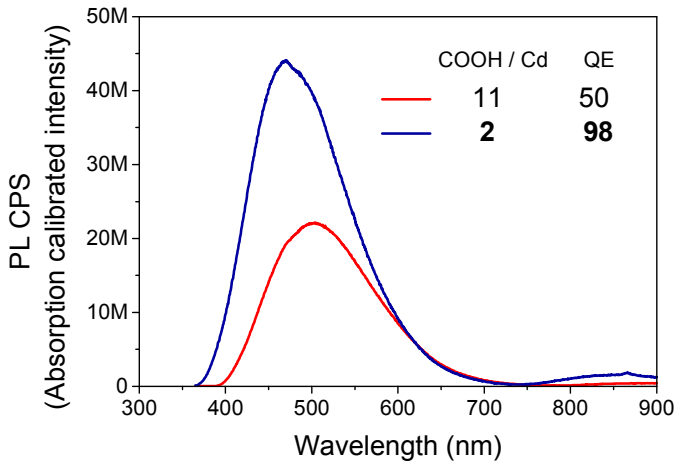

Figure 3.14 PL spectra of of PAA/MAA 40/60 – CdS at a COOH/Cd of 11 and 2. (QY is in the form of %)

3.5 Conclusions

In this study, we demonstrated the first examples of CdS nanoparticles capped with PAA/MAA binary mixture and investigated the influence of coating composition and temperature on particle properties. Compared sizes of the binary systems were relatively lower than those of PAA and MAA stabilized ones. Small size particles around green emission with relatively broad size distribution were obtained for all the binary coated particles except that the 80/20 PAA/MAA % coated one synthesized at 30 ºC which has relatively bluer emission compared to others. The X-ray spectra support cubic structure where peaks had a small shift towards higher two-theta values. Size of the crystals calculated by Brus eqn. from UV-visible spectra and measures from TEM images are comparable. TEM images indicate no excessive particle aggregation. It is also important to report that the highest fluorescence emission of the PAA/MAA–CdS was obtained at PAA/MAA ratio of 40/60. Particles size can be tuned at the expense of QY. Surfactant conformations and adsorption should be investigated further for better explanation of the dependence of size and QY to the composition. Observations suggest a synergistic effect of binary system in reducing the particle size around 2.5 nm and a fine tuning with temperature especially at compositions with less than 60 % PAA. The QY of the CdS QDs coated with the binary surfactant system can be improved further if COOH/Cd ratio of 2 is adopted in the light of the findings detailed in Chapter 2. So far, in an optimized composition of Cd/S, COOH/Cd and PAA/MAA ratios of 2.5, 2, 40/60, respectively, CdS QDs exhibit 98% QY (with respect to rhodamine B) which is the highest QY reported for the CdS QDs to the best of our knowledge.

Chapter 4

KINETIC STUDY OF THE PAA/MAA-CDS SYSTEM

In Chapter 3, synthesis and properties of PAA/MAA-CdS particles as a function of temperature and composition were discussed. In this chapter, we will discuss the growth kinetics of PAA/MAA-CdS system in detail.

4.1 Experimental section

CdS nanoparticles were synthesized at 30 ºC with 90/10 PAA/MAA at a Cd/S ratio of 2.5 and COOH/Cd ratio of 11 in water as described lengthily in Chapter 3.1. Na_2S solution was added in portions in every 5 min and addition is completed in 45 min. Reaction was tracked by taking 5 mL aliquot from the reaction mixture in every 5 min for the first 45 min and then in every 10 min. So, the first aliquot was taken out right before the addition of second Na_2S portion (Figure 4.1). Each aliquot was frozen in the refrigerator, immediately. Absorbance and luminescence of each aliquot were analyzed by UV-Vis spectrophotometer and spectrofluorometer as described in Appendix A and B.

4.2 Results and discussion

4.2.1 Synthesis of PAA/MAA (90/10) – CdS

Nucleation and growth of PAA/MAA (90/10) coated CdS were tracked by analyzing aliquots taken during sulfide addition and for the next 60 min. Addition of the full amount of Na_2S took 45 min, therefore the first nine aliquots represented the nucleation and growth during the sulfide addition. Next six aliquots were taken in 10 minutes intervals addressing

the growth kinetics after the completion of Na_2S addition. The last part was very important to understand how long the reaction needed to be continued.

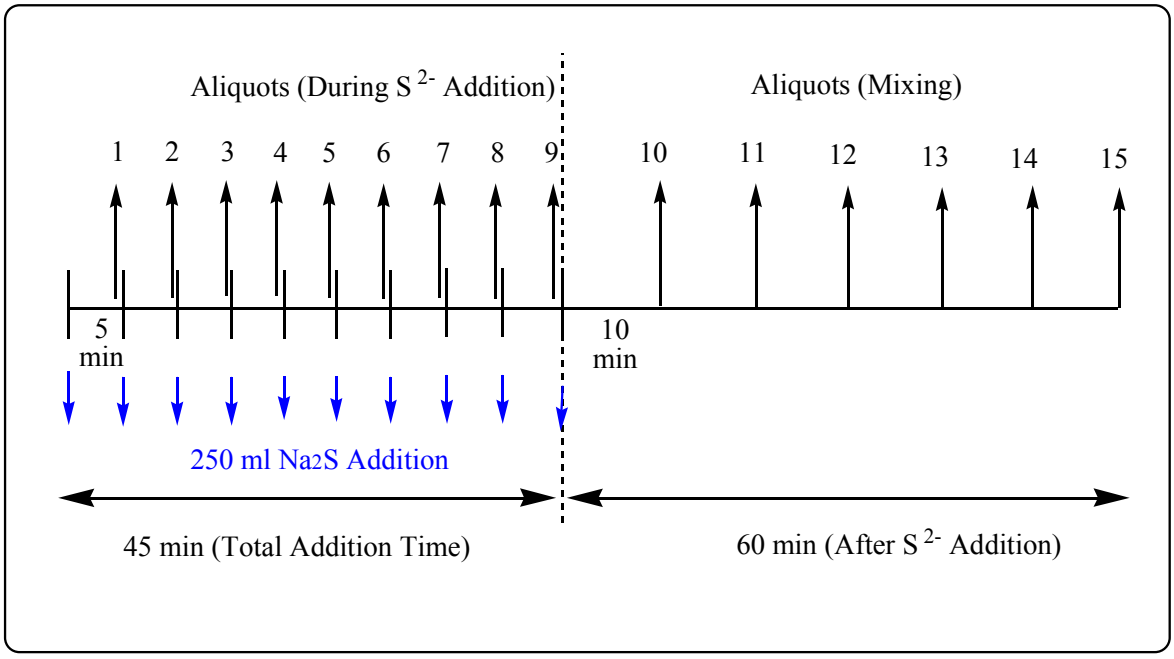

Figure 4.1 Schematic of the Na_2S addition and sampling sequence.

4.2.2 UV – Visible absorbance study of the aliquots

Figure 4.2 shows the absorbance spectra of the first six aliquots. Spectra of aliquots 1 to 5 are almost superimposable indicating no significant growth within the first 30 min of the reaction. We have stated in Chapter 3 that Cd^{2+} ions form complexes with PAA and MAA. Besides, based on the DLS data (Figure 3.11), we believe that a ternary compact complex is formed between the PAA, MAA and Cd^{2+} ions, which can be considered as nanocontainer (NC). This complex would be very important in the nucleation and growth. Almost identical spectra of the first 5 aliquots, where only half of Na_2S is added (roughly Cd/S=5), indicates the nucleation process. At this stage, as sulfide is added to the Cd-OOR

and Cd-SR complexes, S^{2-} replaces ligands to form Cd-S bond in a mechanism similar to ligand exchange.

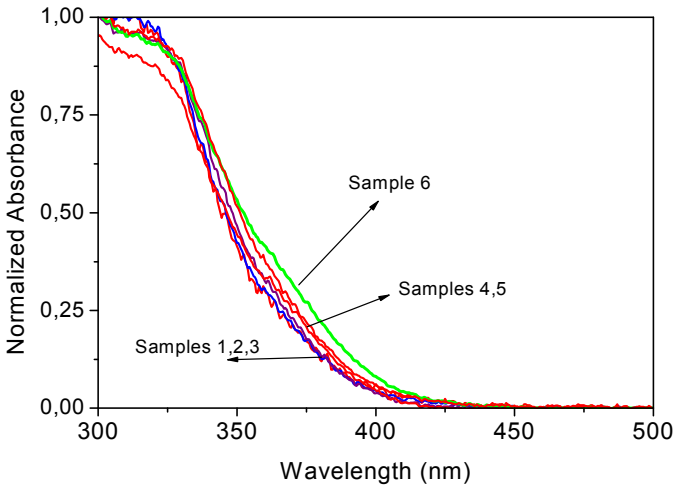

Figure 4.2 Normalized absorption spectra of the PAA/MAA (90/10) - CdS nanoparticles prepared at 30 ºC (samples 1-6)

A gradual red shift started after the addition of 6th portion of Na_2S (Figure 4.3), indicating major growth. No important red shift could be seen after the addition of 8th portion of the Na_2S (80 % of the full charge) and within the 50 min after the addition of last portion (Figure 4.4). It was interesting that in the last 20 min, for the last two aliquots, a blue shift was observed (Figure 4.4). We are not sure about the origin of the blue shift.

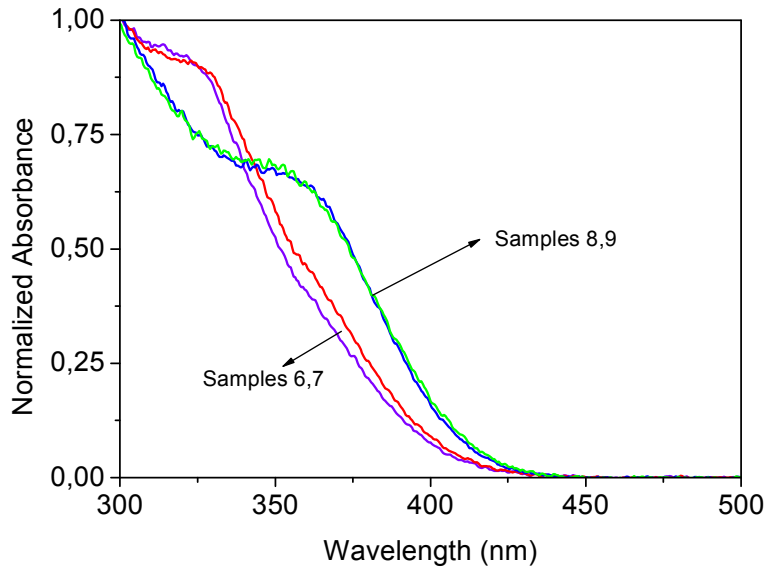

Figure 4.3 Normalized absorption spectra of the PAA/MAA (90/10) - CdS nanoparticles prepared at 30 ºC (samples 6-9)

Sizes of the QDs were calculated from the absorbance edge values of the samples using Brus equation as described in Chapter 1 and Appendix A. When the sizes of the nanoparticles were compared, a gradual increase in size during the addition of Na_2S was observed till 80 % of the Na_2S was added, and it stayed almost constant for the next 50 min of stirring and decreased afterwards. Particle diameter increased about 0.4 nm with respect to the starting point.

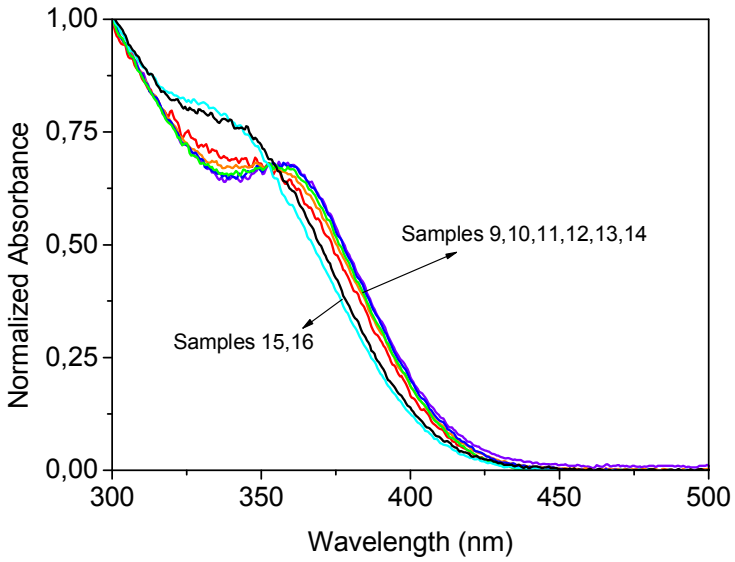

Figure 4.4 Normalized absorption spectra of the PAA/MAA (90/10) - CdS nanoparticles prepared at 30 ºC (samples 9-16)

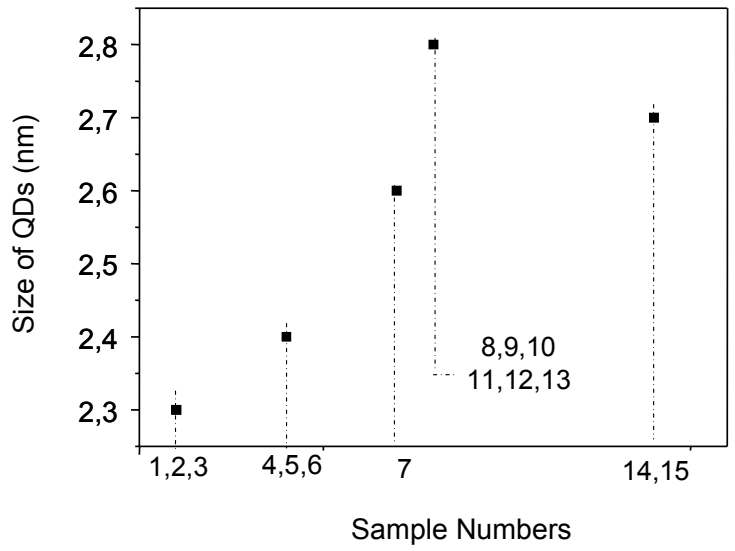

Figure 4.5 Size of the PAA/MAA (90/10) - CdS nanoparticles prepared at 30 ºC

Absorbance data and the calculated sizes indicated that particle size increases as Na_2S was added to the Cd^{2+}/PAA-MAA mixture. Major growth is possibly originating from S^{2-} addition on the crystal surface through a sort of ligand-exchange mechanism as well as Ostwald ripening process where the concentration of the Cd^{2+} and S^{2-} decreases, small crystals dissolve and add to the larger ones. This is generally accompanied by an increase in the particle size distribution. Figure 4.6 shows increasing FWHM during the Na_2S addition that confirms such discussion. During the mixing stage where all Na_2S is added, size does not change (Figure 4.5) but FWHM shows a slight decrease.

The trend observed in size was also accompanied with a linear red shift in the PL maximum during the S^{2-} addition (Figure 4.7). This is reasonable since the particle size is increasing during the S^{2-} addition.

However, after the sulfide addition was completed, a jump in the PL maximum occurred in more than 10 nm. The same jump was observed for the FWHM. Considering no significant size change for the majority of this time, an increase in the PL_{max} is quite interesting. During the 50 min stirring after full charge of sulfide is added, a regime of low precursor concentration is reached. During the earlier stages of the reaction, smaller particles grow faster than the larger ones, but as the concentration of the precursors decrease and majority of the crystallites reaches a critical size, smaller crystals slowly dissolve while the larger particles continue to grow. During the short time period right after full charge of the sulfide is added, it is possible to suggest such growth that can validate the jump seen in the PL_{max} and the FWHM. One possibility of not seeing a parallel increase in the size of the crystal could be due to the diffusion limited growth process exerted by the presence of PAA. We have discussed in Chapter 3 that cadmium ions form a ternary complex, rather collapsed, with MAA and PAA. Such network like structure may prevent diffusion of clusters at long distance. Dissolved species may add to the faster growing smaller sized particles, which could also account for the small decrease in the PL_{max} and FWHM during the mixing period.

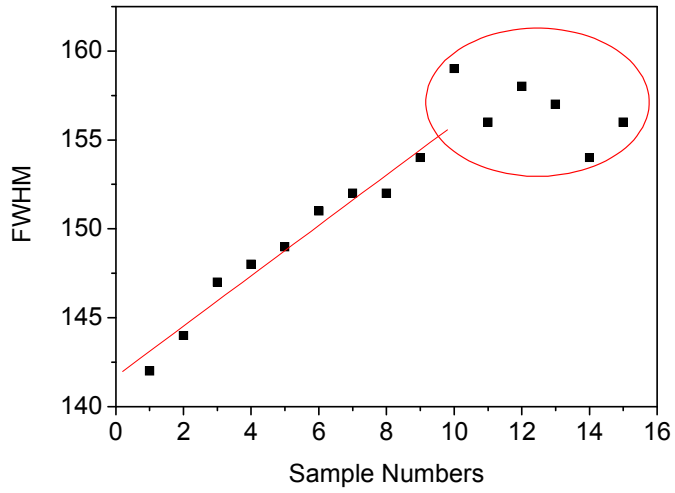

Figure 4.6 Full width at half maximum of the emission peak of the aliquots.

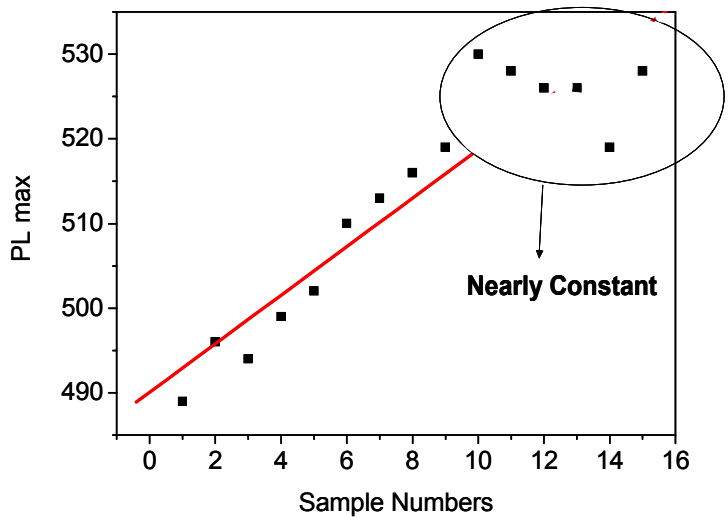

Figure 4.7 PL max shifts of the PAA/MAA (90/10) - CdS nanoparticles prepared at 30 ºC

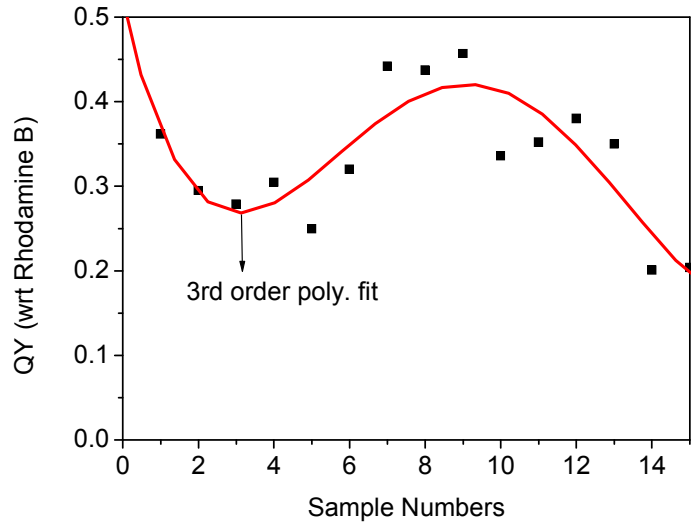

Figure 4.8 QY of the PAA/MAA (90/10) - CdS nanoparticles prepared at 30 ºC

In Figure 4.8, QY yield of all aliquots are shown. It is very interesting that QY reached maximum for samples 7 to 9 where particle size reachs 2.6-2.8 nm. For the smaller size particles, surface to volume ratio is relatively larger and surface defects are very important. These results indicate formation of CdS at around 2.6-2.8 nm with MAA/PAA coating of 90/10. However, the QY decreased considerably during the mixing period after S^{2-} addition is complete. It could be possible that, late growing crystals do not achieve good surface passivization with the organic coating, since the mobility of the coating is more restricted at the later stages due to already adsorbed segments. Last two data points are intriguing. If larger number of defects based on volume/surface ratio is considered, size and QY data are in agreement for these last two data points. Yet, it is not clear why the size of the crystal decreased in the last 10 min. One possibility could be the oxidation of the surface causing the blue shift of the PL maximum and absorption onset with the decrease in size. However, during the removal of aliquot, sufficient amount of air leaked into the reaction and surface oxidation results into the increase the in QY since CdO is a wider band-gap material (2.5

eV) surrounding the CdS core. On the contrary, QY decreased as well in that final 10 min. Besides, the reaction is run under continuous nitrogen blanket to eliminate the possibility of such processes.

4.3 Conclusions

NP synthesis in PAA/MAA binary surfactant system was investigated in detail. Evolution of the nanocrystals showed that at the initial stages of sulfide addition nucleation was the dominant process yet with increasing concentration of the sulfide, significant particle growth took place. Particle size remained constant at around 2.8 nm after 80% of the sulfide precursor was added. Mixing regime after the entire load of sulfide was added did not impact the size of the particle for about 50 min followed by a slight decrease afterward. Reason of such decrease is not clear, yet. Size and the particle size distribution increases during the sulfide addition as a result of particle growth. Yet, particle size reaches a plateau around 2.8 nm. QY of the samples initially were the same however, particle growth also increased the QY. After the completion of the sulfide addition, QY was gradually decreased unexpectedly which may be resulted from the ineffective passivization of the surface of the particles. It has been shown that the FWHM and the PL_{max} of the aliquots were increased as the particles grow. These nanoparticles had a green/blue emission which was not compatible with the large size distribution.

The most important observation was the decrease in QY during the mixing after S^{2-} addition. In chapter 3, Figure 3.8a, the QY of 90/10 (PAA/MAA) was reported as 0.2. The QY for the same composition here was 0.18 which was in agreement with the previous finding. The ratio between two aliquots taken right after all sulfide was added and after 60 min mixing was 0.5/0.2 = 2.5. This suggests a dramatic improvement in the QY when the reactions can be stopped short after the sulfide addition.

Chapter 5

MAGNETIC AND LUMINESCENT HYBRID NANOPARTICLES

5.1 Introduction

MQD can be used for a variety of applications since they can be tracked both optically and magnetically. They can be used as bimodal contrast agents. The mentioned nanoparticles can be attached to various drugs and molecular labels for target specific therapy and therapy (Figure 5.1).

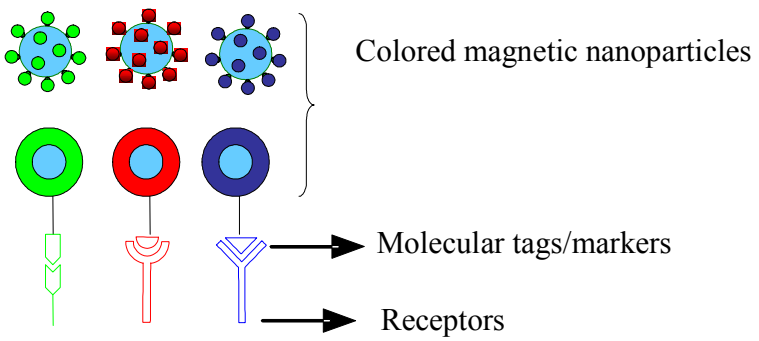

Figure 5.1 Schematic of magnetic nanoparticles labeled in different QD colors and representative molecular tags.

In the preparation of the MQDs, we desire to eliminate the ligand and solvent exchange processes that changes the particle properties in an undesirable way as discussed in length in chapter 1. Therefore, synthesis of both particles in water with a compatible surfactant

was attempted in this study. Stabilization of CdS QDs with PAA provides a valuable opportunity for the construction of MQDs since PAA is an effective coating for SPIOs as well. Demirer, in her MS thesis, reports a detailed study on PAA stabilized SPIOs.[1] Conditions that are most suitable for the preparation of different size (color) QDs with high QY and different size MNPs need to be determined to provide colloidally and optically stable colored SPIOs.

In general, MQD synthesis is non-trivial and both synthesis and characterization is relatively harder than the individual QD or MNP systems. Based on the experience gained with QD and MNP systems, reaction concentration, surfactant to cation ratios and reaction temperature are important parameters to control and optimize. Besides, QD/MNP ratio would be crucial as well.

Our ultimate desire was to develop a single pot methodology for the MQD synthesis. The critical problem in such approach is the choice of the surfactant. It should be water soluble, able to stabilize both CdS and iron oxide nanoparticles and last but not the least should form a stable colloidal suspension. PAA seems to satisfy these requirements. Especially when used with MAA, highly luminescent and stable QDs can be obtained. CdS QDs developed and detailed in previous chapters were used for the MQD preparation.

We considered two different approaches for the synthesis of MQDs;

1. *Synthesis of QDs in aqueous MNP solution.* However, when mercaptoacetic acid (MAA; stabilizer for CdS) is added into PAA coated Fe_3O_4 solution, all Fe_3O_4 decomposes in five minutes. MAA acts as an etching agent for the iron oxide and makes this approach quite problematic for the MQD synthesis. Another potential problem seems to be the synthesis of small CdS nanoparticles (1-5 nm) in a relatively narrow size distribution around the bigger SPIOs. Considering that main color differentiation will depend on the QD, control of the size and the color is very important and easier if QDs are prepared separately.
2. *Synthesis of MNPs in aqueous QD solution.* This requires the preparation of aqueous CdS first which ensures the quality (QY), size and the color of the QD. Iron oxide

nanoparticles can then be synthesized in CdS solution. Coating provided for the CdS would also stabilize the iron oxide. It is crucial to choose the right surfactant and the sufficient amount since both of these influences the QY of the QD and the size of both QDs and MNPs.

In an effort to produce MQD in a process that would eventually support a one-pot synthesis, adaptation of the second strategy will be discussed in this chapter. At the end of the chapter, suggestions for the following work will be detailed for successful synthesis and characterization of MQDs.

5.2 Experimental section

5.2.1 Materials

All chemicals were analytical grade or of the highest purity available. Sodium sulfide trihydrate ($Na_2S{\cdot}3H_2O$) and cadmium acetate twohydrate ($Cd(Ac)_2{\cdot}2H_2O$), rhodamine B, acetic acid (99.8 %), mercaptoacetic acid (MAA) were purchased from Merck. Iron (III) chloride hexahydrate ($FeCl_3{\cdot}6H_2O$) and iron (II) chloride tetrahydrate ($FeCl_2{\cdot}4H_2O$) were supplied from Fluka. Ammonium hydroxide (26% NH_3 in water, w/w) was purchased from Riedel-de Haen. NaOH pellets and poly(acrylic acid) sodium salt (PAA, Mn 2100) were purchased from Aldrich. Doubled distilled Milli-Q water (Millipore) was used as solvent.

5.2.1.1. Preparation of Fe_3O_4-CdS

In system, SPIOs were prepared in aqueous CdS solutions prepared ahead of time. For the synthesis of iron oxide nanoparticles, experimental procedure developed by Demirer and Acar was adopted. [40] In a typical synthesis, 50 ml PAA or PAA/MAA coated CdS QD solution put into 100 ml 3-necked round bottom flask and deoxygenated. Required amount of $FeCl_3{\cdot}6H_2O$ and than $FeCl_2{\cdot}4H_2O$ was added to the solution (Table 5.1). This addition sequence is important. The pH of the CdS solution is around 8.0. Addition of Fe^{3+} lowers the pH to ca 2.0. The effect of the pH decrease is different for PAA and MAA/PAA coated CdS solutions. In PAA coated CdS, pH drop is accompanied by the formation of white-yellow insoluble complex. At this pH, no iron oxide nanoparticle formation was

observed, expectedly. Then, Fe^{2+} is added to the solution. However, if it was added first, pH of the reaction mixture would maintain and at this pH (ca 8), iron oxide would start to form in an uncontrolled fashion. The different acidic behavior of the iron ions is responsible from such difference in behavior. The formation of the Fe_3O_4 nanoparticles starts by the injection of the ammonium hydroxide to the iron salt solution. At this stage, PAA is added as an excess surfactant. MAA, however, can not be added since free MAA groups react with iron ions forming iron sulfide. The solution is deoxygenated for 15 minutes by using a slow nitrogen flow. Then, the solution is heated to 85 ºC and charged with required amount of NH_4OH with rapid injection. The color of the solution turned into black immediately. The system was left 30 minutes for stabilization and growth and then cooled down to room temperature.

Table 5.1 Specifications for the magnetic QD synthesis.

	COOH/Fe		
	1.01	1.61	2.03
$Cd(NO_3)_2$▪4H2O (mg)	64	64	64
Na_2S▪$3H_2O$ (mg)	25	26	25
PAA (2100) (mg)	**20**	**30**	**40**
Total Iron Conc (M)	0.030	0.030	0.030
$FeCl_3$▪$6H_2O$ (mg)	270.0	270.0	270.0
$FeCl_2$▪$4H_2O$ (mg)	100.8	100.8	100.8
PAA (2100) (mg) (excess)	0	0	0
NH_3 solution (25 %) (ml)	2.9	2.9	2.9
Starting Sol. Volume of corresponding QD sol. (ml)	50	50	50
Effective CdS- Iron Oxide Ratio (approximate)	3.2	3.2	3.2

5.2.1.2. Characterization of the nanocomposites

UV-visible absorption of the nanocrystals was recorded on a Schimadzu UV visible spectrophotometer in the 300-500 nm range. Particle sizes of QDs were calculated from absorption edges using Brus equation.[3] Photoluminescence measurements were performed on Horiba Jobin Yvon–Fluoromax 3 spectrophotometer at 355 nm excitation wavelength. DLS measurements were performed on a Malvern Zeta Sizer. Recorded sizes are the average of three subsequent measurements.

5.3 Results and discussions

5.3.1 Synthesis of MQDs

MNPs are prepared at around 80-90 ºC in water from iron salts in an aqueous colloidal solution of CdS where PAA was used as a coating. Since PAA can stabilize iron oxide crystals as well, PAA coated QDs would adsorb on the growing iron oxide crystal and/or iron oxide would form in the PAA network that partly stabilizes the CdS crystals as well. At the end, the same surfactant would stabilize both of the nanoparticles to create a hybrid structure. It is very important to note that during the MNP synthesis excess surfactant should not be used to eliminate the possibility of forming independent/unconjugated MNPs.

As demonstrated in previous chapters synthesis temperature of CdS influences the crystal size, therefore the color of the QD. An advantage of PAA coating of QD is the insensitivity of size to temperature. This otherwise not desirable property is essential in the preparation of hybrid nanoparticles where in the second step CdS QDs are taken to relatively higher reaction temperatures. Otherwise, all QDs could grow or aggregated into larger crystals where all compositions would emit red.

It is also necessary to make suitable selection for the total iron concentration and for the CdS to Fe_3O_4 ratio. Former is an effective factor in determining the size of the magnetic nanoparticles and the later in the fluorescence intensity. Demirer and Acar reported that

SPIOs of 100nm and less can be prepared at iron concentration of 3-30 mM at PAA/Fe ratio between 4-0.4.[40] Concentration of the CdS in the starting solution is 0.63 mM. Assuming that iron oxide molecules are in the form of Fe_3O_4, then total Fe_3O_4 concentration is 1 mM if the total iron concentration is selected as 3 mM.

Rosenzweig et al proposed the following equation to calculate the maximum number of QD that can be attached to an iron oxide nanoparticle considering a hexagonal packing on iron oxide surface.[34]

$$N_{QD} = \frac{2 \times \pi \times (R_{Fe_3O_4}{}^2 + R_{QD}{}^2)}{\sqrt{3} \times R_{QD}{}^2},$$

N_{QD}, $R_{Fe_3O_4}$ and R_{QD} are the number of QDs, radius of iron oxide and QD, respectively. N_{QD} is found as 30 if the same of the iron oxide and CdS crystal, are considered as 8 and 2.2 nm, respectively. However, there are two important points to be considered here: 1. this equation regards a single layer of QD coating around a single MNP and does not take the possible clusters into consideration. 2. This approach does not consider the coating as a globular structure where MNPs can be formed inside.

In practice, Cd/Fe molar ratio of 125 is tested here. When a smaller ratio is not used, particle stabilization is not successful and particles aggregated right after the synthesis. Among many difficulties one of the major one is the QY calculation of the MQD. Since iron oxide nanoparticles absorb the excitation radiation at 355 nm, the florescence emission decreases significantly. QY calculations for the QD can't be performed accurately with the current method. Moreover, since some of the fluorescence emission is absorbed by iron oxides, iron oxide concentration has to be determined and the fluorescence intensities should be calibrated with respect to the iron concentration determined by the ICP.

5.3.2 Absorbance and photoluminescence study of the MQDs

In Figure 5.3, absorption spectra of the PAA-CdS and the PAA-CdS-Fe_3O_4 prepared in three different PAA concentrations are shown. Absorbance edges of QD solutions as discussed in chapter 2 were not changed with COOH/Cd. In other words, all particles have the same size. The absorbance plots of MQDs do not provide information about the change in size of QDs, if any exist, since iron oxides absorb the incoming and emitted light, considerably.

Photoluminescence (PL) studies were carried out to determine qualitative luminescence of the hybrid nanoparticles and to investigate the change in the QD size during the MNP synthesis. In Figure 5.4 andFigure 5.5, PL maximum of MQDs (650 nm) are red shifted (50 nm) with respect to QD PL maximum (600nm). This shift indicates a corresponding size increase in QDs which can't be evaluated by the UV-visible spectra. Normally, the size of CdS crystal does not increase with the increasing reaction temperature when PAA used as a coating (Figure 3.5a). However, if partial desorption of the surfactant occurs, QDs may aggregate into larger ones during the iron oxide synthesis. The dominant reasons behind this phenomenon are also under investigation.

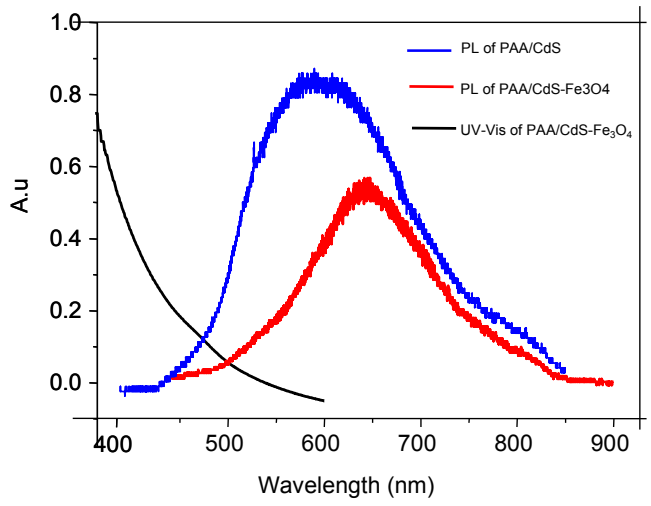

Figure 5.2 UV-Vis and PL plots of CdS-Fe_3O_4 and CdS QDs

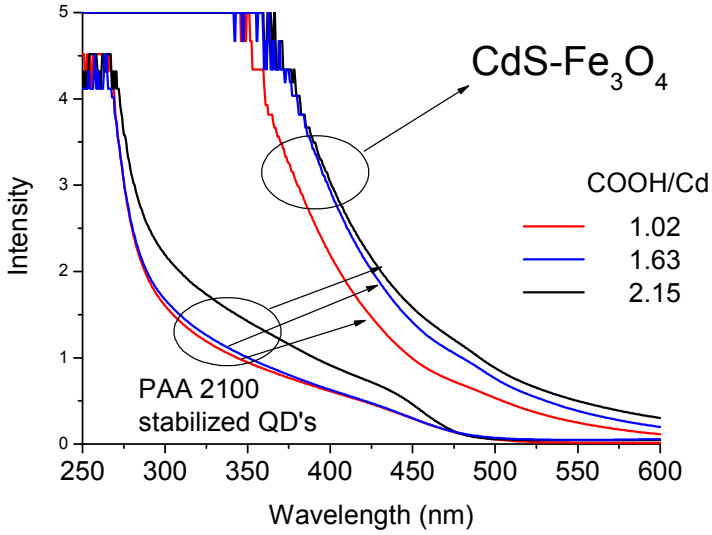

Figure 5.3 Absorbance spectrum of CdS coated iron oxide nanoparticles. (All ratios are kept constant)

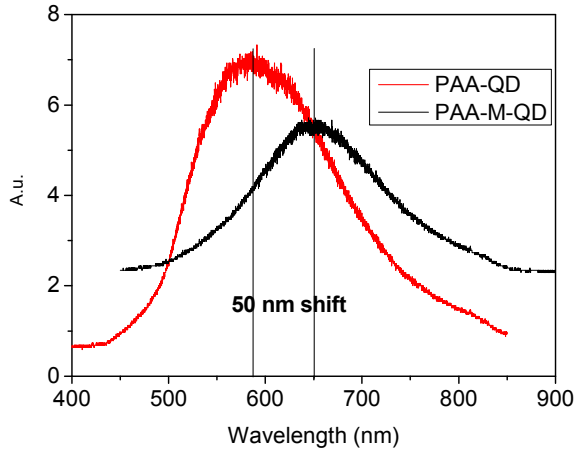

Figure 5.4. PL spectrum of (COOH/Cd=2.15) QD and MQD solutions. Cd/Fe=125 Cd/S=1.1, PAA 2100 is the surfactant. (Ratios are listed in molar otherwise stated.)

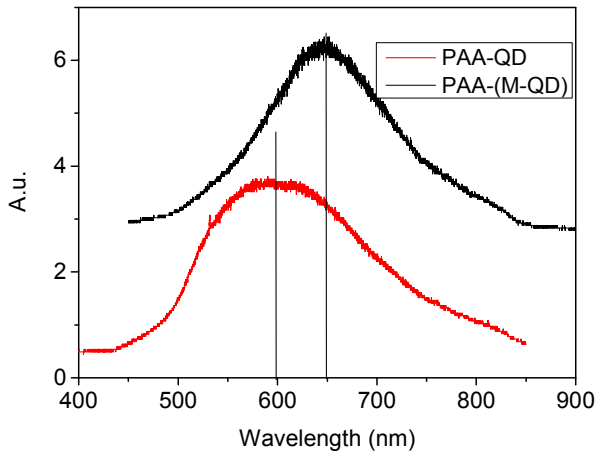

Figure 5.5 PL spectrum of (COOH/Cd=1.02) QD and MQD solutions.

Figure 5.6 shows these MQDs before and after UV illumination. It should be noted that the solution is not fluorescent in high MNP concentrations. However, when the solution is diluted, fluorescent QDs are easily detectable. Brown color of the MQDs are typical for SPIO solutions (Figure 5.6a). Orange luminescence under UV excitation shows the luminescence character (Figure 5.6b).

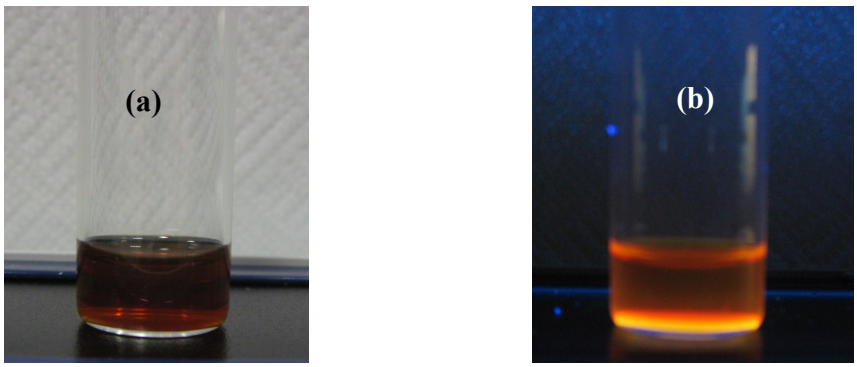

Figure 5.6 Pictures of MQDs a) before illumination b) after illumination with 366 nm UV-lamb.

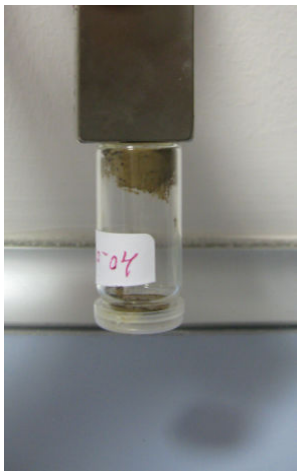

Figure 5.7 Representation of the magnetization strength of dried powder of MQD.

Improvement in MQDs has been achieved by adopting PAA/MAA coated CdS. Dried powders of MQD PAA/MAA ratio of 40/60 and a COOH/Cd ratio of 2 were rinsed with isopropanol under magnetic field to remove any unbound QD. Figure 5.7 shows the response of these particles to magnetic field. In Figure 5.8a and b, size distributions of QDs and MQDs are shown. In MQD solution, there is no particle population around 2-5 nm as found in QD solution. This may be an important indication for the binding of the QDs onto MNPs.

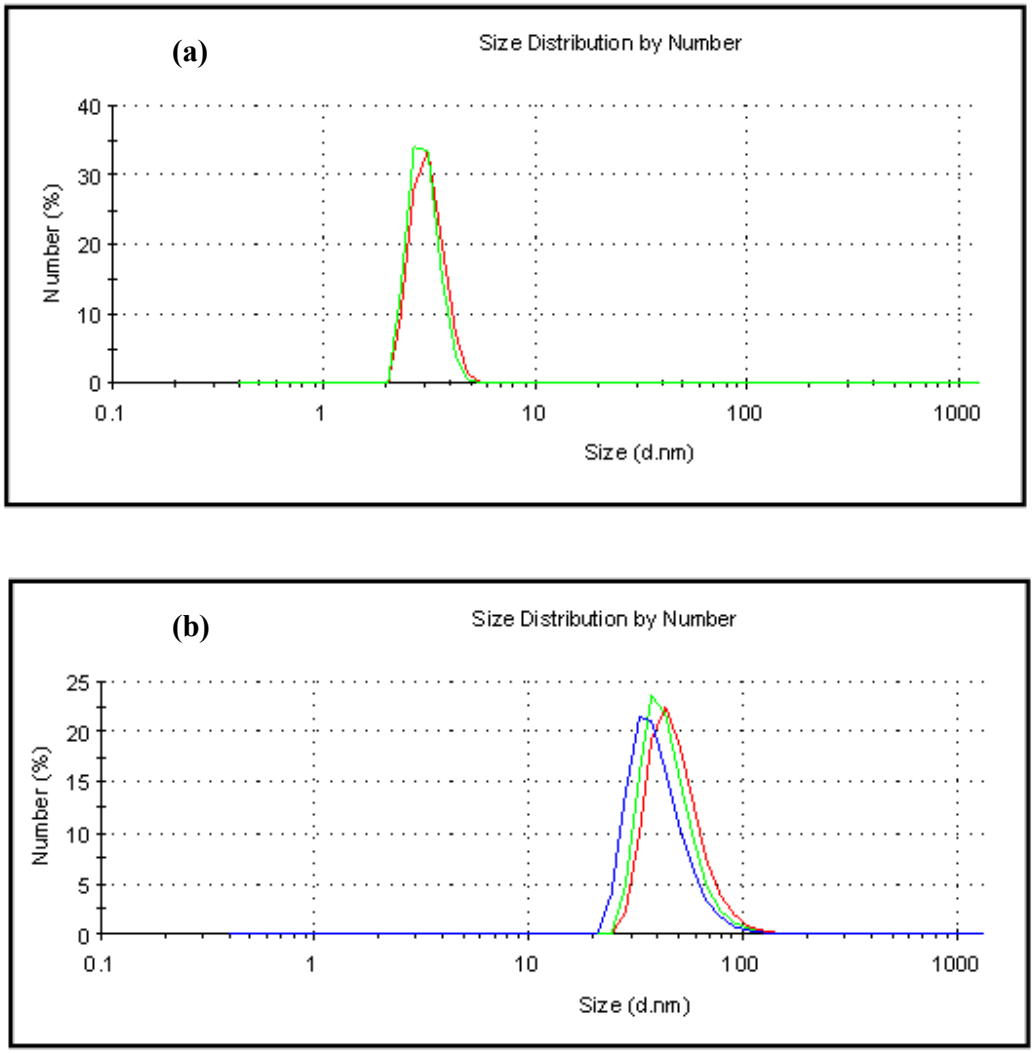

Figure 5.8 DLS plots of a) QD and b) MQD solutions.

5.4 Conclusions and future suggestions

In this chapter, we discussed the first one-pot examples of PAA capped MQDs and investigated the influence of PAA amount on particle size, and Fe_3O_4/CdS ratio on the fluorescence of the MQDs, qualitatively. Our experience on the MQD synthesis showed that without the use of excess surfactant, MQDs are stable whereas excess surfactant addition results into precipitation of the particles (data not shown). At high concentration of iron oxide, detection of luminescence is hindered as iron oxide absorbs strongly in the visible region. Future investigations should be concentrated on the effective QY determination and calibration of the MQD fluorescence. If the amount of the absorption by MQDs is known, then QY of the QDs can be compared with QY of the individual QDs. In order to obtain different colored MQDs by applying this method, iron oxides should be synthesized in pre-characterized QD solutions in different colors since the control of the QD reaction is rather difficult than iron oxide nanoparticle reaction.

Chapter 6

CONCLUSIONS

Primary focus of this thesis was the development of CdS QDs in a simple aqueous and environmentally safe method. For this purpose, PAA coated CdS nanoparticles (CdS-PAA) were investigated in detail in an effort to achieve such goal. This first in-depth study of PAA-CdS nanoparticles, revealed important and surprising characteristics of the system: CdS nanoparticles can be easily stabilized by PAA through carboxylate adsorption on the crystal surface. Nanoparticles surrounded by the polymeric network have superior long-term colloidal stability over the monomeric surfactants such as MAA and MPA. Unbound carboxylates provide aqueous dispersions and functional surfaces where electrostatic repulsion between particles is effective. PAA molecular weight, COOH/Cd ratio, Cd/S ratio, reaction pH and reaction temperature were studied to investigate the influence of such factors on QD properties as means to control and tailor particles for desired applications. In chapter 2, we demonstrated that Cd/S ratio over 1 is required for practical QY and colloidal stability. Reaction pH around 7.5 is desirable where the PAA is mostly deprotonated. When molecular weight of the PAA is considered many short chains were more effective in surface passivization than few longer chains. Therefore, reactions at pH 7.5 with PAA of 2100 g/mol at Cd/S ratio above 1 emerged as the preferred variables for the preparation of stable and luminescent CdS nanoparticles in water. Regardless of the PAA molecular weight or reaction pH, PAA-CdS NPs were luminescent in color emissions between yellow-orange with absorption edges ranging from 460 to 508 nm. As discussed in chapter 2, ability to tune size and emitted color is relatively limited with respect to MAA

capped CdS nanoparticles. Polymeric nature of the coating is discussed as the source of such behavior. Although more stable than the thiol stabilized CdS, luminescent properties of PAA coated CdS are inferior to MAA-CdS. QYs around 5-17 % were achieved with PAA coating, possibly due to less effective passivization of the CdS surface with the carboxylate groups. Most spectacular result of the experiments is the determination of the carboxylic acid concentration which gives the highest QY. By considering the colloidal stability, optimum COOH/Cd ratio was determined as 1.5-2.0 for both molecular weights and different pH values.

In chapter 3, CdS NPs capped with PAA/MAA binary surfactant system were studied and the influence of coating composition and reaction temperature on the particle properties was investigated. Such strategy was followed in order to combine the good properties of MAA and PAA coated particles together to get colloidally stable, highly luminescent nanoparticles in tunable sizes. Increasing reaction temperature increases the crystal size and dramatically decreases the QY of MAA-CdS nanoparticles. On the contrary, PAA coated nanoparticles do not get influenced from the reaction temperature as much. Again, monomeric versus polymeric coating nature was discussed as an important contributor in such difference in their response to temperature. When the mixed coating was adopted, surprisingly, sizes of the particles were rather lower than those of MAA-CdS or PAA-CdS, and QYs were higher than PAA-CdS nanoparticles. Moreover, at some compositions QYs as good as MAA-CdS nanoparticles were achieved. Maximum QY was obtained at PAA/MAA-40/60. It is possible to tune size and color at this composition by changing the reaction temperature with penalty in QY. Further improvement to the PAA/MAA-CdS nanoparticles was achieved by adjusting the COOH/Cd ratio to 2 as this ratio emerged as the optimum ratio for the best QY in Chapter 2. Such optimization of the system increased QY from 50 % to almost 100% (with respect to Rhodamine B) at PAA/MAA 40/60. Optimization of the coating amount and surfactant ratios provided a synergy and allowed to prepare stable CdS QDs in water with small and tunable sizes and in high QY, as good as Rhodamine B, so far.

In chapter 4, kinetics of 90/10 PAA/MAA coated CdS synthesis was investigated in order to understand the size, FWHM, QY and PL_{max} changes during the reaction (addition of sulfide) and mixing (after all reagents were introduced). A continuous increase in size was observed as the sulfide is introduced slowly to the PAA-Cd solution, yet the crystal reaches its final size at about 80 % of the total sulfide addition. Highest QY was reached at the end of the sulfide addition and shows a downward trend during the post addition mixing (1h). Ratio of the QY after 1 h mixing and right after full amount of sulfide introduction is 2.5. Considering this, it should be possible to improve the QY of all particles dramatically when the reactions are quenched shortly after sulfide addition is over. This assumption is under investigation.

Secondary focus of this thesis is preparing hybrid nanoparticles of dual character, namely *MQDs*, or *fluoresencent SPIOs*. MAA is not an appropriate coating for SPIOs but PAA is. Ability to achieve CdS QDs of good stability and QY with PAA and relative insensitivity of PAA coated nanoparticles to temperature is invaluable in the design and preparation of such hybrid structures. In chapter 5, first examples of PAA capped MQD is reported. Besides, this is the first *one pot synthesis* reported for such hybrid structure. System has few drawbacks to be resolved: MQD absorbs the light emitted from the QDs that decreases the observed luminescence of the hybrid nanoparticles. This makes blue emitting MQDs and QY calculations difficult. Yet, system is suitable for the development of green, yellow and red luminescing MQDs with further adjustments in composition and reaction temperature.

The ultimate goal of the project is to develop hybrid MQD nanoparticles in aqueous system. In order to achieve such goal, QDs with high QY in tunable sizes needed to be achieved with a coating that is also suitable for the iron oxide nanoparticles. Then, the proposed method for the hybrid MQDs can be followed. Our investigations are at the point of obtaining MQDs of various colors. However, there are some difficulties in the characterization of MQDs that need to be overcome and some non-trivial points to be considered in the construction of the hybrid system in the future.

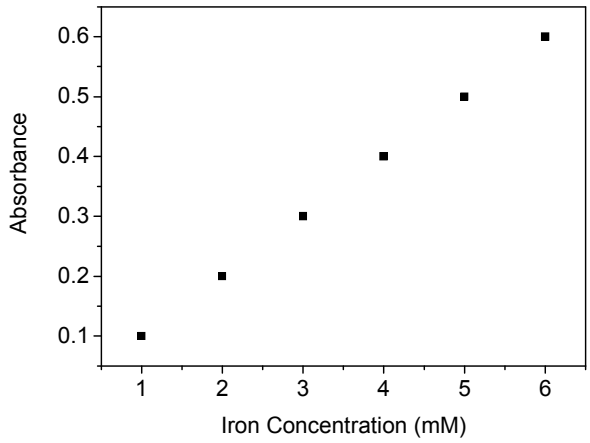

Figure F Concentration dependence on luminescence of SPIOs

For QY calculations, quantity of the absorbed photons at the excitation wavelength by the CdS needed to be known. This is not trivial since iron oxide starts to absorb at longer wavelengths than CdS covering also the whole range absorbed by the CdS. In order to quantify the amount absorbed by CdS, amount of absorption by the iron oxide needed to be determined. This can be done by an investigation of the concentration dependent absorption of iron oxides at the excitation wavelength. A theoretical plot is provided in Figure F.

Iron oxide content of the MQD can be determined on the etched samples by inductively coupled plasma (ICP) and the absorption amount originating from the iron oxide content can be determined using the absorption-concentration plot of the iron oxide. However, one should always remember that the observed luminescence will be lower than the initial QD solutions since SPIOs absorb the fluorescence light considerably. When the QD emission is in red, higher luminescent MQDs can be obtained since the absorption of SPIOs is rather low at that wavelength. Use of QDs with absorption and emission wavelength at longer wavelengths than CdS, such as CdSe and CdTe, may be used alternatively.

Appendix A

CALCULATION OF NANOPARTICLE DIAMETER FROM ABSORBANCE SPECTRUM

A-1 Introduction to absorption spectrophotometry

Ultraviolet-Visible (UV-Vis) spectroscopy is a type of optical spectroscopy technique which gives information about the structure of a material in the solution. Absorption spectra are produced when ions or molecules absorb electromagnetic radiation in the ultraviolet or visible regions. The intensity of the absorption peak varies with the number of the molecules (concentration) of the material in the solution.

We have scanned our samples between 300-700nm which covers the range where our QDs absorb.

A-2 Application of the Brus equation

In 1984, Brus proposed an equation to estimate the particle size of the nanoparticles from their absorption edges. The equation (A-2.1), which is also called as the "*effective mass approximation (EMA)",* was based on quantum well approximation and coulombic interactions between the atoms. Equation A-2.1 is the expanded form of the equation 1.4 presented in chapter 1.

$$\Delta E = \left(\frac{\hbar^2\pi^2}{2R^2}\right)\left(\frac{1}{m_e}+\frac{1}{m_h}\right) - 1.8\frac{e^2}{\varepsilon_{CdS}\times 4\pi\varepsilon_0\times R} \quad \text{EMA [3, 93] approximation.} \qquad \text{(A-2.1)}$$

The simplified form of equation (A-2.1) can be written as

$$A = B - C\,, \qquad \text{(A-2.2)}$$

where A, B and C define the band gap difference, quantum well approximation term and coulomb interaction term, respectively.

For CdS core, $m_e = 0.3m_0$, $m_h = 0.8m_0$, $\varepsilon_{CdS} = 5.7$, $\varepsilon_0 = 8.854\times 10^{-12}\,\frac{F}{m}$ (A-2.3)

$$m_0 = 9.10938188 \times 10^{-31}[\text{kg}] \qquad \text{(A-2.4)}$$

$$\hbar = \frac{h}{2\pi} = 1.054571\times 10^{-34}[J.s] \quad \text{or} \quad \hbar = \frac{h}{2\pi} = 6.582119\times 10^{-16}[eV.s] \qquad \text{(A-2.5)}$$

A-2.1 Calculation of band gap difference

$$\Delta E = E_{Nanocrystal} - E_{Bulk} \qquad \text{(A-2.6)}$$

The Planck equation for the calculation of the band gap energy is given as;

$$E_{nanocrsytal} = \frac{hc}{\lambda} \qquad \text{(A-2.7)}$$

By using (A-2.7), band gap of our particles can be calculated with the following equation.

$$E_{nanocrsytal} = \frac{hc}{\lambda} = \frac{6.582119\times 10^{-16}[eV.s]\times 2\pi\times 3\times 10^{8}[\frac{m}{s}]\times 10^{9}[\frac{nm}{m}]}{\lambda_{nm}} = \frac{1240.7[eV]}{\lambda_{nm}} \qquad \text{(A-2.8)}$$

From (A-2.6), (A-2.8) and considering $E_{Bulk} = 2.42\ [eV]$ for CdS [85]

$$A = \Delta E = \frac{1240.7eV}{\lambda_{nm}} - 2.42[eV] \qquad \text{(A-2.9)}$$

λ_{nm} is the absorbance edge which can be found from the UV spectrum of the sample as shown in Figure A-1.1. First, a linear line is drawn from the linear region of the absorbance plot (blue linear line). Then, the red line from the reference region is plotted and the intersection point of the blue and red lines gives the absorption edge of the sample.

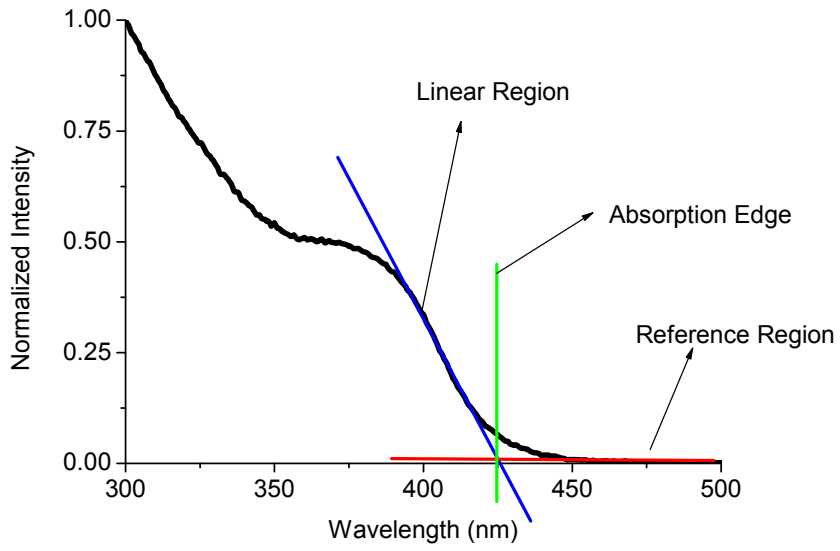

Figure A-1.1 Representative plot for the determination of the absorption edge.

A-2.2 Calculation of the second term (Quantum well approximation)

$$\mathrm{B} = \left(\frac{\hbar^2\pi^2}{2R^2}\right)\left(\frac{1}{m_e}+\frac{1}{m_h}\right) \tag{A-2.10}$$

$$[eV] = 1.60\times10^{-19}[j] = 1.60\times10^{-19}[\frac{kg\times m^2}{s^2}] \tag{A-2.11}$$

$$\varepsilon_0 = 8.854\times10^{-12}[\frac{F}{m}] = 8.854\times10^{-12}[\frac{C\times V}{m}] \tag{A-2.12}$$

by combining (A-2.3), (A-2.4), (A-2.5) and (A-2.10)

$$B = \left(\frac{(6.58\times10^{-16}[eV.s])^2 \times \pi^2}{2(R_m)^2} \right)\left(\frac{1.1}{0.24\times9.11 \times 10^{-31}[\text{kg}]} \right)$$

$$B = \left(\frac{(4.27\times10^{-30}([eV.s])^2}{2(R_m)^2} \right)\left(\frac{5.031\times10^{30}}{[\text{kg}]} \right)\times\left(\frac{[kg\times m^2/s^2]}{[\text{j}]} \right)\times\left(\frac{1.6\times10^{-19}[j]}{[\text{ev}]} \right)$$

$$B = \frac{1.719\times10^{-18}[eV]}{(R_m)^2} = \frac{1.719[eV]}{(R_{nm})^2} \qquad \text{(A-2.13)}$$

A-2.3 Calculation of the third term (Coulomb interaction)

$$\text{C}=1.8\frac{e^2}{\varepsilon_{CdS}\times4\pi\varepsilon_0\times R_m} \qquad \text{(A-2.14)}$$

by combining (A-2.3), (A-2.12) and (A-2.14)

$$C = 1.8\frac{([eV])^2}{5.7\times4\pi\times8.854\times10^{-12}[\frac{CV}{m}]\times R_m}$$

$$C = 1.8\frac{([eV])^2}{5.7\times4\pi\times8.854\times10^{-12}[\frac{CV}{m}]\times R_m}\times\frac{[CV]}{[j]}\times\frac{1.6\times10^{-19}[j]}{[eV]}$$

$$C = \frac{4.54\times10^{-10}[ev]}{R_m} = \frac{4.54\times10^{-1}[ev]}{R_{nm}} \tag{A-2.15}$$

A-2.4 Representation of final equation

From (A-2.2), (A-2.9), (A-2.13) and (A-2.15)

$$\frac{1240.7[eV]}{\lambda_{nm}} - 2.42[eV] = \frac{1.72[eV]}{(R_{nm})^2} - \frac{4.54\times10^{-1}[eV]}{R_{nm}}$$

since $D_{nm} = 2\times R_{nm}$,

$$\frac{1240.7[eV]}{\lambda_{nm}} - 2.42[eV] = \frac{6.88[eV]}{(D_{nm})^2} - \frac{9.08\times10^{-1}[eV]}{D_{nm}} \tag{A-2.16}$$

Equation (A-2.16) is only valid for CdS nanocrystals.

A-3 Matlab code for the calculation of particle diameter

A Matlab code presented below is used to calculate the particle size of the QDs from their absorption edges by using equations A-2.1 to A-2.15. This program can also be applied to other QD's such as ZnO, CdSe or PbS as long as ε_{rel}, ΔE_{bulk}, m_e, m_h are corrected for the new material. Table A-3.1 shows the list of particle size and band gap energies calculated accordingly.

```
int L23
% relative, relative permittvity of vacuum, bulk bandgap [ev].
Cdsprop=[0.3 0.8 5.7 2.42];
% mo is the mass of electron (kg)
m0=9.1095*10^-31;
% planck constant in (Js)
h=6.63*10^-34;
% permittivity of vacuum in [F/m]=C*V/m
e0=8.854*10^-12;
% 1 ev = 1.6*10^-19 C
c=3.0*10^8;
N1=264
landa=linspace(250e-9,513e-9,N1);
wavelength_entered=landa*10^9
for i=1:N1
bandgap_found(i)=h*c/(landa(i)*1.602*10^-19);
deltaband(i)=bandgap_found(i)-Cdsprop(4);
z=deltaband(i);
mstar=1/(1/(Cdsprop(1)*m0)+1/(Cdsprop(2)*m0))
A=h^2/(8*mstar*10^-18*1.602*10^-19);
```

```
B=1.8*(1.602*10^-19)/(4*pi*Cdsprop(3)*e0*10^-9);
p=[z 0 -A];
r=roots(p);
   If r(1)>r(2)
      a=r(1);
   Else
      a=r(2);
   End
   P1=[z B -A];
r1=roots(p1);
   If r1(1)>r1(2)
      a1=r1(1);
   Else
      a1=r1(2);
   End
diameter(i)=a;
diameter2(i)=a*2;
diametera1(i)=a1;
diameter2a1(i)=a1*2;
End
diameter_r=diameter2';
wavelength_entered1=wavelength_entered';
bandgap_found1=bandgap_found';
deltaband1=deltaband';
diameter_ra1=diameter2a1';
```

Table A-3.1 CdS particle diameters with respect to absorption edge

Wavelength (nm)	Diameter (nm)	Diameter (nm) wrt First term	Band Gap (eV)	Delta Band Gap (eV)
250	1.5	1.6	4.97	2.55
251	1.5	1.7	4.95	2.53
252	1.5	1.7	4.93	2.51
253	1.5	1.7	4.91	2.49
254	1.5	1.7	4.89	2.47
255	1.5	1.7	4.87	2.45
256	1.5	1.7	4.85	2.43
257	1.5	1.7	4.83	2.41
258	1.5	1.7	4.81	2.39
259	1.5	1.7	4.79	2.37
260	1.5	1.7	4.78	2.36
261	1.5	1.7	4.76	2.34
262	1.5	1.7	4.74	2.32
263	1.5	1.7	4.72	2.30
264	1.6	1.7	4.70	2.28
265	1.6	1.7	4.69	2.27
266	1.6	1.8	4.67	2.25
267	1.6	1.8	4.65	2.23
268	1.6	1.8	4.63	2.21
269	1.6	1.8	4.62	2.20
270	1.6	1.8	4.60	2.18
271	1.6	1.8	4.58	2.16
272	1.6	1.8	4.56	2.14
273	1.6	1.8	4.55	2.13
274	1.6	1.8	4.53	2.11
275	1.6	1.8	4.51	2.09
276	1.6	1.8	4.50	2.08
277	1.6	1.8	4.48	2.06
278	1.6	1.8	4.47	2.05
279	1.6	1.8	4.45	2.03
280	1.6	1.9	4.43	2.01
281	1.6	1.9	4.42	2.00
282	1.7	1.9	4.40	1.98
283	1.7	1.9	4.39	1.97
284	1.7	1.9	4.37	1.95

* **Diameter** is the calculated diameter according to (A.2-15).

Diameter wrt First term represents the diameter of the particles without considering the third term in (A.2-15).

Band gap defines the band Gap of the nanocrystals with respect to absorption edge.

Delta Band Gap defines the difference between the band gap of CdS nanocrystals and bulk form of the CdS.

Wavelength (nm)	Diameter (nm)	Diameter (nm) wrt First term	Band Gap (eV)	Delta Band Gap (eV)
285	1.7	1.9	4.36	1.94
286	1.7	1.9	4.34	1.92
287	1.7	1.9	4.33	1.91
288	1.7	1.9	4.31	1.89
289	1.7	1.9	4.30	1.88
290	1.7	1.9	4.28	1.86
291	1.7	1.9	4.27	1.85
292	1.7	1.9	4.25	1.83
293	1.7	1.9	4.24	1.82
294	1.7	2.0	4.22	1.80
295	1.7	2.0	4.21	1.79
296	1.7	2.0	4.19	1.77
297	1.7	2.0	4.18	1.76
298	1.7	2.0	4.17	1.75
299	1.8	2.0	4.15	1.73
300	1.8	2.0	4.14	1.72
301	1.8	2.0	4.12	1.70
302	1.8	2.0	4.11	1.69
303	1.8	2.0	4.10	1.68
304	1.8	2.0	4.08	1.66
305	1.8	2.0	4.07	1.65
306	1.8	2.1	4.06	1.64
307	1.8	2.1	4.04	1.62
308	1.8	2.1	4.03	1.61
309	1.8	2.1	4.02	1.60
310	1.8	2.1	4.01	1.59
311	1.8	2.1	3.99	1.57
312	1.8	2.1	3.98	1.56
313	1.8	2.1	3.97	1.55
314	1.8	2.1	3.95	1.53
315	1.9	2.1	3.94	1.52
316	1.9	2.1	3.93	1.51
317	1.9	2.1	3.92	1.50
318	1.9	2.2	3.90	1.48
319	1.9	2.2	3.89	1.47
320	1.9	2.2	3.88	1.46

Wavelength (nm)	Diameter (nm)	Diameter (nm) wrt First term	Band Gap (eV)	Delta Band Gap (eV)
357	2.2	2.6	3.48	1.06
358	2.2	2.6	3.47	1.05
359	2.2	2.6	3.46	1.04
360	2.2	2.6	3.45	1.03
361	2.2	2.6	3.44	1.02
362	2.2	2.6	3.43	1.01
363	2.2	2.6	3.42	1.00
364	2.2	2.6	3.41	0.99
365	2.2	2.7	3.40	0.98
366	2.2	2.7	3.39	0.97
367	2.2	2.7	3.38	0.96
368	2.3	2.7	3.37	0.95
369	2.3	2.7	3.36	0.94
370	2.3	2.7	3.36	0.94
371	2.3	2.7	3.35	0.93
372	2.3	2.7	3.34	0.92
373	2.3	2.8	3.33	0.91
374	2.3	2.8	3.32	0.90
375	2.3	2.8	3.31	0.89
376	2.3	2.8	3.30	0.88
377	2.3	2.8	3.29	0.87
378	2.3	2.8	3.28	0.86
379	2.4	2.8	3.28	0.86
380	2.4	2.9	3.27	0.85
381	2.4	2.9	3.26	0.84
382	2.4	2.9	3.25	0.83
383	2.4	2.9	3.24	0.82
384	2.4	2.9	3.23	0.81
385	2.4	2.9	3.22	0.80
386	2.4	2.9	3.22	0.80
387	2.4	3.0	3.21	0.79
388	2.4	3.0	3.20	0.78
389	2.5	3.0	3.19	0.77
390	2.5	3.0	3.18	0.76
391	2.5	3.0	3.18	0.76
392	2.5	3.0	3.17	0.75

Wavelength (nm)	Diameter (nm)	Diameter (nm) wrt First term	Band Gap (eV)	Delta Band Gap (eV)
393	2.5	3.1	3.16	0.74
394	2.5	3.1	3.15	0.73
395	2.5	3.1	3.14	0.72
396	2.5	3.1	3.14	0.72
397	2.5	3.1	3.13	0.71
398	2.6	3.1	3.12	0.70
399	2.6	3.2	3.11	0.69
400	2.6	3.2	3.10	0.68
401	2.6	3.2	3.10	0.68
402	2.6	3.2	3.09	0.67
403	2.6	3.2	3.08	0.66
404	2.6	3.3	3.07	0.65
405	2.6	3.3	3.07	0.65
406	2.7	3.3	3.06	0.64
407	2.7	3.3	3.05	0.63
408	2.7	3.3	3.04	0.62
409	2.7	3.3	3.04	0.62
410	2.7	3.4	3.03	0.61
411	2.7	3.4	3.02	0.60
412	2.7	3.4	3.01	0.59
413	2.7	3.4	3.01	0.59
414	2.8	3.5	3.00	0.58
415	2.8	3.5	2.99	0.57
416	2.8	3.5	2.98	0.56
417	2.8	3.5	2.98	0.56
418	2.8	3.5	2.97	0.55
419	2.8	3.6	2.96	0.54
420	2.8	3.6	2.96	0.54
421	2.9	3.6	2.95	0.53
422	2.9	3.6	2.94	0.52
423	2.9	3.7	2.94	0.52
424	2.9	3.7	2.93	0.51
425	2.9	3.7	2.92	0.50
426	2.9	3.7	2.91	0.49
427	2.9	3.8	2.91	0.49
428	3.0	3.8	2.90	0.48

Wavelength (nm)	Diameter (nm)	Diameter (nm) wrt First term	Band Gap (eV)	Delta Band Gap (eV)
429	3.0	3.8	2.89	0.47
430	3.0	3.8	2.89	0.47
431	3.0	3.9	2.88	0.46
432	3.0	3.9	2.87	0.45
433	3.0	3.9	2.87	0.45
434	3.1	4.0	2.86	0.44
435	3.1	4.0	2.85	0.43
436	3.1	4.0	2.85	0.43
437	3.1	4.0	2.84	0.42
438	3.1	4.1	2.83	0.41
439	3.1	4.1	2.83	0.41
440	3.2	4.1	2.82	0.40
441	3.2	4.2	2.82	0.40
442	3.2	4.2	2.81	0.39
443	3.2	4.2	2.80	0.38
444	3.2	4.3	2.80	0.38
445	3.3	4.3	2.79	0.37
446	3.3	4.4	2.78	0.36
447	3.3	4.4	2.78	0.36
448	3.3	4.4	2.77	0.35
449	3.3	4.5	2.77	0.35
450	3.4	4.5	2.76	0.34
451	3.4	4.6	2.75	0.33
452	3.4	4.6	2.75	0.33
453	3.4	4.6	2.74	0.32
454	3.5	4.7	2.73	0.31
455	3.5	4.7	2.73	0.31
456	3.5	4.8	2.72	0.30
457	3.5	4.8	2.72	0.30
458	3.6	4.9	2.71	0.29
459	3.6	4.9	2.71	0.28
460	3.6	5.0	2.70	0.28
461	3.6	5.0	2.69	0.27
462	3.7	5.1	2.69	0.27
463	3.7	5.1	2.68	0.26
464	3.7	5.2	2.68	0.26

Wavelength (nm)	Diameter (nm)	Diameter (nm) wrt First term	Band Gap (eV)	Delta Band Gap (eV)
465	3.7	5.3	2.67	0.25
466	3.8	5.3	2.66	0.24
467	3.8	5.4	2.66	0.24
468	3.8	5.4	2.65	0.23
469	3.9	5.5	2.65	0.23
470	3.9	5.6	2.64	0.22
471	3.9	5.7	2.64	0.22
472	4.0	5.7	2.63	0.21
473	4.0	5.8	2.62	0.20
474	4.0	5.9	2.62	0.20
475	4.1	6.0	2.61	0.19
476	4.1	6.1	2.61	0.19
477	4.1	6.1	2.60	0.18
478	4.2	6.2	2.60	0.18
479	4.2	6.3	2.59	0.17
480	4.3	6.4	2.59	0.17
481	4.3	6.5	2.58	0.16
482	4.3	6.7	2.58	0.16
483	4.4	6.8	2.57	0.15
484	4.4	6.9	2.57	0.15
485	4.5	7.0	2.56	0.14
486	4.5	7.2	2.55	0.13
487	4.6	7.3	2.55	0.13
488	4.6	7.5	2.54	0.12
489	4.7	7.6	2.54	0.12
490	4.8	7.8	2.53	0.11
491	4.8	8.0	2.53	0.11
492	4.9	8.2	2.52	0.10
493	4.9	8.4	2.52	0.10
494	5.0	8.6	2.51	0.09
495	5.1	8.8	2.51	0.09
496	5.2	9.1	2.50	0.08
497	5.2	9.4	2.50	0.08
498	5.3	9.7	2.49	0.07
499	5.4	10.1	2.49	0.07
500	5.5	10.5	2.48	0.06

Wavelength (nm)	Diameter (nm)	Diameter (nm) wrt First term	Band Gap (eV)	Delta Band Gap (eV)
501	5.6	10.9	2.48	0.06
502	5.7	11.4	2.47	0.05
503	5.8	12.0	2.47	0.05
504	5.9	12.6	2.46	0.04
505	6.0	13.4	2.46	0.04
506	6.2	14.3	2.45	0.03
507	6.3	15.5	2.45	0.03
508	6.5	16.9	2.44	0.02
509	6.7	18.9	2.44	0.02
510	6.8	21.9	2.43	0.01
511	7.1	26.7	2.43	0.01

Appendix B

FLOURESCENCE MEASUREMENTS AND QY (QY) DETERMINATION

B-1 Introduction to fluorescence spectrophotometry

In this section, the detailed explanation about the fluorescence spectrophotometer and the fluorescence theory will be given.

B-1.1 Fluorescence spectrophotometer

The working principle of any fluorescence spectrophotometer is relatively simple than the principles of the complex spectroscopic techniques. Simply, the light from an excitation source passes through a filter or monochromator, and then passes through the sample in the sample holder. As a result, absorbed light generates fluorescence in the sample. A part of the fluorescent light is focused on a filter or monochromator, which often is placed at a 90° angle to the excitation light. Focused light is then detected by a detection device and delivered to the computer (Figure B-1.1).

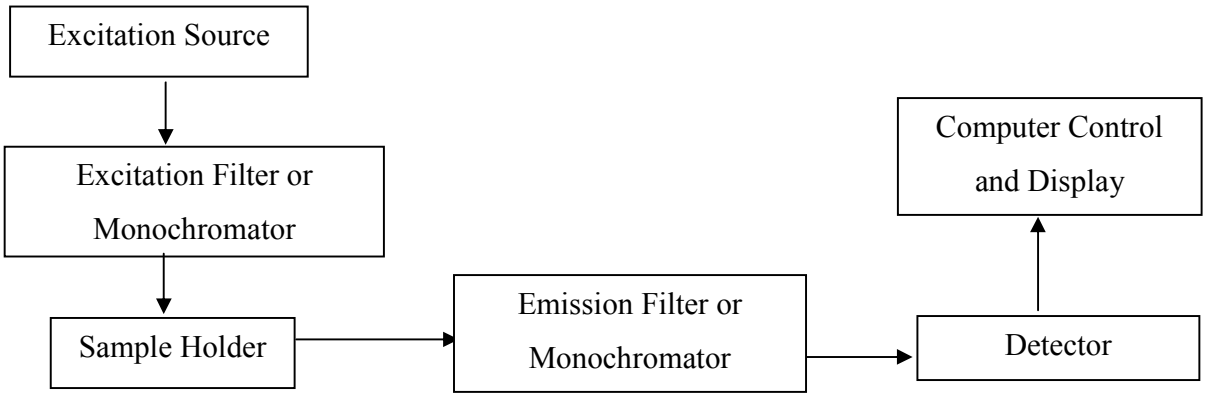

Figure B-1.1 Working principle of a typical fluorescence spectrophotometer.

In our lab, fluorescence measurements were done by using Horiba Jobin Yvon FluoroMax-3 (Figure B-1.2). Excitation light is sent from part A to the sample holder in part B. After the light passed through the emission filter, fluorescence light is collected by the emission detector in part C.

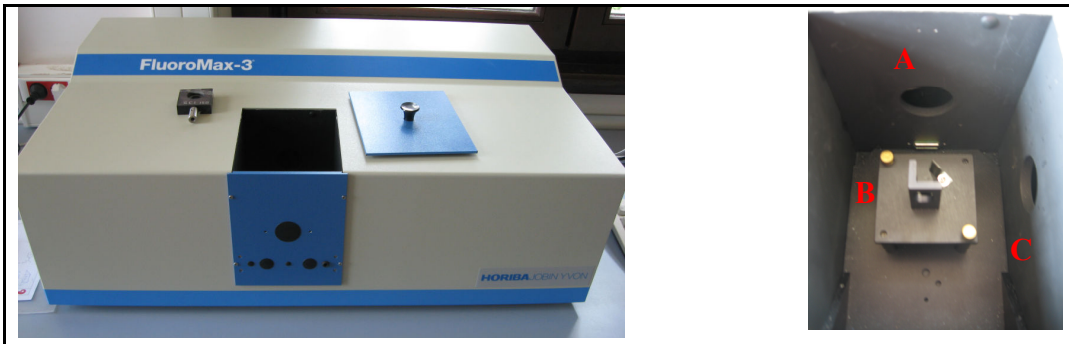

Figure B-1.2 Pictures of Horiba Jobin Yvon Fluoromax-3 spectrophotometer. On the left general view of the spectrophotometer is seen. On the right, excitation window (A), sample holder (B) and emission window (C) are seen.

Fluorescence is often measured at a 90° angle relative to the excitation light. This prevents the interference of the transmitted excitation light and provides detection of the scattered light. Since the monochromator is not a perfect device that only transmits the light at desired wavelength, light at other wavelengths is also sent to the detector. Measurement at 90° angle allows detection of only the scattered light. In the optical spectrophotometers, there are excitation and emission monochromators. Fluorescence is measured at fixed excitation wavelength. Likewise, an excitation spectrum is taken at a constant emission wavelength.

B-1.2 Fluorescence theory

At room temperature, molecules are excited from ground state to excited state by the absorption of light. Figure B-1.3 shows the schematic of the excited and ground states of a molecule that absorbed light. Very simply, when a semiconductor material is excited, electrons jump to the higher vibrational levels. This can be tracked by the absorption bands in the UV-Vis spectroscopy. Energy gained by the electron is lost by the collisions in that state and the molecule rapidly falls to the lowest vibrational level of the excited state emitting its energy in the form of fluorescence. QY of the solution is then calculated as the ratio of emitted light to absorbed light. The transition formed during the energy change from the lowest vibrational level in the ground electronic state to the lowest vibrational level in the first excited state called as the 0-0 transition, and it is common for both the absorption and the emission of light. Other absorption transitions require more energy than the transitions in the fluorescence emission. Then, the 0-0 transition can be considered as the overlapping of the energy levels on the absorption and fluorescence spectrum at the same region. Other than that transition, the emission spectrum is of lower energy, or longer wavelength (Figure B-1.4).

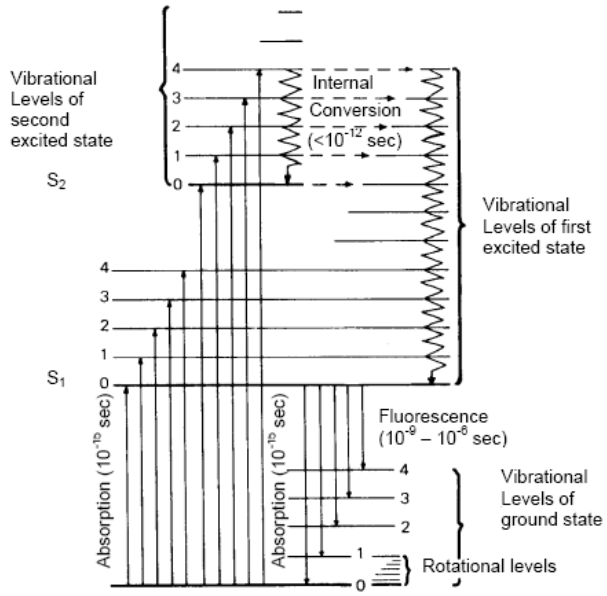

Figure B-1.3 Transitions giving rise to absorption and fluorescence emission spectra.[94]

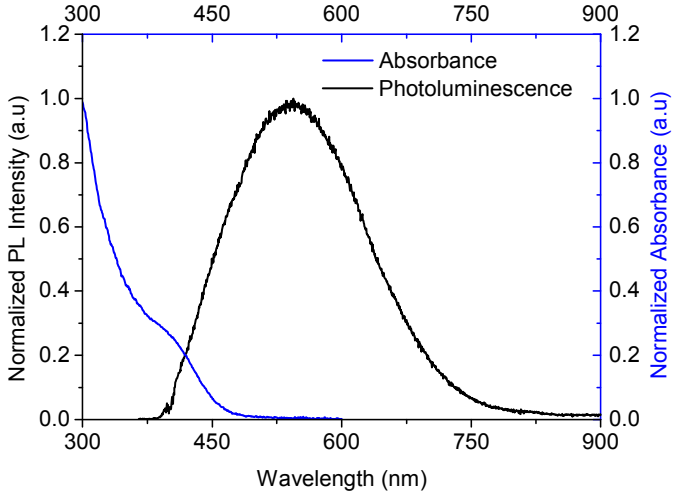

Figure B-1.4 Absorbance and fluorescence emission spectrum of 30 ºC synthesized MAA-PAA coated CdS-QDots.

B-1.3 Quantum yield (QY)

QY is defined as the ratio of the number of fluorescence photons emitted per number of incident photons absorbed. QY are generally reported in comparison to known organic fluorophores. For most efficient calculation, sample and the reference should absorb approximately at the same wavelengths, and their fluorescence spectra should overlap as much as possible.

B-2 PL measurements

B-2.1 QY Determination with a single measurement (SM)

In this type of characterization, the solution is diluted below the absorbance of 0.1 at the excitation wavelength in order to prevent the nonlinear effects of concentration for the fluorescence.

The QY of two different materials can be related by equation B-2.1.

$$\frac{QY(A)}{QY(B)} = \frac{iei(A)/Abs(A)}{iei(B)/Abs(B)} \times \frac{n^2(A)}{n^2(B)} \qquad \text{(eqn B-2.1)}$$

where;

QY **q**uantum **y**ield,

iei **i**ntegrated **e**mission **i**ntensity,

Abs **abs**orbance at the excitation wavelength ; of the samples A and B

n refractive index of the solvents for A and B

B-2.2 QY determination with multiple measurements (MM)

QY calculation of the QDs was done by applying the procedure explained by Horiba Jobin Yvon. In this characterization method, at least three different dilutions from the stock solution were prepared. The most important point is that the absorbance of the samples at the fluorescence excitation wavelength should be smaller that 0.1 in order to avoid any concentration effects on fluorescence.[95] After the absorbance measurements, fluorescence measurements of the same samples were performed. Then, the total integrated

emission intensities (i.e.i) of the particles were calculated by using the Origin software (FluorEscence) supplied from Horiba. I.e.i of the particles was plotted against the absorbance of the samples shown in Figure B-2.1.

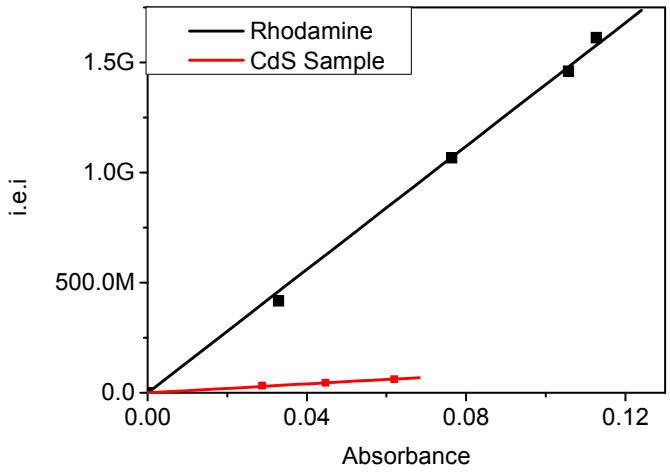

Figure B-2.1 Linear plots for Rhodamine standard sample and CdS sample. The gradient for each sample is proportional to that sample's fluorescence QY as shown in the plot.

It is expected that the absorbed light is proportional to the i.e.i of the particles linearly. Conversion into an absolute QY is achieved through the equation B-2.2.

$$\Phi_X = \Phi_{ST} \times \left(\frac{Grad_X}{Grad_{ST}} \right) \times \left(\frac{n_X}{n_{ST}} \right)^2 \qquad \text{(eqn B-2.2)}$$

Φ_X and Φ_{ST}	QYs of the unknown sample and standard (Rhodamine B), respectively.
$Grad_X$ and $Grad_{ST}$	Gradient of the linear lines for the unknown and standard sample, respectively.
n_X and n_{ST}	Refractive index of the solvents used for unknown and standard sample, respectively.

B-2.3 PL plots

Diluted solutions of the sample (at least three dilutions) are put into the 10 mm four-sided quartz cuvette. The fluorescence measurements are taken at 365-900 nm emission intervals and the excitation wavelength was set at 355 nm. The slit widths were adjusted to 2 nm for both emission and excitation monochromators. Slit width is very important since it changes the intensity of the incoming light from the excitation monochromator and outgoing light to the emission monochromator. If it is too low, for example 0.5, signal to noise ratio will be increased considerably. On the other hand if it is too high for example at the upper limit (5 nm), signal intensity will be very high resulting into the saturation of the light emitted from the sample on the emission detector. The saturation from Rhodamine B sample (reference used in this work) is shown on Figure B-2.2.

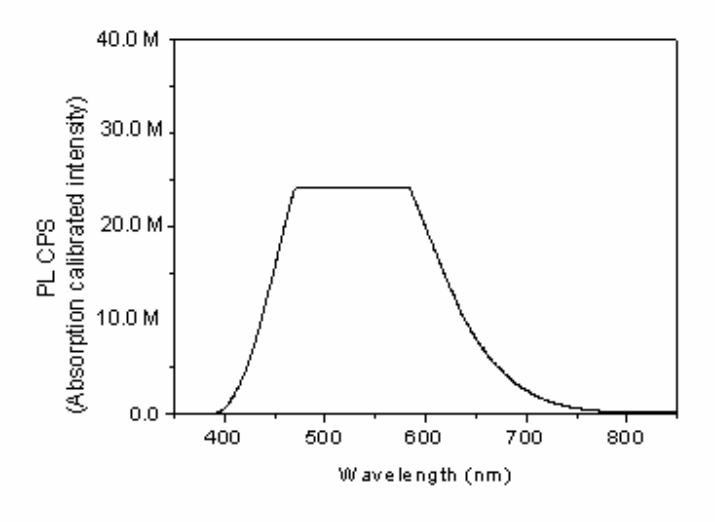

Figure B-2.2 Saturation of the emitted light on emission detector at the excitation wavelength of 355 nm.

PL spectra of the three samples should be different than each other with respect to absorption values. However, after the calibration with absorptions at the excitation wavelength, there should be no difference between the spectra as seen Figure B-2.3 a, b.

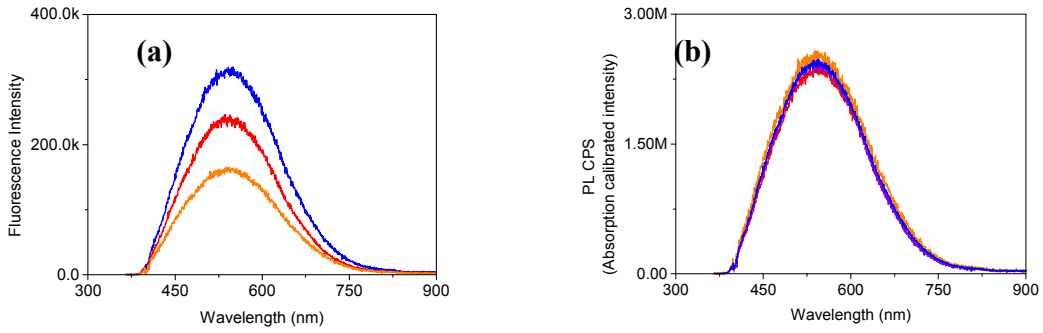

Figure B-2.3 Fluorescence of an arbitrary CdS sample in three different dilution was plotted (a) before and (b) after being calibrated by the absorption at the excitation wavelength

BIBLIOGRAPHY

1. Smith, A.M., X.H. Gao, and S.M. Nie, *Quantum dot nanocrystals for in vivo molecular and cellular imaging.* Photochemistry and Photobiology, 2004. 80(3): p. 377-385.
2. Alivisatos, A.P., *Perspectives on the physical chemistry of semiconductor nanocrystals.* Journal of Physical Chemistry, 1996. 100(31): p. 13226-13239.
3. Brus, L.E., *Electron-electron and electron-hole interactions in small semiconductor crystallites: The size dependence of the lowest excited electronic state.* J. Chem. Phys., 1984. 80(9): p. 4403-4409.
4. Schmid, G., *Nanoparticles: From Theory to Application* 3ed. 2005: Wiley-VCH. 444.
5. Murray, C.B. and D.J. Norris, *Synthesis and characterization of nearly monodisperse CdE (E=S, Se, Te) semiconductor.* Journal of the American Chemical Society, 1993. 115(19): p. 8706.
6. Reiss, P., J. Bleuse, and A. Pron, *Highly luminescent CdSe/ZnSe core/shell nanocrystals of low size dispersion.* Nano Letters, 2002. 2(7): p. 781-784.
7. Guo, W.H., J.J. Li, Y.A. Wang, and X.G. Peng, *Luminescent CdSe/CdS core/shell nanocrystals in dendron boxes: Superior chemical, photochemical and thermal stability.* Journal of the American Chemical Society, 2003. 125(13): p. 3901-3909.
8. Esteves, A.C.C. and T. Trindade, *Synthetic studies on II/VI semiconductor quantum dots.* Current Opinion in Solid State & Materials Science, 2002. 6(4): p. 347-353.

9. Puzder, A., A.J. Williamson, N. Zaitseva, G. Galli, L. Manna, and A.P. Alivisatos, *The effect of organic ligand binding on the growth of CdSe nanoparticles probed by Ab initio calculations.* Nano Letters, 2004. 4(12): p. 2361-2365.
10. Hines, M.A. and P. Guyot-Sionnest, *Synthesis and characterization of strongly luminescing ZnS-Capped CdSe nanocrystals.* Journal of Physical Chemistry, 1996. 100(2): p. 468-471.
11. yBullen, C.R. and P. Mulvaney, *Nucleation and growth kinetics of CdSe nanocrystals in octadecene.* Nano Letters, 2004. 4(12): p. 2303-2307.
12. Yu, W.W. and X.G. Peng, *Formation of high-quality CdS and other II-VI semiconductor nanocrystals in noncoordinating solvents: Tunable reactivity of monomers.* Angewandte Chemie-International Edition, 2002. 41(13): p. 2368-2371.
13. Ji, J., N. Rosenzweig, I. Jones, and Z. Rosenzweig, *Molecular oxygen-sensitive fluorescent lipobeads for intracellular oxygen measurements in murine macrophages.* Analytical Chemistry, 2001. 73(15): p. 3521-3527.
14. Luccardini, C., C. Tribet, F. Vial, V. Marchi-Artzner, and M. Dahan, *Size, charge, and interactions with giant lipid vesicles of quantum dots coated with an amphiphilic macromolecule.* Langmuir, 2006. 22(5): p. 2304-2310.
15. Fan, H.Y., E.W. Leve, C. Scullin, J. Gabaldon, D. Tallant, S. Bunge, T. Boyle, M.C. Wilson, and C.J. Brinker, *Surfactant-assisted synthesis of water-soluble and biocompatible semiconductor quantum dot micelles.* Nano Letters, 2005. 5(4): p. 645-648.
16. Kim, S. and M.G. Bawendi, *Oligomeric Ligands for luminescent and stable nanocrystal quantum dots.* Journal of the American Chemical Society, 2003. 125(48): p. 14652-14653.
17. Libert, S., V. Gorshkov, V. Privman, D. Goia, and E. Matijevic, *Formation of monodispersed cadmium sulfide particles by aggregation of nanosize precursors.* Advances in Colloid and Interface Science, 2003. 100: p. 169-183.

18. Priyam, A., A. Chatterjee, S.K. Das, and A. Saha, *Synthesis and spectral studies of cysteinee-capped CdS nanoparticles.* Research on Chemical Intermediates, 2005. 31(7-8): p. 691-702.
19. Young, A.G., D.P. Green, and A.J. McQuillan, *Infrared spectroscopic studies of monothiol ligand adsorption on CdS nanocrystal films in aqueous solutions.* Langmuir, 2006. 22(26): p. 11106-11112.
20. Zhang, H., Z. Zhou, B. Yang, and M.Y. Gao, *The influence of carboxyl groups on the photoluminescence of mercaptocarboxylic acid-stabilized CdTe nanoparticles.* Journal of Physical Chemistry B, 2003. 107(1): p. 8-13.
21. Righini, G.C., A. Verciani, S. Pelli, M. Guglielmi, A. Martucci, J. Fick, and G. Vitrant, *Sol–gel glasses for nonlinear optics.* Pure Appl. Optics, 1996. 5: p. 655-666.
22. Winter, J.O., N. Gomez, S. Gatzert, C.E. Schmidt, and B.A. Korgel, *Variation of cadmium sulfide nanoparticle size and photoluminescence intensity with altered aqueous synthesis conditions.* Colloids and Surfaces a-Physicochemical and Engineering Aspects, 2005. 254(1-3): p. 147-157.
23. Mang, P. and L. Gao, *Synthesis and characterization of CdS nanorods via hydrothermal microemulsion.* Langmuir, 2003. 19(1): p. 208-210.
24. Liu, B., G.Q. Xu, L.M. Gan, C.H. Chew, W.S. Li, and Z.X. Shen, *Photoluminescence and structural characteristics of CdS nanoclusters synthesized by hydrothermal microemulsion.* Journal of Applied Physics, 2001. 89(2): p. 1059-1063.
25. Zhang, Q.M., F.Z. Huang, and Y. Li, *Cadmium sulfide nanorods formed in microemulsions.* Colloids and Surfaces a-Physicochemical and Engineering Aspects, 2005. 257-58: p. 497-501.
26. Dutz, S., W. Andra, R. Hergt, R. Muller, C. Oestreich, C. Schmidt, J. Topfer, M. Zeisberger, and M.E. Bellemann, *Influence of dextran coating on the magnetic behaviour of iron oxide nanoparticles.* Journal of Magnetism and Magnetic Materials, 2007. 311(1): p. 51-54.

27. Pardoe, H., W. Chua-anusorn, T.G. St Pierre, and J. Dobson, *Structural and magnetic properties of nanoscale iron oxide particles synthesized in the presence of dextran or polyvinyl alcohol.* Journal of Magnetism and Magnetic Materials, 2001. 225(1-2): p. 41-46.

28. Acar, H.Y.C., R.S. Garaas, F. Syud, P. Bonitatebus, and A.M. Kulkarni, *Superparamagnetic nanoparticles stabilized by polymerized PEGylated coatings.* Journal of Magnetism and Magnetic Materials, 2005. 293(1): p. 1-7.

29. Chen, D.H. and S.H. Huang, *Fast separation of bromelain by polyacrylic acid-bound iron oxide magnetic nanoparticles.* Process Biochemistry, 2004. 39(12): p. 2207-2211.

30. Graham, D.L., H.A. Ferreira, and P.P. Freitas, *Magnetoresistive-based biosensors and biochips.* Trends in Biotechnology, 2004. 22(9): p. 455-462.

31. Poeckler-Schoeniger, C., J. Koepke, F. Gueckel, J. Sturm, and M. Georgi, *MRI with superparamagnetic iron oxide: Efficacy in the detection and characterization of focal hepatic lesions.* Magnetic Resonance Imaging, 1999. 17(3): p. 383-392.

32. Bulte, J.W.M., I.D. Duncan, and J.A. Frank, *In vivo magnetic resonance tracking of magnetically labeled cells after transplantation.* Journal of Cerebral Blood Flow and Metabolism, 2002. 22(8): p. 899-907.

33. Brzeska, M., M. Panhorst, P.B. Kamp, J. Schotter, G. Reiss, A. Puhler, A. Becker, and H. Bruckl, *Detection and manipulation of biomolecules by magnetic carriers.* Journal of Biotechnology, 2004. 112(1-2): p. 25-33.

34. Wang, D.S., J.B. He, N. Rosenzweig, and Z. Rosenzweig, *Superparamagnetic Fe_2O_3 Beads-CdSe/ZnS quantum dots core-shell nanocomposite particles for cell separation.* Nano Letters, 2004. 4(3): p. 409-413.

35. Hong, X., J. Li, M.J. Wang, J.J. Xu, W. Guo, J.H. Li, Y.B. Bai, and T.J. Li, *Fabrication of magnetic luminescent nanocomposites by a layer-by-layer self-assembly approach.* Chemistry of Materials, 2004. 16(21): p. 4022-4027.

36. Mandal, S.K., N. Lequeux, B. Rotenberg, M. Tramier, J. Fattaccioli, J. Bibette, and B. Dubertret, *Encapsulation of magnetic and fluorescent nanoparticles in emulsion droplets.* Langmuir, 2005. 21(9): p. 4175-4179.

37. Kim, J., J.E. Lee, J. Lee, J.H. Yu, B.C. Kim, K. An, Y. Hwang, C.H. Shin, J.G. Park, J. Kim, and T. Hyeon, *Magnetic fluorescent delivery vehicle using uniform mesoporous silica spheres embedded with monodisperse magnetic and semiconductor nanocrystals.* Journal of the American Chemical Society, 2006. 128(3): p. 688-689.

38. Muller-Schulte, D., T. Schmitz-Rode, and P. Borm, *Ultra-fast synthesis of magnetic and luminescent silica beads for versatile bioanalytical applications.* Journal of Magnetism and Magnetic Materials, 2005. 293(1): p. 135-143.

39. Mulvaney, S.P., H.M. Mattoussi, and L.J. Whitman, *Incorporating fluorescent dyes and quantum dots into magnetic microbeads for immunoassays.* Biotechniques, 2004. 36(4): p. 602-+.

40. Demirer, M., *Controlled synthesis of superparamagnetic iron oxide nanoparticles in the presence of poly(acrylic acid)*, in *Material Science&Engineering*. 2006, Koc University: Istanbul. p. 100.

41. Yu, W.W., L.H. Qu, W.Z. Guo, and X.G. Peng, *Experimental determination of the extinction coefficient of CdTe, CdSe and CdS nanocrystals (vol 15, pg 2854, 2003).* Chemistry of Materials, 2004. 16(3): p. 560-560.

42. Aldana, J., Y.A. Wang, and X.G. Peng, *Photochemical instability of CdSe nanocrystals coated by hydrophilic thiols.* Journal of the American Chemical Society, 2001. 123(36): p. 8844-8850.

43. Ozkan, M., *Quantum dots and other nanopartciles: what can they offer to drug discovery?* Drug Discovery Today, 2004. 9(24): p. 1065-1071.

44. Marti, A., N. Lopez, E. Antolin, E. Canovas, C. Stanley, C. Farmer, L. Cuadra, and A. Luque, *Novel Semiconductor solar cell structures: The quantum dot intermediate band solar cell.* Thin Solid Films, 2006. 511-512: p. 638-644.

45. Landi, B.J., S.L. Castro, H.J. Ruf, C.M. Evans, S.G. Bailey, and R.P. Raffaelle, *CdSe quantum dot-single wall carbon nanotube complexes for polymeric solar cells.* Solar Energy Materials & Solar Cells, 2005. 87: p. 733-746.

46. Weng, J.F., X.T. Song, L.A. Li, H.F. Qian, K.Y. Chen, X.M. Xu, C.X. Cao, and J.C. Ren, *Highly luminescent CdTe quantum dots prepared in aqueous phase as an alternative fluorescent probe for cell imaging.* Talanta, 2006. 70(2): p. 397-402.

47. Henini, M. and M. Bugajski, *Advances in self-assembled semiconductor quantum dot lasers.* Microelectronics Journal, 2005. 36(11): p. 950-956.

48. Mattheakis, L.C., J.M. Dias, Y.J. Choi, J. Gong, M.P. Bruchez, and E.W. J. Liu, *Optical coding of mammalian cells using semiconductor quantum dots.* Analytical Biochemistry, 2004. 327: p. 200-208.

49. Yin, Y. and A.P. Alivisatos, *Colloidal nanocrystal synthesis and the organic-inorganic interface.* Nature, 2005. 437(7059): p. 664-670.

50. Spanhel, L., M. Haase, H. Weller, and A. Henglein, *Photochemistry of Colloidal Semiconductors .20. Surface Modification and Stability of Strong Luminescing Cds Particles.* Journal of the American Chemical Society, 1987. 109(19): p. 5649-5655.

51. Yusuf, H., W.G. Kim, D.H. Lee, Y.Y. Guo, and M.G. Moffitt, *Size control of mesoscale aqueous assemblies of quantum dots and block copolymers.* Langmuir, 2007. 23(2): p. 868-878.

52. Wang, C.W. and M.G. Moffitt, *Surface-tunable photoluminescence from block copolymer-stabilized cadmium sulfide quantum dots.* Langmuir, 2004. 20(26): p. 11784-11796.

53. Duxin, N., F.T. Liu, H. Vali, and A. Eisenberg, *Cadmium sulphide quantum dots in morphologically tunable triblock copolymer aggregates.* Journal of the American Chemical Society, 2005. 127(28): p. 10063-10069.

54. Lu, X.F., H. Gao, J.Y. Chen, D.M. Chao, W.J. Zhang, and Y. Wei, *Poly(acrylic acid)-guided synthesis of helical polyaniline/CdS composite microwires.* Nanotechnology, 2005. 16(1): p. 113-117.

55. Erdamar, A.K., *Spectroscopic Investigation of CdS Quantum Dots and Fe^{2+}:ZnSe*, in *Physics Department*. 2007, Koç University: Istanbul. p. 67.

56. Chung, C.K. and M. Lee, *Self-assembled monolayers of mercaptoacetic acid on Ag powder: Characterization by FT-IR diffuse reflection spectroscopy.* Bulletin of the Korean Chemical Society, 2004. 25(10): p. 1461-1462.

57. Guinier, A., *X-ray Diffraction*. 1963, San Francisco: Freeman.

58. Wang, W., Z. Liu, C. Zheng, C. Xu, Y. Liu, and G. Wang, *Synthesis of CdS nanoparticles by a novel and simple one-step, solid-state reaction in the presence of a nonionic surfactant.* Materials Letters, 2003. 57(18): p. 2755.

59. Whelan, C.M., J. Ghijsen, J.-J. Pireaux, and K. Maex, *Cu adsorption on carboxylic acid-terminated self-assembled monolayers: a high-resolution X-ray photoelectron spectroscopy study.* Thin Solid Films, 2004. 464/465: p. 388.

60. Farah, A.A., S.H. Zheng, S. Morin, F. Bensebaa, and W.J. Pietro, *Thiolated poly(ε-caprolactone) macroligand with vacant coordination sites on gold substrate: Synthesis and surface characterization.* Surface Science, 2007. 601(7): p. 1677.

61. Kar, S. and S. Chaudhuri, *Shape selective growth of CdS one-dimensional nanostructures by a thermal evaporation process.* Journal of Physical Chemistry B, 2006. 110(10): p. 4542-4547.

62. Chowdhury, P.S., P. Ghosh, and A. Patra, *Study of photophysical properties of capped CdS nanocrystals*. Journal of Luminescence, 2007. 124: p. 327-332.

63. Wang, Y., A. Suna, W. Mahler, and R. Kasowki, *PbS in polymers. From molecules to bulk solids.* Journal of Chemical Physics, 1987. 87(12): p. 7315.

64. Wuister, S.F. and A. Meijerink, *Synthesis and luminescence of (3-mercaptopropyl)trimethoxysilane capped CdS quantum dots.* Journal of Luminescence, 2003. 102: p. 338-343.

65. Trindade, T., P. OBrien, and X.M. Zhang, *Synthesis of CdS and CdSe nanocrystallites using a novel single-molecule precursors approach.* Chemistry of Materials, 1997. 9(2): p. 523-530.

66. Swayambunathan, V., D. Hayes, K.H. Schmidt, Y.X. Liao, and D. Meisel, *Thiol Surface Complexation on Growing Cds Clusters.* Journal of the American Chemical Society, 1990. 112(10): p. 3831-3837.

67. Moffitt, M., L. Mcmahon, V. Pessel, and A. Eisenberg, *Size Control of Nanoparticles in Semiconductor-Polymer Composites .2. Control Via Sizes of Spherical Ionic Microdomains in Styrene-Based Diblock Ionomers.* Chemistry of Materials, 1995. 7(6): p. 1185-1192.

68. Rivas, B.L., E.D. Pereira, and I. Moreno-Villoslada, *Water-soluble polymer-metal ion interactions.* Progress in Polymer Science, 2003. 28(2): p. 173.

69. Reiss, P., S. Carayon, J. Bleuse, and A. Pron, *Low polydispersity core/shell nanocrystals of CdSe/ZnSe and CdSe/ZnSe/ZnS type: preparation and optical studies.* Synthetic Metals, 2003. 139(3): p. 649-652.

70. Gerion, D., F. Pinaud, S.C. Williams, W.J. Parak, D. Zanchet, S. Weiss, and A.P. Alivisatos, *Synthesis and properties of biocompatible water-soluble silica-coated CdSe/ZnS semiconductor quantum dots.* Journal of Physical Chemistry B, 2001. 105(37): p. 8861-8871.

71. Sukhanova, A., M. Devy, L. Venteo, H. Kaplan, M. Artemyev, V. Oleinikov, D. Klinov, M. Pluot, J.H.M. Cohen, and I. Nabiev, *Biocompatible fluorescent nanocrystals for immunolabeling of membrane proteins and cells.* Analytical Biochemistry, 2004. 324(1): p. 60-67.

72. Wang, Y., Z.Y. Tang, M.A. Correa-Duarte, I. Pastoriza-Santos, M. Giersig, N.A. Kotov, and L.M. Liz-Marzan, *Mechanism of strong luminescence photoactivation of citrate-stabilized water-soluble nanoparticles with CdSe cores.* Journal of Physical Chemistry B, 2004. 108(40): p. 15461-15469.

73. Wang, M., N. Felorzabihi, G. Guerin, J.C. Haley, G.D. Scholes, and M.A. Winnik, *Water-Soluble CdSe Quantum Dots Passivated by a Multidentate Diblock Copolymer.* Macromolecules, 2007. 40: p. 6377-6384.

74. Lin, Y.W., M.M. Hsieh, C.P. Liu, and H.T. Chang, *Photoassisted synthesis of CdSe and core-shell CdSe/CdS quantum dots.* Langmuir, 2005. 21(2): p. 728-734.

75. Yuan, C.-T., W.-C. Chou, D.-S. Chuu, W.H. Chang, H.-S. Lin, and R.-C. Ruaan, *Fluorescence Properties of Colloidal CdSe/ZnS Quantum Dots with Various Surface Modifications.* Journal of Medical and Biological Engineering, 2006. 26(3): p. 131-135.

76. Chen, H.M., X.F. Huang, L. Xu, J. Xu, K.J. Chen, and D. Feng, *Self-assembly and photoluminescence of CdS-mercaptoacetic clusters with internal structures.* Superlattices and Microstructures, 2000. 27(1): p. 1-5.

77. Zhang, X.J., Q.R. Zhao, Y.P. Tian, and Y. Xie, *Fabrication of CdS micropatterns: Effects of intermolecular hydrogen bonding and decreasing capping ligand.* Crystal Growth & Design, 2004. 4(2): p. 355-359.

78. Jang, J.S., S. Kim, and K.J. Lee, *Fabrication of CdS/PMMA core/shell nanoparticles by dispersion mediated interfacial polymerization.* Chemical Communications, 2007(26): p. 2689-2691.

79. Zhang, H., C.L. Wang, M.J. Li, X.L. Ji, J.H. Zhang, and B. Yang, *Fluorescent nanocrystal-polymer composites from aqueous nanocrystals: Methods without ligand exchange.* Chemistry of Materials, 2005. 17(19): p. 4783-4788.

80. Lei, Y., H. Tang, C. Zhou, T. Zhang, M. Feng, and B. Zou, *Incorporating fluorescent quantum dots into watersoluble polymer*, in *Journal of Luminescence*. 2007.

81. Chen, M., L. Pan, J. Cao, H. Ji, G. Ji, X. Ma, and Y. Zheng, *Synthesis of CdS nanoplates by PAA-assisted hydrothermal approach.* Materials Letters, 2006. 60(29/30): p. 3842.

82. Celebi, S., A.K. Erdamar, A. Sennaroglu, A. Kurt, and H.Y. Acar. *NanoTr-III*. in *NanoScience ,Nanotechnology,Nanobiotechnology,Nanomedicine*. 2007. Bilkent,Ankara/Turkey.

83. Magde, D., G.E. Rojas, and P.G. Seybold, *Solvent dependence of the fluorescence lifetimes of xanthene dyes.* Photochemistry and Photobiology, 1999. 70(5): p. 737-744.

84. Horiba, J.Y. *A Guide to Recording Fluorescence Quantum Yields*. Volume, 1-6

85. Raji, P., C. Sanjeeviraja, and K. Ramachandran, *Thermal properties of nano crystalline CdS.* Crystal Research and Technology, 2004. 39(7): p. 617-622.

86. Yao, J., G. Zhao, and G. Han, *Synthesis and characterization of the thiourea-capped CdS nanoparticles.* Journal of Materials Science Letters, 2003. 22(21): p. 1491.

87. Ste-Marie, J., A.E. Torma, and A.O. Gübeli, *The stability of Thiocomplexes and solubility products of metal sulphides.* Canadian Journal of Chemistry, 1964. 42: p. 662-668.

88. Nosaka, Y., H. Shigeno, and T. Ikeuchi, *Formation of Polynuclear Cadmium-Thiolate Complexes and Cds Clusters in Aqueous-Solution Studied by Means of Stopped-Flow and Nmr Spectroscopies.* Journal of Physical Chemistry, 1995. 99(20): p. 8317-8322.

89. Floroiu, R.M., A.P. Davis, and A. Torrents, *Cadmium adsorption on aluminum oxide in the presence of polyacrylic acid.* Environmental Science & Technology, 2001. 35(2): p. 348-353.

90. Acar, H.Y., S. Celebi, A.K. Erdamar, A. Sennaroglu, and A. Kurt, *Synthesis and Characterization of Poly(acrylic acid) Stabilized CdS Quantum Dots.* Journal of Physical Chemistry B, 2007.

91. Kavlak, S., H.K. Can, Z.M.O. Rzaev, and A. Guner, *Thermal properties of poly(maleic anhydride-alt-acrylic acid) in the presence of certain metal chlorides.* Journal of Applied Polymer Science, 2006. 100(5): p. 3926-3930.

92. Karlsson, T., K. Elgh-Dalgren, E. Bjorn, and U. Skyllberg, *Complexation of cadmium to sulfur and oxygen functional groups in an organic soil.* Geochimica Et Cosmochimica Acta, 2007. 71(3): p. 604-614.

93. van Dijken, A., A.H. Janssen, M.H.P. Smitsmans, D. Vanmaekelbergh, and A. Meijerink, *Size-selective photoetching of nanocrystalline semiconductor particles.* Chemistry of Materials, 1998. 10(11): p. 3513-3522.

94. *An Introduction to Fluorescence Spectroscopy*. 2000 [cited; Available from: http://homepages.wmich.edu/~rsung/files/IntroFluor.pdf.

95. Dhami, S., A.J. Demello, G. Rumbles, S.M. Bishop, D. Phillips, and A. Beeby, *Phthalocyanine Fluorescence at High-Concentration - Dimers or Reabsorption Effect.* Photochemistry and Photobiology, 1995. 61(4): p. 341-346.

VITA

Serdar Çelebi was born in Istanbul, Turkey in 1982. He completed the high school in Çapa Anatolian teacher training high school in 2000. He received his B.S. degree from the Department of Chemical Engineering, Middle East Technical University (Ankara) in 2005. In 2005, he started his M.S. degree in Material Science& Engineering department at Koc University. He will be starting his doctorate degree in Chemical Reactor engineering at the department of Chemical Engineering and Chemistry, Technical University of Eindhoven.